Sediment Transport Predictions and Bed Surface Adjustments in Spatially Variable Flow

A Dissertation
Presented in Partial Fulfillment of the Requirements for the
Degree of Doctorate of Philosophy
with a
Major in Civil Engineering
in the
College of Graduate Studies
University of Idaho
by

Angel D. Monsalve Sepúlveda

Major Professor: Elowyn Yager, Ph.D
Committee Members: Daniele Tonina, Ph.D,; John Buffington, Ph.D.; Peter Nelson, Ph.D.
Department Administrator: Patricia Colberg, Ph.D.

April 2016

Authorization to Submit Dissertation

This dissertation of Angel D. Monsalve Sepúlveda, submitted for the degree of Doctor of Philosophy with a Major in Civil Engineering and titled "Sediment Transport Predictions and Bed Surface Adjustments in Spatially Variable Flow," has been reviewed in final form. Permission, as indicated by the signatures and dates below, is now granted to submit final copies to the College of Graduate Studies for approval.

Major Professor: _____ Date: _____
Elowyn Yager, Ph.D.

Committee Members: _____ Date: _____
Daniele Tonina, Ph.D.

_____ Date: _____
John Buffington, Ph.D.

_____ Date: _____
Peter Nelson, Ph.D.

Department Administrator: _____ Date: _____
Patricia Colberg, Ph.D.

Abstract

In mountainous rivers bedforms, large relatively immobile grains, and bed texture and topographic variability can significantly alter local and reach-averaged flow characteristics. However, this variability is often omitted in bed load calculations. To explore the influence of spatially variable flow in sediment transport fluxes and bed adjustments I conducted a field study in which I obtained all the measurements to test a novel probabilistic bed load transport equation that explicitly includes local variations in the flow field and grain size distribution. I also conducted a set of flume experiments in which the relative submergence was varied to obtain different shear stress divergences around large immobile grains which created dissimilar bedforms between experiments. Spatially variable flow parameters were calculated using a quasi-3D and 3D RANS-VOF model in the field and flume studies, respectively. The boundary shear stress in the field study displayed substantial variability between sediment patch classes, but the patch mean dimensionless shear stress varied inversely with patch median grain size. I developed an empirical relation between the applied shear stress on each patch class and the reach averaged shear stress and median grain size which when used in my bed load equation was more accurate than current bed load transport equations. In the laboratory experiments the bed surface in each experiment was adjusted through surface elevations and GSD changes. Upstream the hemispheres a coarse sediment patch was developed and little to no change occurred in the downstream region. Commonly used theoretical velocity profiles only performed correctly at the reach scale when the roughness length of the relatively mobile sediment was considered, at the local scale large deviations from these profiles were observed. The presence of bedforms altered the spatial distribution of boundary shear stresses and caused significant deviations from hydrostatic pressure. Zones of high turbulent kinetic energy occurred near the water surface and were controlled by the immobile grains and plunging flow. Our results suggest spatially variable grain size distributions must be explicitly included in bed load transport calculations. Simple methods to estimate boundary shear stresses based on velocity profiles may not perform correctly at the local scale.

Acknowledgements

I would like to express the deepest appreciation to my major professor, Dr. Elowyn Yager, without her advice, expertise, encouragement, and persistent help this research and dissertation would not have been possible. I greatly appreciate the time we spent discussing about sediment transport and rivers in general and the freedom she gave me to develop all my ideas. Her guidance was fundamental throughout all my Ph.D. program.

I would also like to thank the other members of my dissertation committee: Dr. Daniele Tonina, Dr. John Buffington, and Dr. Peter Nelson. All of them are an inspiration for my future career as scientist and their insight, feedback, and advice was essential during the dissertation writing process.

I am greatly thankful to Dr. Peter Goodwin and the staff Center for Ecohydraulics Research for giving me the opportunity to conduct my research here. It has been my pleasure and honor to work during almost five years in this amazing environment.

I would like to thank my wife, Marcela, for all her patience and support. Leaving her career to let me pursue my dreams was and still is the most generous act I could ever imagine. I will be forever thankful for taking care of our three children while I was doing my research.

Finally to all my friends and colleges that made this time a fantastic experience – Thanks to Dr. Diego Caamaño, Heidi Smith, Megan Kenworthy, Miguel Aguayo, and Mohammad Sohrabi and their families. Funding for this research was provided by an NSF Career award to E.M. Yager (0847799) and the Chilean Government - CONICYT “Becas de Doctorado en el Extranjero – Becas Chile”

Dedication

To Marcela, Felipe, Sebastián, and Matías

Table of Contents

List of Figures

List of Tables

Chapter 1: Introduction

Mountain rivers with steep slopes (> 3 percent) are different than lowland rivers in a number of characteristics. They typically have low discharges and relative submergences (ratio of the average flow depth and a characteristic grain size) and their beds are often composed of sediment patches. [*Yager et al*., 2007, 2012a; *Comiti and Mao*, 2012]. Patches of sediment, which are areas of the bed with relatively narrow grain size distribution (GSD) compared to the reach [*Laronne et al*., 2000; *Dietrich et al*., 2005], affect the flow field and induce large spatial and temporal variations in bed load transport rates and grain size distributions [*Paola and Seal*, 1995; *Ferguson*, 2003]. Including the effects of sediment patches in bedload transport predictions is challenging because most equations were developed for lowland rivers and do not consider the characteristics of a typical mountain river. For instance, they do not account for spatial the variability of shear stresses, increased total flow resistance caused by large roughness elements or the limited upstream sediment supply. Using these types of bedload transport equations often result in overpredictions of sediment transport rates by several orders of magnitude [*Bathurst et al*., 1987; *Lenzi M.A. and D'agostino V*., 1999; *Rickenmann*, 2001; *Yager et al*., 2007, 2012a, 2012b; *Mueller et al*., 2008; *Nitsche et al.*, 2011; *Schneider et al*., 2015]. Sediment transport equations developed for steep channels improve the predictions, however, they are only accurate to an order of magnitude at best and do not account for the spatial variability in the flow caused by sediment patches and bedforms [e.g. *Smart*, 1984; *Bathurst et al*., 1987; *Graf and Suszka*, 1987; *Aziz and Scott*, 1989; *Rickenmann*, 1997, 2005; *Lenzi et al*., 1999; *Yager et al*., 2007, 2012b; *Nitsche et al.*, 2011]. Accurate predictions of bedload transport in steep rivers are important because they control the design of hydraulic structures such as bridges and are a key component in hazard management projects, for instance in the mitigation of the flood effects [*Nitsche et al.*, 2011].

The mechanisms controlling patch formation, evolution, and characteristics (such as area, grain size distribution, and location) are also unclear, partly because of the lack of correlation between local hydraulic properties (e.g. velocity or shear stress) and local surface grain texture *[Lisle et al*., 2000; *Nelson et al.*, 2010]. It has been proposed that patches arise from a local sediment transport capacity – sediment supply imbalance *[Dietrich et al., 1989; Kinerson, 1990; Lisle et al.*, 1991, 1993; *Yarnell et al.*, 2006; *Nelson et al.*, 2009], grain to grain

interactions [*Lisle et al*., 1991; *Nelson et al.*, 2009; *Nelson*, 2010] or size-selective cross-stream transport in topographically forced heterogeneous flow fields [*Dietrich and Whiting*, 1989; *Lisle et al*., 1991; *Nelson et al*., 2010], but in reality all of these processes interact. Sediment patch formation is important to understand because it has biological implications, for instance salmon may find their preferred spawning-sized gravel in zones of finer textures [*Kondolf and Wolman*, 1993; *Buffington and Montgomery*, 1999; *Buxton et al*., 2015a, 2015b; *Hassan et al*., 2015].

In addition to patches, bedforms and large roughness elements are critical controls on the spatial variability in the flow field, for instance in the distribution of shear stresses *[Einstein, 1950; Einstein and Barbarosa, 1952; Smith and McLean*, 1977; *Nelson et al*., 1993; *Sukhodolov et al*., 2006], which in turn affect the local sediment transport rate and bedload grain size distribution. In particular, dunes can generate flow separation, near-bed accelerations at the downstream dune face, secondary currents (e.g. *Smith and McLean* [1977]; *Mclean and Smith* [1986]; *Nelson et al*. [1993]; *Bennett and Best* [1995]; *McLean et al*. [1999]; *Venditti and Bennett* [2000]; *Maddux et al*. [2003a, 2003b]; *McLean and Nikora* [2006]; *Sukhodolov et al*. [2006]; *Keylock et al*. [2014]), velocity intermittency [*Keylock et al.*, 2014] and are a key control of turbulence kinetic energy [*Sukhodolov et al*., 2006] and intensity [*Bennett and Best*, 1995]. Understanding the effects of bedforms and roughness elements on flow velocity is not only important for sediment transport studies but is crucial to develop accurate predictive models of nutrient transport [*Webel and Schatzmann*, 1984], plant growth [*Sutcliffe*, 2014] and salmonid migration [*Tritico and Hotchkiss*, 2005].

In mountain rivers the spatial variability of the bed surface elevation (e.g. bedforms) and texture (i.e. patches) and the presence of large relatively immobile boulders create highly spatially variable flow fields, which in turn affect the variability of grain sizes. This study is focused on these spatial variations and their effects on sediment transport. The questions that motivate this research are: i) Is it important to include the variability in flow and grain size distributions in sediment transport predictions? if these variations are important, how should they be included?, ii) What is the effect of bedforms and large roughness elements on flow hydraulics? iii) What is the mechanism that controls patch formation and stability? To answer these questions a field study and a series of laboratory and numerical modeling experiments

were conducted. For question i) a novel approach that explicitly includes spatial variations of shear stresses and grain size distributions was proposed and tested in a 10% gradient river. The accuracy of the approach was evaluated by comparing its results to measured sediment transport volumes. In question ii) three flume experiments were conducted with large immobile boulders and mobile gravel and flow hydraulics were compared at the beginning (no bedforms) and end of the runs (bedforms were present). Finally, in question iii) the same flume experiments were used to study the formation and stability of sediment patches around immobile boulders. In all cases the spatial distributions of flow variables were obtained using numerical flow models, where the irregularities of the bed and the presence of large roughness elements were explicitly included.

1.1 References

Aziz, N. M., and D. E. Scott (1989), Experiments on sediment transport in shallow flows in high gradient channels, Hydrol. Sci. J., 34(4), 465–478, doi:doi:10.1080/02626668909491352.

Bathurst, J. C., W. H. Graf, and H. H. Cao (1987), Bed load discharge equations for steep mountain rivers, in Sediment Transport in Gravel Bed Rivers, edited by C. R. Thorne, J. C. Bathurst, and R. D. Hey, pp. 453–477, John Wiley, Chichester, UK.

Bennett, S. J., and J. L. Best (1995), Mean flow and turbulence structure over fixed, two-dimensional dunes implications for sediment transport and bedform stability, Sedimentology, 42, 491–513.

Buffington, J. M., and D. R. Montgomery (1999), Effects of hydraulic roughness on surface textures of gravel-bedded rivers, Water Resour. Res., 35(11), 3507–3521.

Buxton, T. H., J. M. Buffington, D. Tonina, A. K. Fremier, and E. M. Yager (2015a), Modeling the Influence of Salmon Spawning on Hyporheic Exchange of Marine-Derived Nutrients in Gravel Stream beds, Can. J. Fish. Aquat. Sci., 72, 1146–1158, doi:10.1139/cjfas-2014-0413.

Buxton, T. H., J. M. Buffington, E. M. Yager, M. A. Hassan, and A. K. Fremier (2015b), The relative stability of salmon redds and unspawned streambeds, Water Resour. Res., 51, 6074–6092, doi:10.1002/ 2015WR016908.

Comiti, F., and L. Mao (2012), Recent Advances in the Dynamics of Steep Channels, in Gravel-Bed Rivers: Processes, Tools, Environments, edited by M. Church, P. M. Biron, and A. G. Roy, pp. 351–377, John Wiley & Sons, Ltd, Chichester, UK.

Dietrich, W. E., and P. Whiting (1989), Boundary Shear Stress and Sediment Transport In River Meanders of Sand and Gravel, in River Meandering, American Geophysical Union - Water Resources. Monographs, vol. 12, edited by S. Ikeda and G. Parker, pp. 1–50, American Geophysical Union, Washington, D.C., USA.

Dietrich, W. E., J. W. Kirchner, H. Ikeda, and F. Iseya (1989), Sediment supply and the development of the coarse surface layer in gravel-bedded rivers, Nature, 340, 215–217, doi:10.1038/340215a0.

Dietrich, W. E., P. a. Nelson, E. Yager, J. G. Venditti, M. P. Lamb, and L. Collins (2005), Sediment patches, sediment supply, and channel morphology, in 4th IAHR Symposium on River, Coastal and Estuarine., edited by G. Parker and M. H. Garcia, pp. 79–90, Taylor & Francis Group, Urbana, Illinois, USA.

Einstein, H. A. (1950), The Bed-Load Function for Sediment Transportation in Open Channel Flows, Soil Conserv. Serv., (1026), 1–31.

Einstein, H. A., and N. L. Barbarosa (1952), River Channel Roughness, Trans. Am. Soc. Civ. Eng., 117(1), 1121–1132.

Ferguson, R. I. (2003), The missing dimension: Effects of lateral variation on 1-D calculations of fluvial bedload transport, Geomorphology, 56, 1–14, doi:10.1016/S0169-555X(03)00042-4.

Graf, W. H., and L. Suszka (1987), Sediment transport in steep channels, J. Hydrosci. Hydraul. Eng., 5, 11–26.

Hassan, M. A., D. Tonina, and T. H. Buxton (2015), Does small-bodied salmon spawning activity enhance streambed mobility?, Water Resour. Res., 51, 1–18, doi:10.1002/2015WR017079.

Keylock, C. J., A. Singh, J. G. Venditti, and E. Foufoula-Georgiou (2014), Robust classification for the joint velocity-intermittency structure of turbulent flow over fixed and mobile bedforms, Earth Surf. Process. Landforms, 39(13), 1717–1728, doi:10.1002/esp.3550.

Kinerson, D. (1990), Surface response to sediment supply, M.S., Thesis. University of California, Berkeley, CA. 108 pp.

Kondolf, G. M., and M. G. Wolman (1993), The sizes of salmonid spawning gravels, Water Resour. Res., 29(7), 2275–2285, doi:10.1029/93WR00402.

Laronne, J. B., C. García, and I. Reid (2000), Mobility of patch sediment in gravel bed streams: patch character and its implications for bedload, in Gravel-Bed Rivers V, edited by M. P. Mosley, pp. 249–289, New Zealand Hydrological Society Inc., Wellington, New Zealand.

Lenzi, M. A., V. D'Agostino, and P. Billi (1999), Bedload transport in the instrumented catchment of the Rio Cordon PArt I: Analysis of bedload records, conditions and threshold of bedload entrainment, Catena, 36, 171–190, doi:10.1016/S0341-8162(99)00017-X.

Lenzi M.A., and D'agostino V. (1999), Bedload transport in the instrumented catchment of the Rio Cordon Part II: Analysis of the bedload rate, Catena, 36, 191–204.

Lisle, T. E., H. Ikeda, and F. Iseya (1991), Formation of stationary alternate bars in a steep channel with mixed-size sediment: A flume experiment, Earth Surf. Process. Landforms, 16(5), 463–469, doi:10.1002/esp.3290160507.

Lisle, T. E., F. Iseya, and H. Ikeda (1993), Response of a channel with alternate bars to a decrease in supply of mixed-size bed load: A flume experiment, Water Resour. Res., 29(11), 3623–3629, doi:10.1029/93WR01673.

Lisle, T. E., J. M. Nelson, J. Pitlick, M. A. Madej, and B. L. Barkett (2000), Variability of bed mobility in natural, gravel-bed channels and adjustments to sediment load at local and reach scales, Water Resour. Res., 36(12), 3743–3755, doi:10.1029/2000WR900238.

Maddux, T. B., J. M. Nelson, and S. R. McLean (2003a), Turbulent flow over three-dimensional dunes: 1. Free surface and flow response, J. Geophys. Res. Surf., 108(F1), F16009, doi:F16009\r10.1029/2003jf000017.

Maddux, T. B., S. R. McLean, and J. M. Nelson (2003b), Turbulent flow over three-dimensional dunes: 2. Fluid and bed stresses, J. Geophys. Res. Surf., 108(F1), F16010, doi:F16010\r10.1029/2003jf000018.

McLean, S. R., and V. I. Nikora (2006), Characteristics of turbulent unidirectional flow over rough beds: Double-averaging perspective with particular focus on sand dunes and gravel beds, Water Resour. Res., 42(10), 1–19, doi:10.1029/2005WR004708.

Mclean, S. R., and J. D. Smith (1986), A model for flow over two-dimensional bed forms, J. Hydraul. Eng., 112(4), 300–317.

McLean, S. R., S. R. Wolfe, and J. M. Nelson (1999), Spatially averaged flow over a wavy surface revisited, J. Geophys. Res., 104(C7), 743–753, doi:10.1029/1999JC900116.

Mueller, E., R. Batalla, C. Garcia, and A. Bronstert (2008), Modeling Bed-Load Rates from Fine Grain-Size Patches during Small Floods in a Gravel-Bed River, J. Hydraul. Eng., 134(10), 1430–1439, doi:10.1061/(ASCE)0733-9429(2008)134:10(1430).

Nelson, J. M., S. R. McLean, and S. R. Wolfe (1993), Mean flow and turbulence fields over two-dimensional bed forms, Water Resour. Res., 29(12), 3935, doi:10.1029/93WR01932.

Nelson, P. A. (2010), Bed Surface Patchiness in Gravel-Bed Rivers, PhD Thesis. University of California, Berkeley, CA. 154 pp.

Nelson, P. A., J. G. Venditti, W. E. Dietrich, J. W. Kirchner, H. Ikeda, F. Iseya, and L. S. Sklar (2009), Response of bed surface patchiness to reductions in sediment supply, J. Geophys. Res. Earth Surf., 114(2), 1–18, doi:10.1029/2008JF001144.

Nelson, P. A., W. E. Dietrich, and J. G. Venditti (2010), Bed topography and the development of forced bed surface patches, J. Geophys. Res. Earth Surf., 115, F04024, doi:10.1029/2010JF001747.

Nitsche, M., D. Rickenmann, J. M. Turowski, A. Badoux, and J. W. Kirchner (2011), Evaluation of bedload transport predictions using flow resistance equations to account for macro-roughness in steep mountain streams, Water Resour. Res., 47, W08513, doi:10.1029/2011WR010645.

Paola, C., and R. Seal (1995), Grain size patchiness as a cause of selective deposition and downstream fining, Water Resour. Res., 31(5), 1395–1407.

Rickenmann, D. (1997), Sediment transport in Swiss torrents, Earth Surf. Process. Landforms, 22(10), 937–951, doi:10.1002/(SICI)1096-9837(199710)22:10<937::AID-ESP786>3.0.CO;2-R.

Rickenmann, D. (2001), Comparison of bed load transport in torrents and gravel bed streams, Water Resour. Res., 37(12), 3295–3305, doi:10.1029/2001WR000319.

Rickenmann, D. (2005), Geschiebetransport bei steilen Gefällen, in Festkolloquium, edited, Versuchsanstalt für Wasserbau, Hydrologie und Glaziologie.

Schneider, J. M., D. Rickenmann, J. M. Turowski, K. Bunte, and J. W. Kirchner (2015), Applicability of bed load transport models for mixed-size sediments in steep streams considering macro-roughness, Water Resour. Res., 51, 5260–5283, doi:10.1002/2014WR016417.Received.

Smart, G. (1984), Sediment Transport Formula for Steep Channels, J. Hydraul. Eng., 110(3), 267–276, doi:10.1061/(ASCE)0733-9429(1984)110:3(267).

Smith, J. D., and S. R. McLean (1977), Spatially averaged flow over a wavy surface, J. Geophys. Res., 82(12), 1735, doi:10.1029/JC082i012p01735.

Sukhodolov, A. N., J. J. Fedele, and B. L. Rhoads (2006), Structure of flow over alluvial bedforms: an experiment on linking field and laboratory methods, Earth Surf. Process. Landforms, 31(10), 1292–1310, doi:10.1002/esp.1330.

Sutcliffe, A. G. (2014), Modelling the effects of aquatic plant growth and management on the hydraulics of a chalk stream, University of London.

Tritico, H. M., and R. H. Hotchkiss (2005), Unobstructed and Obstructed Turbulent Flow in Gravel Bed Rivers, J. Hydraul. Eng., 131(8), 635–645, doi:10.1061/(ASCE)0733-9429(2005)131:8(635).

Venditti, J. G., and S. J. Bennett (2000), Spectral analysis of turbulent flow and suspended sediment transport over fixed dunes, J. Geophys. Res., 105(C9), 22,035–22,047.

Webel, G., and M. Schatzmann (1984), Transverse Mixing in Open Channel Flow, J. Hydraul. Eng., 110(4), 423–435, doi:10.1061/(ASCE)0733-9429(1984)110:4(423).

Yager, E. M., J. W. Kirchner, and W. E. Dietrich (2007), Calculating bed load transport in steep boulder bed channels, Water Resour. Res., 43(7), 1–24, doi:10.1029/2006WR005432.

Yager, E. M., W. E. Dietrich, J. W. Kirchner, and B. W. McArdell (2012a), Prediction of sediment transport in step-pool channels, Water Resour. Res., 48(1), 1–20, doi:10.1029/2011WR010829.

Yager, E. M., J. M. Turowski, D. Rickenman, and B. W. McArdell (2012b), Sediment supply, grain protrusion, and bedload transport in mountain streams, Geophys. Res. Lett., 39, L10402, doi:10.1029/2012GL051654.

Yarnell, S. M., J. F. Mount, and E. W. Larsen (2006), The influence of relative sediment supply on riverine habitat heterogeneity, Geomorphology, 80(3-4), 310–324, doi:10.1016/j.geomorph.2006.03.005.

Chapter 2: A probabilistic formulation of bed load transport to include spatial variability of flow and surface grain size distributions

Submitted to Water Resources Research

Monsalve, A., Yager, E.M., Turowski, J. M., Rickenmann, D. (2016) A probabilistic formulation of bed load transport to include spatial variability of flow and surface grain size distributions. *Water Resour. Res.*

2.1 Abstract

Bed load fluxes are typically calculated as a function of the reach averaged boundary shear stress and a representative bed grain size distribution. In steep, rough channels, heterogeneous bed surface texture and macro-roughness elements cause significant local deviations from the mean shear stress but this variability is often omitted in bed load calculations. Here we present a probabilistic bed load transport formulation that explicitly includes local variations in the flow field and grain size distribution. The model is then tested in a 10% gradient stream, to evaluate its predictive capability and to explore relations between surface grain size sorting and boundary shear stress. The boundary shear stress field, calculated using a quasi-3D hydraulic model, displayed substantial variability between patch classes, but the patch mean dimensionless shear stress varied inversely with patch median grain size. We developed an empirical relation between the applied shear stress on each patch class and the reach averaged shear stress and median grain size. Predicted sediment volumes using this relation in our bed load equation were as accurate as those using complete shear stress distributions and more accurate than current bed load transport equations. Our results suggest that when spatially variable grain size distributions (e.g. patches of sediment) are present they must be explicitly included in bed load transport calculations. Spatial variability in shear stress was relatively more important than grain size variations for sediment transport predictions.

2.1.1 Key points

Including sediment patches improve sediment transport predictions

Patch and reach averaged shear stress are related through median grain size

2.2 Introduction

Mountain rivers with steep slopes (longitudinal gradients greater than 3 percent) differ from those with lower slopes through a number of characteristics. Such channels are located in headwater catchments, their drainage area is relatively small, and they typically have low discharges and low relative submergences (h / D where h is the average flow depth and D is the characteristic grain size) [*Comiti and Mao*, 2012]. Their channel beds feature wide grain size distributions (GSD) from sand to rarely mobile boulders [*Yager et al.*, 2012a] and episodic landslides and debris flows may alter this composition. Additionally, these riverbeds are often composed of patches of sediment, which consist of distinct areas of the bed with relatively narrow GSD and greater sorting compared to the reach [*Laronne et al.*, 2000; *Dietrich et al.*, 2005]. Patches of sediment affect the flow and boundary shear stress field, the rate and composition of sediment fluxes [*Paola and Seal*, 1995; *Ferguson*, 2003] and can also have biological implications, for instance salmon may find their preferred spawning-sized gravel in zones of finer textures [*Kondolf and Wolman*, 1993; *Buffington and Montgomery*, 1999b; *Buxton et al.*, 2015a, 2015b; *Hassan et al.*, 2015].

Although sediment patches are common, their formation mechanism is still unclear. When bar morphology or channel obstructions exist, patches can form from topographically induced divergences in boundary shear stress [*Dietrich and Whiting*, 1989; *Lisle et al.*, 1991; *Nelson et al.*, 2010]. Imbalances in local transport capacity and sediment supply have also been identified as a cause of patch formation [*Dietrich et al.*, 1989; *Lisle et al.*, 1993, 2000; *Nelson et al.*, 2009]. Predicting the formation and location of patches is challenging because of the lack of correlation between local hydraulic properties (e.g. velocity or shear stress) and local surface grain texture [*Lisle et al.*, 2000; *Nelson et al.*, 2010]. However, most of these correlations were conducted for a single discharge. Shear stress and median grain size could correlate if a range of discharges is considered, or if scales larger than individual grains (e.g. patches) are analyzed. A relation between shear stress and patch median grain size could also have important consequences for sediment transport predictions.

Sediment patches can lead to large spatial and temporal variations in bed load transport rates, as has been documented in field [*Yager et al.*, 2012a; *Segura and Pitlick*, 2015] and laboratory [*Nelson et al.*, 2010] measurements and by theoretical modeling [*Lisle et al.*, 1993;

Paola and Seal, 1995; *Ferguson*, 2003; *Chen and Stone*, 2008]. Large relatively immobile boulders, which are a common feature of steep mountain channels, also create a three-dimensional and discharge-dependent flow structure, in which the flow velocity and turbulence intensity can significantly vary [*Comiti et al.*, 2007; *Strom and Papanicolaou*, 2007; *Lacey and Roy*, 2008] even in zones not immediately adjacent to the roughness elements, especially in wake zones [*Shvidchenko and Pender*, 2000; *Shamloo et al.*, 2001; *Papanicolaou and Kramer*, 2005; *Tritico and Hotchkiss*, 2005; *Ghilardi et al.*, 2014; *Hajimirzaie et al.*, 2014; *Tsakiris et al.*, 2014]. Studies on low gradient rivers have found that spatial-temporal variations of shear stresses are a key factor in determining the areas of the bed that are highly active during sediment transport events [*Segura and Pitlick*, 2015].

Most sediment transport equations are inaccurate in steep streams because they do not include the energy losses or increased total flow resistance caused by macro- roughness elements (e.g. boulders and steps), the limited upstream sediment supply, and the wide GSD that are typical of high gradient channels [*Bathurst et al.*, 1987; *Lenzi M.A. and D'agostino V.*, 1999; *Rickenmann*, 2001; *Yager et al.*, 2007, 2012b, 2012c; *Mueller et al.*, 2008; *Nitsche et al.*, 2011; *Scheider et al.*, 2015]. Even equations developed for steep channels [e.g. *Smart*, 1984; *Bathurst et al.*, 1987; *Graf and Suszka*, 1987; *Aziz and Scott*, 1989] and those that explicitly [*Yager et al.*, 2007, 2012c] or implicitly [e.g. *Rickenmann*, 1997, 2005; *Lenzi et al.*, 1999; *Nitsche et al.*, 2011] account for macro-roughness elements are only accurate to an order of magnitude at best. No investigation has determined if including spatial variability in flow and GSD at a scale smaller than the reach (e.g. patch) can improve bed load transport predictions in steep channels. At the patch scale, local hiding/exposure effects and the relative mobility of different grain sizes may be better captured if the patch's median grain size and local flow conditions are considered instead those of the reach.

Probabilistic formulations of sediment transport [*Einstein*, 1950; *Paintal*, 1971; *Lisle et al.*, 1998] can, theoretically, include the variability of flow and surface texture but their application is generally more difficult than deterministic equations. Probabilistic equations require detailed measurements of flow and bed properties that are not commonly available, or involve extrapolation far beyond the conditions (typically flume experiments) where they were developed. For instance the sediment continuity equations of *Parker et al.* [2000] require

functions for the probability of erosion and deposition, which, to date, have not been generalized. The bed load transport equation of *Sun and Donahue* [2000] works well for non-uniform sediment under full motion, but requires the time when a particle is in motion, which has also not been generalized. The use of probabilistic formulations in real field applications is even more unusual. In gravel bed streams, under partial motion conditions, the equation of *Sun and Donahue* [2000] does not perform as well [*Sun and Donahue*, 2000]. However, the field results of *Wu and Yang's* [2004] fractional transport model suggest that a probabilistic approach has enormous potential.

The objectives of this study are to: (1) investigate whether sediment transport predictions in steep streams are improved when spatial variability in the flow field and grain size, in the form of sediment patches, are explicitly included, (2) explore the correlation between reach and patch averaged shear stresses; and its application in bed load flux predictions, and (3) analyze individual contributions of different patch classes to the total transported sediment volume. To meet our objectives, we use bedload transport, bed conditions and shear stress distributions for a steep stream and develop a new bedload transport formulation.

2.3 Field measurements, sediment transport equations and flow modelling

Our field work was conducted at the Erlenbach, a steep (10% gradient) stream located in central Switzerland. This stream has been described in detail in several studies [i.e. *Rickenmann*, 1997; *Turowski et al.*, 2009; *Nitsche et al.*, 2011; *Yager et al.*, 2012a, 2012b; *Beer et al.*, 2015] and we only focus on characteristics needed for flow modelling and bed load measurements and predictions. Bedload transport rates have been continuously recorded since 1986 using a series of Piezoelectric Bedload Impact Sensors (PBIS) or geophone based bed load impact sensors, both hereinafter called bed load sensors [*Rickenmann and McArdell*, 2007; *Rickenmann et al.*, 2012]. The installation, sensitivities and other operating characteristics of these sensors have been described in detail in several studies [*Rickenmann*, 1997; *Rickenmann and McArdell*, 2007; *Turowski and Rickenmann*, 2011]. Our field site is a 40 m long and 4.7 m wide reach composed of a series of steps, formed by large, relatively immobile boulders, and intervening finer, more mobile sediment patches whose GSD ranges from gravel to cobble [*Yager et al.*, 2012a]. The bed load sensors are located directly downstream of our study site,

in a steep concrete ramp designed to easily transport all sediment until it reaches a retention basin.

Our field measurement plan was designed to: a) obtain the detailed bed topography, including large roughness elements and banks, b) define each patch class GSD, c) determine the location and area of different patch classes that are potentially active (submerged) during each discharge, and d) estimate reach averaged properties such as step protrusion [*Yager et al.*, 2012b].

2.3.1 Channel geometry

On August 1st 2010 an extreme event [*Turowski et al.*, 2013] re-arranged the bed configuration, mobilized boulder steps, increased the in-channel sediment supply, and changed the bed surface packing and armoring. We split our data to account for these changes and conducted measurements during June-July 2010 (hereinafter called 2010 data set) and during July-August 2011 and July 2012 (2011 data set).

We surveyed the bed with a high-resolution ground-based light detection and ranging system (terrestrial LiDAR, Leica ScanStation C10, average point spacing 2 cm) and a total station (Leica-system 1200). Terrestrial LiDAR captured the banks, large boulders, and bed surface above the water level and the total station was used to measure the steps, pools, submerged bed, and any other zones the terrestrial LiDAR was unable to capture (average point spacing of 5 cm). We combined both datasets using AutoCAD® Civil 3D 2014 to obtain a digital elevation model (DEM) that was interpolated, using a linear Kriging algorithm, into a rectangular grid with an average point spacing of 5 cm. The grid size of our numerical simulation (~10 cm) would not have benefited from a more detailed topography.

2.3.2 Patch mapping and grain size

Patch boundaries were visually identified as gradual or sharp gradations in GSD and were mapped with the total station. Delineation of patch boundaries has a certain degree of subjectivity [*Nelson et al.*, 2014] and one of the same operators was present in all field campaigns to ensure the same criteria was applied. Patches were grouped in different classes following the classification of *Buffington and Montgomery* [1999a], where a certain patch is

named based on the relative frequency of the surface grain sizes (gravel (2-64 mm), cobble (64-256), and boulder (>256 mm)). Surface grain sizes that occupied less than 5% of the patch area were excluded from the classification. We conducted pebble-counts (counting ≥ 100 grains using the grid method on mostly dry patches) on each patch class and divided all patches into immobile (Boulder patches, steps) or relatively mobile sediment (see *Yager et al.* [2012b]). Nine patch classes distributed into 74 individual patches and 6 patch classes with 62 individual patches composed the 2010 and 2011 data set, respectively (Table 2.1, Figure 2.1 and Figure 2.2). The difference between data sets was likely due to bed restructuring and instability after the extreme event of August 2010 [*Turowski et al.*, 2013].

2.3.3 Flow measurements

We installed 6 and 5 staff plates in different cross-sections for the 2010 and 2011 data sets, respectively (Figure 2.1). We measured water surface elevation (WSE) at each plate throughout 5 and 6 flow events with a total of 8 and 35 measurements for each cross section for the 2010 and 2011 data, respectively. Because of the unsteadiness of the water surface, flow depth (h) at each staff plate was the average of the maximum and minimum h over a period of 60 s. We developed rating curves between h at each cross-section and the flow discharge (Q), which is measured at 1 min intervals (stream gage operated by the Swiss Federal Research Institute, WSL [*Nitsche et al.*, 2011]) at the downstream end of our reach. For all cross-section the average coefficient (R^2) of determination was 0.84 and 0.83 for the 2010 and 2011 data sets, respectively. We tried to simultaneously measure WSE and local flow velocity in each cross section, but even for moderate flows the conditions were too dangerous to wade. We therefore calculated the reach averaged velocity (U) using the method of *Yager et al.* [2012b] (see Appendix B for equation and details), which was originally calibrated for our study reach in 2004. The calibration was prior to extreme events in 2007 and 2010 [*Yager et al.*, 2012b] and to further ensure that our velocities were in the appropriate range, we compared our calculated U (from FaSTMECH, see section 2.3.4) to those from other resistance equations [*Whittaker*, 1986; *Egashira and Ashida*, 1991; *Pagliara and Chiavaccini*, 2006; *Rickenmann and Recking*, 2011] and to the cross sectional averaged velocity ($U_{xs} = Q / A_{xs}$, where the cross sectional area (A_{xs}) was calculated using the measured cross sections and the $h - Q$ rating curves).

2.3.4 Flow modelling and shear stress distributions

We modified *Parker*'s [1990] equations to include the spatially variable boundary shear stress (τ_b) and GSD. To obtain τ_b we used the quasi-3D hydrodynamic model, FaSTMECH, which is included in the iRIC software package V2.3 (*www.i-ric.org*) and was developed by the U.S. Geological Survey. The model has been described in detail elsewhere [e.g. *Nelson and Smith*, 1989; *Nelson and McDonald*, 1995; *Lisle et al.*, 2000; *Nelson et al.*, 2003; *Mcdonald et al.*, 2005; *Kinzel et al.*, 2009] and used in several studies [*Clayton and Pitlick*, 2007; *Nelson et al.*, 2010; *Conner and Tonina*, 2014; *Maturana et al.*, 2014; *Mueller and Pitlick*, 2014; *Segura and Pitlick*, 2015], so only its major characteristics are mentioned here. The model solves the vertically integrated conservation of mass and momentum equations in a curvilinear grid coordinate system. Approximated vertical velocity profiles are calculated from the two dimensional (2D) solution using an assumed eddy viscosity structure [*Rattray and Mitsuda*, 1974]. A zero-equation model for the lateral eddy viscosity, which assumes homogenous and isotropic turbulence, is used for turbulence closure [*Miller and Cluer*, 1998; *Nelson et al.*, 2003; *Barton et al.*, 2005]. The lateral eddy viscosity was constant and equal to 0.005 m^2/s for all our simulated discharges.

Discharges ranging from 0.10 to 3.5 m^3/s, in increments of 0.05 m^3/s, were simulated to include the entire range of flows during which sediment transport was calculated. Flows below 0.10 m^3/s were not simulated because they produce almost no bed load transport. We used a spatially constant drag coefficient (C_d), that was calibrated for each discharge using the $h-Q$ rating curves and the estimated U from *Yager et al.* [2012b]. The use of a constant C_d can result in similar local shear stresses *Lisle et al.* [2000] and *Nelson et al.* [2010] or better predictions of WSE and U [*Segura and Pitlick*, 2015] (see Appendix C for more details on C_d). For both data sets (2010 and 2011) C_d (range of 0.12 to 0.26) varied inversely with depth, which is consistent with the results of *Pasternack et al.* [2006] and *Jarrett* [1984].

The boundary shear stress was calculated at every node (τ_{bn}, where n is a node in the 10 cm mesh, see Appendix C) using the model's outputs for the vertically averaged streamwise (u_n) and cross-stream (v_n) velocities,

$$\tau_{bn} = \rho C_d \left(u_n^2 + v_n^2 \right) , \quad (2.1)$$

where ρ is the water density. Two different approaches were used to describe τ_{bn} for a given patch class: a) patch class averaged τ_{bn} (hereinafter "Patch mean"), and b) patch class variable τ_{bn} distribution (hereinafter "Variable distribution"). We could have used individual patches instead of patch classes, but their areas in most cases were often too small to have enough τ_{bn} values (less than 15) to fit probability distributions. For each patch class, data set (2010 or 2011), and discharge we fit five different probability distributions (normal, lognormal, gamma, exponential, and generalized extreme value) to the modeled shear stresses. The normal, lognormal [*Bridge and Bennett*, 1992; *Kleinhans and van Rijn*, 2002], and gamma [*Paola*, 1996; *Nicholas*, 2000; *Bertoldi et al.*, 2009; *Recking*, 2013; *Segura and Pitlick*, 2015] have been used in previous studies and the exponential and generalized extreme value were included to extend our analysis. Parameters in each distribution were estimated using the maximum likelihood estimation (MLE) method and we used the nonparametric test Chi-Square ($\chi 2$) to determine whether or not the observed shear stresses came from the hypothesized continuous distribution at a 95% significance level. Of those distributions that met the $\chi 2$ test, we selected the one with the highest R^2 from the fit between predicted (from the distribution) and modeled (FaSTMECH) shear stresses. We did this for every discharge and every patch class. If a patch class had less than 15 shear stress values for a given discharge we did not calculate any distribution and bed load transport was determined using the patch class averaged shear stress (see section 2.3.5). A more detailed analysis of the methods, results and implications of using continuous probability distribution with our probabilistic equations (see section 2.3.5) is described in Appendix D.

2.3.5 Sediment transport equations

Our modified version of *Parker's* [1990] equations explicitly includes the grain sizes of different patch classes, spatial distribution of shear stresses, and limited sediment supply. The bed was divided into J patch classes that were further divided into N grain size classes with characteristic diameters D_{ij}, where i ranges from 1 to N and j ranges from 1 to J. The

geometric mean size ($D_{sg\,j}$) and arithmetic standard deviation ($\sigma_{\phi\,j}$ in ϕ units) for each patch class were calculated as:

$$\ln D_{sg\,j} = \sum_{i=1}^{N} F_{i\,j} \ln D_{i\,j}\,, \tag{2.2}$$

$$\sigma_{\phi\,j}^2 = \sum_{i=1}^{N} \left[\ln\left(\frac{D_{i\,j}}{D_{sg\,j}} \right) \left(\ln 2 \right)^{-1} \right]^2 F_{i\,j}\,, \tag{2.3}$$

where $F_{i\,j}$ is the volume fraction of the i^{th} grain-size class in the j^{th} patch class . The local applied dimensionless shear stress ($\tau^*_{sg\,j}$, hereinafter the superscript * denotes a dimensionless quantity) at the j^{th} patch class was calculated as:

$$\tau^*_{sg\,j} = \frac{\tau_{b\,n\,j}}{\rho R_s g D_{sg\,j}}\,, \tag{2.4}$$

where $\tau_{b\,n\,j}$ is a local applied shear stress at the j^{th} patch class, R_s is the dimensionless submerged specific gravity of sediment and g the acceleration due to gravity. Hereinafter we refer to $\tau^*_{sg\,j}$ simply as τ^*_j. For sediment transport, the only relevant locations were where the local dimensionless shear stress was higher than the dimensionless critical shear stress (assumed τ^*_c=0.045, *Buffington and Montgomery*, [1997]); we only used locations in which $\tau^*_j \geq \tau^*_c$. Although the smaller fractions of fine sediment patches could be in motion for these low shear stresses, their contribution to the total transported volume was negligible and neglecting low τ^*_j allowed us to simplify our calculations. The probability density function ($P_{\tau^*_j}$, see Figure 2.3 for definitions) of τ^*_j follows the best-fit distribution that may change with the discharge. The lower, τ^*_{jl}, and upper, τ^*_{ju}, limits of the distribution were set as the 1st and 99th percentile of the best-fit distribution. Bedload transport rates were calculated at discrete intervals of τ^*_j, where the width of each interval ($\Delta\tau^*_j$) is given by:

$$\Delta\tau_j^* = \frac{\tau_{ju}^* - \tau_{jl}^*}{K}, \tag{2.5}$$

with K=25 as the number of intervals. Since the patch mean approach does not require a discrete interval, τ_j^* is simply the average of all shear stresses for each discharge and patch class. Within a patch class the fraction of the bed area, A_{jk}, where a certain τ_j^* acts is:

$$A_{jk} = \Delta\tau_j^* P_{\tau_j^*}\ , \tag{2.6}$$

with k ranging from 1 to K, therefore the τ_j^* acting on A_{jk} is defined as τ_{jk}^*. The process for calculating τ_j^*, A_{jk} and τ_{jk}^* is shown in Figure 2.3. The hiding function (ϕ_{ijk}) for the k^{th} sub-region in the j^{th} patch class is:

$$\phi_{ijk} = \omega_{jk}\phi_{sgojk}\left(\frac{D_{ij}}{D_{sgj}}\right)^{-\beta}\ , \tag{2.7}$$

where ϕ_{sgojk} is:

$$\phi_{sgojk} = \frac{\tau_{jk}^*}{\tau_{rsgo}^*}, \tag{2.8}$$

The exponent β is 0.16 for all patch classes and was calculated using tracer particles installed in our reach [*Yager et al.*, 2012b] and τ_{rsgo}^* is a dimensionless reference stress (0.0386, in the original *Parker* [1990] equation). A sensitivity analysis of the bed load transport predictions to this hiding function is provided in Appendix E). The empirical function ω_{jk} is defined as:

$$\omega_{jk} = 1 + \frac{\sigma_{\phi j}}{\sigma_{\phi 0}\left(\phi_{sgojk}\right)}\left(\omega_0\left(\phi_{sgojk}\right) - 1\right), \tag{2.9}$$

where $\sigma_{\phi 0}\left(\phi_{sgo\,j\,k}\right)$ and $\omega_0\left(\phi_{sgo\,j\,k}\right)$ are graphical functions from *Parker* [1990]. The dimensionless bed load transport rate $W^*_{s\,i\,j\,k}$ for each i^{th} size class in for each k^{th} sub-region on the j^{th} patch class is:

$$W^*_{s\,i\,j\,k} = 0.00218 G\left(\phi_{i\,j\,k}\right), \tag{2.10}$$

where

$$G\left(\phi_{i\,j\,k}\right) = \begin{cases} 5474\left(1-\dfrac{0.853}{\phi_{i\,j\,k}}\right)^{4.5} & ,\phi_{i\,j\,k} > 1.59 \\ \exp\left[14.2\left(\phi_{i\,j\,k}-1\right)-9.28\left(\phi_{i\,j\,k}-1\right)^2\right] & ,1 \le \phi_{i\,j\,k} \le 1.5 \\ {\phi_{i\,j\,k}}^{14.2} & ,\phi_{i\,j\,k} < 1 \end{cases}, \tag{2.11}$$

The volumetric transport rate per unit width ($q_{i\,j\,k}$) for the i^{th} size class in the k^{th} sub-region on the j^{th} patch class:

$$q_{i\,j\,k} = \frac{\left(\dfrac{\tau_{j\,k}}{\rho}\right)^{1.5} F_{i\,j}\, W^*_{s\,i\,j\,k}}{R_s g} A_{j\,k}, \tag{2.12}$$

The volumetric transport rate per unit width for each i^{th} size class on the j^{th} patch class is:

$$q_{i\,j} = \sum_{k=1}^{K} q_{i\,j\,k}\ , \tag{2.13}$$

and the volumetric transport rate per unit width for the j^{th} patch class is $q_j = \sum_{i=1}^{N} q_{i\,j}$. The total transport rate per unit width (q_T) is:

$$q_T = \left(\sum_{j=1}^{J} q_j \frac{A_j}{A_{T\,w}} \right) \frac{A_m}{A_T} Z_m^*, \tag{2.14}$$

where A_j is the wetted, or submerged, bed area of the j^{th} patch class, A_{Tw} is the total wetted bed area, A_m is the area fraction occupied by relatively mobile grains (i.e. the bed excluding immobile steps) sand A_T is the total bed area. The ratio A_j / A_{Tw} is a weighting factor that accounts for the individual contributions of each patch class to the total bed load. Z_m^* is the ratio of the mobile sediment deposit thickness at the time of an individual flow event (Z_t) to that immediately after the last extreme event (Z_{t0}).

$$Z_m^* = \frac{Z_t}{Z_{t0}}, \tag{2.15}$$

If the mean immobile-grain diameter (D_I) does not vary with time (t, in units of months, see Appendix F for details) then Z_m^* can be approximated as:

$$Z_m^* = \frac{1}{0.85}\left(1 - 0.15 t^{0.21}\right), \tag{2.16}$$

The upstream sediment supply, which is typically limited in steep streams, is included by scaling the predicted total transport rate by the volumetric proportion of the bed covered by relatively mobile sediment, $\left(Am / A_T\right) Z_m^*$, which is a proxy for sediment supply and a modification of the approach used by *Yager et al. [2012c]*. The ratio A_m / A_T changed between the two data sets (0.70 and 0.74 for the 2010 and 2011 data sets, respectively), but it was assumed constant within each set.

2.3.6 Sediment flux measurements and predictions

Our transport predictions depend on bed topography, patch class GSD, and assumed relative sediment supply, which in turn depend on the time elapsed since the last extreme event. The last recorded extreme events occurred on June 20, 2007 and August 1, 2010 [*Turowski et al.*, 2009, 2013], and therefore we limit our analysis to events after 2007. The bed load sensors

were not calibrated for low sediment yield events [*Rickenmann and McArdell*, 2007], and all events with less than 3 m^3 of transported sediment were excluded from our analysis (~37% of the events). In addition, events containing discharges larger than 9 m^3/s (the two extreme events) were also omitted for two reasons: (i) there are likely large uncertainties in extrapolating our WSE to those high discharges, and (ii) the WSE is likely outside our numerical domain boundaries (overbank flow). Measured transported volumes were corrected for porosity (assumed 40%) (details on measured transport in *Rickenmann and McArdell* [2007]; *Rickenmann et al.* [2012]; *Yager et al.* [2012b]). Although our simulations do not cover all possible individual discharges throughout each hydrograph (see section 2.3.4), they bracket the measured values. To obtain $q_{i\,j}$ and A_j for any specific discharge within the measured hydrograph we used spline cubic interpolations between known values. We did not analyze if modifications to sediment transport equations other than the *Parker* [1990] equation would further improve predictions (but see *Schneider et al.* [2015] for accuracy of other equations).

2.4 Results

2.4.1 Hydrodynamic model simulations and results

Water surface elevation RMSE (root mean squared error) for our simulated discharges was 0.06 m (standard deviation (std) 0.06 m; 10% of mean flow depth) and 0.04 m (std 0.04 m; 7% of mean flow depth) for the 2010 data 2011 data, respectively. The RMSE of the reach-averaged velocity from the hydrodynamic model versus the *Yager et al.* [2012b] method, for both data sets was 0.014 m/s. The equation of *Ferguson* [2007] that uses the coefficient from *Rickenmann and Recking* [2011], gave similar velocities, although slightly larger, to those predicted by the hydrodynamic model (differences of 5-9% and 2-8% for the 2010 and 2011 data sets). This similitude between velocities confirms the successful calibration of our hydrodynamic model (Figure 2.4). The equations of *Whittaker* [1986], *Egashira and Ashida* [1991] and *Pagliara and Chiavaccini* [2006] gave larger velocities than *Rickenmann and Recking* [2011], *Yager et al.* [2012b], and the hydrodynamic model.

The RMSE between the model's cross-sectionally averaged velocity (hereinafter $U_{xs\ model}$) and U_{xs} for the 2010 and 2011 data sets were 0.081 and 0.076 m/s, respectively. The

major differences between $U_{xs\,model}$ and U_{xs} were observed at high discharges (approximately over 1.5 m/s) and could be partly arise from uncertainties of (i) the stage-discharge and $h-Q$ relations, where fewer calibration measurements for higher discharges exist, (ii) the hydrodynamic model's simplifications of governing equations, (iii) assuming a constant C_d, and (iv) the use of constant cross section geometries for U_{xs} that may not have been perpendicular to the local flow at all discharges.

2.4.2 Patch and reach averaged shear stress

To study the correlation between (τ_{bn}, grid scale) and local grain size we conducted an analysis similar to that of *Lisle et al.* [2000]. We did not have a detailed map of the local median grain size (i.e. at a sub-patch scale) and used the patch class median grain size (D_{50j}) instead. We obtained a very low coefficient of determination between τ_{bn} and D_{50j} (R^2=0.23, $\alpha =$ 0.05, Figure 2.5 a), which confirms the results of *Lisle et al.* [2000] and *Nelson et al.* [2010]. However, the patch class averaged shear stress ($\bar{\tau}_j$) varied directly with D_{50j} for a given discharge (Figure 2.5 b).

Although we use the patch-scale shear stress, the reach averaged dimensionless shear stress ($\bar{\tau}^*$) is typically used for bed load transport calculations. We tested how $\bar{\tau}^*$ varied using two different calculation methods (Figure 2.6 a, b): (i) First, the mean dimensionless shear stress for each patch class ($\bar{\tau}_j^*$) was a function of the mean shear stress of each patch class ($\bar{\tau}_j$) normalized by the median grain size (D_{50j}) of that patch class and then $\bar{\tau}^*$ was the patch class area (only wetted portion) weighted average of all $\bar{\tau}_j^*$ and is hereinafter called $\bar{\tau}^*_{var\,D_{50}}$. (ii) Second, $\bar{\tau}^*$ was calculated in almost the same way but is instead normalized using the reach-averaged surface median grain size (D_{50}), which is normally done in the literature. The entire area of each patch class was used instead of just the wetted area and this method is called $\bar{\tau}^*_{cst\,D_{50}}$. For any given discharge and for both data sets, $\bar{\tau}^*_{cst\,D_{50}}$ was lower than $\bar{\tau}^*_{var\,D_{50}}$ (Figure 2.6 a) because of the use of a single D_{50} and patch area in $\bar{\tau}^*_{cst\,D_{50}}$. Although $\bar{\tau}^*_{cst\,D_{50}}$ was not used in our

bed load transport calculations, it shows that the patch class-scale $D_{50\,j}$ can significantly impact the reach-averaged shear stress.

We also calculated the shear stress acting on the potentially mobile sediment ($\overline{\tau}_m^*$), using the shear stress partitioning method of *Yager et al.* [2012b, 2012c], to compare to $\overline{\tau}_{var\ D_{50}}^*$. This method accounts for immobile grain drag to indirectly reduce the shear stress on mobile patches whereas our hydrodynamic model includes the flow divergence caused by boulders to directly affect the shear stress on mobile patches. For most discharges and both data sets, $\overline{\tau}_{var\ D_{50}}^*$ was lower than $\overline{\tau}_m^*$, with percent differences as high as 50% for large discharges (Figure 2.6 b). However, within the discharge range where most sediment transport occurs (based on a magnitude frequency analysis, light gray area in Figure 2.6 a, see *Nitsche et al.* [2011]), both methods predict similar dimensionless shear stresses for a given discharge, indicating that $\overline{\tau}_m^*$ can roughly capture the effects of boulders on shear stress. Our results are slightly different from *Segura and Pitlick* [2015] who demonstrated that the differences between mean shear stress from a 2D flow model and the total shear stress (slope-depth product) decreased with increasing flow.

Our model captured significant spatial variability in shear stress that was not represented by the approach of *Yager et al.* [2012b] (Figure 2.6 c). The coefficient of variation in $\overline{\tau}_{var\ D_{50}}^*$ (CV), defined as the ratio of the standard deviation to the mean value, was fairly constant for both data sets.

2.4.3 Predictions of sediment flux

We used three different approaches (see section 2.3.4) to calculate bed load transport: (i) Patch mean; (ii) Variable distribution; and (iii) *Yager et al.* [2012c], which does not include the effect of patches (Figure 2.7, method Shear stress – grain size relation within this figure is explained later in section 2.4.4). Predictions of sediment transport for each of the 43 tested events (36 and 7 for 2010 and 2011, respectively) used the bed topography (and associated shear stresses) for that time period. If an event occurred before or after the extreme event of August 2010, we used the 2010 or 2011data sets, respectively. Bedload volumes calculated using the “Patch mean” approach were always within one order magnitude of the measured

values, had the lowest RMSE (m^3), and did not systematically over or under predict the measured volumes (Figure 2.7). 53% of all events for the "Patch mean" approach had a ratio of the predicted to the measured transported volumes between 0.5 and 2 (factor of 2). The "Variable distribution" approach produced similar results for the bulk of the measured events, but the volume of one event was overpredicted by over an order magnitude (Figure 2.7). We chose the *Yager et al.* [2012c] method to compare to the performance of the "Patch mean" and "Variable distribution" approaches because: (a) it was already tested in exactly the same reach, and (b) it has relatively accurate predictions to compare against those of our equation.

The *Yager et al.* [2012b] approach had about double the RMSE (99 m^3) than the "Patch mean" (40 m^3) and "Variable distribution" (51 m^3) approaches. For all three approaches most sediment transport events were overpredicted ("Patch mean" 58%; "Variable distribution": 65%; *Yager et al.* [2012b]: 63%) than underpredicted them (Table 2.2).

2.4.4 Grain size and shear stress relation

Although bed load transport predictions using the "Patch mean" method are more accurate than those using *Yager et al.* [2012c], they rely on very detailed topographic information not commonly available for most rivers. A more broadly applicable equation that empirically includes the effects of patch classes is therefore desired. Given that patch class mean shear stress on the j^{th} patch class ($\overline{\tau}_j$) increases with patch median grain size (D_{50j}) (Figure 2.5 b), we analyzed if this relationship could be used in our sediment transport equation. Since the reach-averaged shear stress ($\overline{\tau}$) in steep rough channels can be easily estimated using flow resistance partitioning techniques (e.g. *Comiti et al.* [2007]; *Yager et al.* [2007, 2012b]; *Nitsche et al.* [2011]; *Rickenmann and Recking*, [2011]), we developed a function that relates $\overline{\tau}_j$ to D_{50j} and $\overline{\tau}$. Two different approaches were used to define $\overline{\tau}$ for all discharges: (i) $\overline{\tau}_{var\ D50}$ as discussed in section 2.4.2 and (ii) total shear stress ($\overline{\tau}_T$) defined $\rho g h S$ (where S is the average bed slope) which is the most accessible flow parameter used in sediment transport predictions.

We used a power law to relate $\overline{\tau}_j$ to $\overline{\tau}$,

$$\overline{\tau}_j = c_p \overline{\tau}^{e_p} \tag{2.17}$$

where the R^2 was 0.75 for both $\overline{\tau}_{var\ D_{50}}$ and $\overline{\tau}_T$. The coefficient (c_p) and exponent (e_p) of equation (2.17) varied with the dimensionless median grain size D_{50j} / D_{50} (Figure 2.8 a and b). When using $\overline{\tau}_{var\ D50}$ a power law and a logarithmic relation with respect to D_{50j} / D_{50} 83% and 75% of the variability in c_p and e_p were explained, respectively (Figure 2.8 a and b),

$$c_p = 5.31\left(\frac{D_{50j}}{D_{50}}\right)^{2.52} \quad , \overline{\tau} = \overline{\tau}_{var\ D_{50}} \tag{2.18a}$$

$$c_p = 6.52\left(\frac{D_{50j}}{D_{50}}\right)^{2.46} \quad , \overline{\tau} = \overline{\tau}_T \tag{2.18b}$$

$$e_p = -0.37\ln\left(\frac{D_{50j}}{D_{50}}\right) + 0.70 \quad , \overline{\tau} = \overline{\tau}_{var\ D_{50}} \tag{2.19a}$$

$$e_p = -0.33\ln\left(\frac{D_{50j}}{D_{50}}\right) + 0.61 \quad , \overline{\tau} = \overline{\tau}_T \tag{2.19b}$$

We analyzed the performance of equations (2.17) - (2.19) (hereinafter called $\overline{\tau}_j - \overline{\tau} - D_{50j}$) by comparing their predicted $\overline{\tau}_j / \overline{\tau}$ to the actual hydrodynamic model results (Figure 2.8 c). The average R^2 between the predicted and measured $\overline{\tau}_j / \overline{\tau}$ was 0.92 and 0.90 ($\alpha =$ 0.05) for $\overline{\tau}_{var\ D_{50}}$ and $\overline{\tau}_T$, respectively. Therefore the $\overline{\tau}_j - \overline{\tau} - D_{50j}$ relations can be used to quantify shear stress variability between patch classes (Figure 2.8 c). At low $\overline{\tau}$ (100 Pa) fine patches have applied shear stresses that are significantly lower than the reach averaged value. As $\overline{\tau}$ increases, $\overline{\tau}_j / \overline{\tau}$ approaches unity for most patch classes (500 Pa occurs at discharges of about 3.0 m^3/s in the Erlenbach), shear stress variability y becomes relatively unimportant, and reach averaged shear stress may be adequate for sediment transport calculations.

We tested the $\overline{\tau}_j - \overline{\tau} - D_{50j}$ (using the $\overline{\tau}_{var\ D_{50}}$ version) relations in sediment transport calculations using the same measured sediment transport events from section 2.4.3. All the predicted volumes were of comparable magnitude with those calculated using the "Patch mean" method (Figure 2.7). The RMSE was 47 m^3, which is slightly higher than that from the "Patch mean" approach (40 m^3,Table 2.2) and less than half of that from *Yager et al.* [2012c] (99 m^3). 53% of the predictions were within a factor of two. The results obtained using the $\overline{\tau}_j - \overline{\tau} - D_{50j}$ relations suggests that they are well suited for bed load predictions.

2.5 Discussion

2.5.1 Predictions of boundary shear stress and sediment transport equations

We demonstrated that bed load transport estimations can be improved, compared to those that use reach averaged properties, when local characteristics of the flow and the spatial distribution of grain sizes are considered. We presented three different approaches for spatially distributed shear stresses: i) "Patch mean"; ii) "Variable distribution"; and iii) $\overline{\tau}_j - \overline{\tau} - D_{50j}$ relations. For the "Variable distribution" approach we found that no single probability distribution was able to represent the observed spatially distributed shear stresses in each patch and simulated discharge with statistical confidence (see Appendix D). This approach predicted the most sediment transport events outside a factor of 2 of the measured volumes because it uses the full range of shear stresses applied on each patch class and all locally high and low values are included (Figure 2.7). Locally high shear stresses normally are accompanied by scour and filling, which are not included in our calculations. It is not the objective of this study to test the accuracy of each probability distribution used in the "Variable distribution" approach.

The "Patch mean" approach was more accurate than the original method of *Yager et al.* [2012c] in terms of sediment volume RMSE (m^3) and reducing systematic over-prediction but generally had a similar percentage of events within a factor of two of the measured values. The "Patch mean" and "Variable distribution" did not dramatically improve bedload estimates over the method of *Yager et al.* [2012c]. It is important, therefore, to consider that the accuracy achieved with these new methods must be contrasted with the field measurements and the numerical modelling efforts, which can be an obstacle for some practical applications. The *Yager et al.* [2012c] equation likely worked well because it predicts the mean shear stress fairly

accurately for most of the sediment transporting flows (Figure 2.6 a). This mean shear stress could have worked well because the shear stresses on each patch class approach the reach-averaged stress with increasing discharge (Figure 2.8 c3). However, if we had tested the *Yager et al.* [2012c] equation for a wider range of discharges, it is likely that its performance compared to our equation would decline because it systematically over-predicts $\overline{\tau}_m^*$ at higher discharges. A variable drag coefficient of the mobile sediment (C_m), instead of constant as assumed by *Yager et al.* [2012b], could result in a lower $\overline{\tau}_m^*$ at high discharge. The $\overline{\tau}_j - \overline{\tau} - D_{50j}$ relations are easier and more broadly applicable than the "Patch mean" and "Variable distribution" methods and can be used where data collection and/or numerical modelling are difficult to perform. The advantage of these equations is that they preserve the simplicity of reach-averaged relations while maintaining the accuracy of the spatially variable method (Figure 2.7). Only areas relevant for sediment transport, defined as $\tau_j^* \geq \tau_c^*$, were considered in our $\overline{\tau}_j - \overline{\tau} - D_{50j}$ relations, similar relations and bedload prediction accuracies were obtained when the whole wetted area was considered (see Appendix G for further details).

2.5.2 Shear stress variations with median grain size

Local shear stress has previosly been poorly correlated with local median grain size [*Lisle et al.*, 2000; *Nelson et al.*, 2010] and in our case it was also poorly correlated with patch class median grain size (section 2.4.2 ,Figure 2.5 a). However, the mean patch class shear stress varied directly with patch class median grain size and scaled fairly well with the reach-averaged shear stress (Figure 2.5 b, Figure 2.8 a and b). This implies that sediment patches may not only be a response to shear stress divergences [*Nelson et al.*, 2010] but also to local stress magnitudes. Such a result is important for predicting the location and stability of sediment patches. In particular, the ideal location for placement of gravel sizes used for spawning salmon could potentially be estimated from a shear stress map.

2.5.3 Relative importance of spatial distribution of shear stresses and grain size

It is challenging to establish whether grain size or shear stress variations are more important in bedload predictions because of the non-linear processes that govern sediment transport [*Recking*, 2013]. Flume experiments have shown that variations in local shear stress

are relatively more important than those in grain size for bar formation [*Nelson et al.*, 2010]. In steep streams, field observations suggest that local flow, and not spatial grain size variations, is the primary driver of local bed load transport variability [*Yager et al.*, 2012a]. However, local grain-induced roughness may influence the initiation of sediment motion and therefore grain size variations could be important [*Scheingross et al.*, 2013].

To analyze whether a spatial distribution of shear stresses or grain sizes is more important we considered three cases: 1) for case $GSD_{cst}\ \overline{\tau}_{var\,T}$, we used each patch class averaged shear stress ("Patch mean" method of section 2.3.4) and assumed that the GSD for all patches was the reach-averaged value. Note that although all patches classes had the same GSD they had different shear stresses applied over different bed areas. 2) Case $GSD_{cst}\ \overline{\tau}_{var\,m}$ is the same except the mobile bed GSD was used (i.e. immobile grains were excluded), which may be more appropriate for bed load transport calculations. 3) In case $GSD_{var}\ \overline{\tau}_{cst}$, the shear stress acting on each patch class was the same for a given discharge and equal to that of the reach-averaged shear stress. The GSD was spatially variable and each patch class used its original measured grain sizes.

Sediment transport volumes in all three cases were less accurate than our "Patch mean" method (Figure 2.9) but were more accurate for the $GSD_{cst}\ \overline{\tau}_{var}$ cases than the $GSD_{var}\ \overline{\tau}_{cst}$ scenario. This suggests that the spatial variability of shear stress is relatively more important for sediment flux predictions than the spatial distribution of grain sizes, which has been also confirmed by the field study of *Segura and Pitlick* [2015]. The results of this experiment would need to be confirmed with sediment fluxes data from other streams but could help to decide how to allocate efforts to maximize sediment transport prediction accuracy with time or economic constrains.

2.5.4 Individual contributions of patch classes to sediment fluxes

While some studies have found that, during low to moderate flow events, relatively fine patches are the only sources of bed sediment [*Garcia et al.*, 1999; *Vericat et al.*, 2008], others have observed motion on all patches [*Dietrich et al.*, 2005; *Yuill et al.*, 2010; *Yager et al.*, 2012a]. In our study, for a given discharge, the individual contributions of each patch class to

the total transported volume depended on the patch's GSD, area (Figure 2.10) and applied stress. In general, patches with $D_{50j} < D_{50}$ contributed at least 80% of the total transported sediment volume. B, gbC and cgB patches in the 2010 data set and B and bgC patches in the 2011 data set had the lowest contribution (Figure 2.10 a, b). Even during low to moderate flow events coarse patches ($D_{50j} > D_{50}$), whose contribution to the total transported volume was very small (Figure 2.10 a ,b), were still active and had some grain sizes in motion (Figure 2.10 c , d).

In both data sets there were no patch classes that consistently contributed the largest fraction of the total transported volume. The contribution of each patch class to the total transported volume class was controlled by local topography, patch area and GSD. The topography determines flow routing throughout the channel, which directly affected the active area and applied shear stresses on each patch class. Patch class GSD influenced the relative mobility of different grain sizes and relative patch class area partly determines the proportional contribution of a patch class to the total sediment flux. Therefore, coarser patches that composed a larger proportion of the streambed could, at some discharges, contribute more sediment than finer patches. The variability of different patch class contributions suggests that all patch classes must be considered in sediment flux predictions.

2.5.5 Transferability of the grain size and shear stress relation

To study the potential transferability of the $\overline{\tau}_j - \overline{\tau} - D_{50j}$ relation we used the published data of *Yager et al.* [2012a, 2012b] during 2004, which includes areas, GSD for each patch class, and channel characteristics used to calculate reach average shear stresses. The data were assumed to be valid during 2002-2006 when a total of 15 sediment transport events occurred. The extreme event of 2007 completely reorganized boulder steps [*Molnar et al.*, 2010] and all of the mobile patches, and therefore, we treat these data as if they were coming from a different stream to test the broader applicability of our equations. We used five different approaches using the 2004 data to estimate reach-averaged shear stress ($\overline{\tau}$) for use in our relation. Three approaches use the total shear stress ($\overline{\tau}_T$), which is easy to calculate in rivers where no detailed information is available. (1) For a given discharge we assumed that the reach-averaged shear stress was the same as what we calculated using the 2010 data and was equal to $\overline{\tau}^*_{var\ D_{50}}$ (see

section 2.4.2). (2) We do the same thing as in (1) but with the 2011 data. Then, for the other three approaches we used the total shear stress calculated using the equations of (3) *Egashira and Ashida* [1991], (4) *Rickenmann and Recking* [2011], and (5) *Yager et al.* [2012b]. Approaches (1) and (2) use equations (2.18a) and (2.19a) (Figure 2.8 a and b), while approaches (3) to (5) use equations (2.18b) and (2.19b) to estimate the patch average shear stress. Note that we are not directly using the total shear stress for bed load transport predictions, we only use it to determine the shear stress on each patch class. Values used for sediment transport predictions in approaches (3) to (5) are summarized in Appendix I and Table I.1. Details of the equations of *Egashira and Ashida* [1991] and *Rickenmann and Recking* [2011] can be found in the original publications and also in *Nitsche et al.* [2011]. For comparison purposes we include the original sediment volumes predicted by *Yager et al.* [2012c] for this time period.

The predicted sediment volumes from all approaches had similar RMSE, ranging from 33 to 52 m^3 (Figure 2.11) and differences were largely caused by how the reach-averaged shear stress was specified. Predictions using the total shear stress (approaches 3-5), were roughly as accurate as those using the reach-averaged stress from the hydrodynamic model (approaches 1-2). Although the total shear stress does not include the effects of large roughness elements our relations for individual patch classes do.

The 2010, 2011 and *Egashira and Ashida* [1991] methods predicted sediment volumes that were within one order magnitude of the measured values. Most approaches using our sediment transport equation had a lower RMSE and more events predicted within a factor of two than those predicted by *Yager et al.* [2012c], which does not include the effects of patches. This improvement suggest that our method could be capable of predicting fluxes of better accuracy than other methods available but we would recommend using this method with caution until it has been further tested.

2.6 Conclusions

Including the spatial variability of flow and GSD in sediment transport calculations improved predictions compared to equations that only used reach-averaged properties. Nonetheless, achieving this increase in accuracy requires intense numerical modelling and detailed field measurements that can limit its applicability in practical cases. However,

predictions were improved mainly because patch class shear stress directly correlated with patch class median grain size, which allowed for a better representation of local sediment mobility and hiding effects. Simple empirical relations of reach and patch class averaged shear stress with median grain size were developed and tested with our sediment transport equation. When using these relations the simplicity of reach averaged equations is preserved while the accuracy of including spatial variability is achieved. The relation between shear stress and surface median grain size is also a first step towards a theory to explain and predict the formation and location of sediment patches. It indicates that, at patch scale, surface grain size and shear stress are coupled and the patch characteristics may not just be controlled by the divergence of shear stress. For accurate sediment transport predictions all patch classes must be considered; no particular patch class was consistently the greatest contributor to the total transported sediment volume. Individual contributions of each patch class depended on both GSD and area occupied. Finally, the spatial variability in the flow was relatively more important for accurate sediment fluxes than the spatial variability of the GSD.

2.7 Acknowledgements

Funding for this research was provided by an NSF Career award to E.M. Yager (0847799), the Chilean Government - CONICYT “Becas de Doctorado en el Extranjero – Becas Chile” , and the Swiss Federal Research Institute WSL. Invaluable field assistance was provided by Heidi Smith, Alex Beer, and Manuel Nitsche. We thank Thomas Lisle and two anonymous reviewers for their constructive comments that helped to improve an earlier version of this manuscript. Please contact the corresponding author (mons0853@vandals.uidaho.edu) if you are interested in the topographic, sediment grain size distributions or hydraulic data. If you are interested in the Swiss bed load data please contact Dieter Rickenmann (dieter.rickenmann@wsl.ch).

2.8 References

Aziz, N. M., and D. E. Scott (1989), Experiments on sediment transport in shallow flows in high gradient channels, *Hydrol. Sci. J.*, *34*(4), 465–478, doi:10.1080/02626668909491352.

Barton, G. J., R. R. McDonald, J. M. Nelson, and R. R. Dinehart (2005), *Simulation of flow and sediment mobility using a multidimensional flow model for the white sturgeon critical-habitat reach, Kootenai River near Bonners Ferry, Idaho. Scientific Investigations Report*.

Bathurst, J. C., W. H. Graf, and H. H. Cao (1987), Bed load discharge equations for steep mountain rivers, in *Sediment Transport in Gravel Bed Rivers*, edited by C. R. Thorne, J. C. Bathurst, and R. D. Hey, pp. 453–477, John Wiley, Chichester, UK.

Beer, A. R., J. M. Turowski, B. Fritschi, and D. H. Rieke-Zapp (2015), Field instrumentation for high-resolution parallel monitoring of bedrock erosion and bedload transport, *Earth Surf. Process. Landforms*, *40*(4), 530–541, doi:10.1002/esp.3652.

Bertoldi, W., P. Ashmore, and M. Tubino (2009), A method for estimating the mean bed load flux in braided rivers, *Geomorphology*, *103*, 330–340, doi:10.1016/j.geomorph.2008.06.014.

Bridge, J. S., and S. J. Bennett (1992), A model for entrainment and Transport of sediment grain of mixed sizes, shapes, and densities, *Water Resour. Res.*, *28*(2), 337–363.

Buffington, J. M., and D. R. Montgomery (1997), A systematic analysis of eight decades of incipient motion studies, with special reference to gravel-bedded rivers, *Water Resour. Res.*, *33*(8), 1993–2029, doi:10.1029/97WR03138.

Buffington, J. M., and D. R. Montgomery (1999a), A procedure for classifying textural facies in gravel-bed rivers, *Water Resour. Res.*, *35*(6), 1903–1914, doi:10.1029/1999WR900041.

Buffington, J. M., and D. R. Montgomery (1999b), Effects of hydraulic roughness on surface textures of gravel-bedded rivers, *Water Resour. Res.*, *35*(11), 3507–3521.

Buxton, T. H., J. M. Buffington, D. Tonina, A. K. Fremier, and E. M. Yager (2015a), Modeling the Influence of Salmon Spawning on Hyporheic Exchange of Marine-Derived Nutrients in Gravel Stream beds, *Can. J. Fish. Aquat. Sci.*, *72*, 1146–1158, doi:10.1139/cjfas-2014-0413.

Buxton, T. H., J. M. Buffington, E. M. Yager, M. A. Hassan, and A. K. Fremier (2015b), The relative stability of salmon redds and unspawned streambeds, *Water Resour. Res.*, *51*, 6074–6092, doi:10.1002/ 2015WR016908.

Chen, L., and M. C. Stone (2008), Influence of bed material size heterogeneity on bedload transport uncertainty, *Water Resour. Res.*, *44*(1), 1–11, doi:10.1029/2006WR005483.

Clayton, J. A., and J. Pitlick (2007), Spatial and temporal variations in bed load transport intensity in a gravel bed river bend, *Water Resour. Res.*, *43*, W02426, doi:10.1029/2006WR005253.

Comiti, F., and L. Mao (2012), Recent Advances in the Dynamics of Steep Channels, in *Gravel-Bed Rivers: Processes, Tools, Environments*, edited by M. Church, P. M. Biron, and A. G. Roy, pp. 351–377, John Wiley & Sons, Ltd, Chichester, UK.

Comiti, F., L. Mao, A. Wilcox, E. E. Wohl, and M. A. Lenzi (2007), Field-derived relationships for flow velocity and resistance in high-gradient streams, *J. Hydrol.*, *340*(1-2), 48–62, doi:10.1016/j.jhydrol.2007.03.021.

Conner, J. T., and D. Tonina (2014), Effect of cross-section interpolated bathymetry on 2D hydrodynamic model results in a large river, *Earth Surf. Process. Landforms*, *39*, 463–475, doi:10.1002/esp.3458.

Dietrich, W. E., and P. Whiting (1989), Boundary Shear Stress and Sediment Transport In River Meanders of Sand and Gravel, in *River Meandering*, *American Geophysical Union - Water Resources. Monographs*, vol. 12, edited by S. Ikeda and G. Parker, pp. 1–50, American Geophysical Union, Washington, D.C., USA.

Dietrich, W. E., J. W. Kirchner, H. Ikeda, and F. Iseya (1989), Sediment supply and the development of the coarse surface layer in gravel-bedded rivers, *Nature*, *340*, 215–217, doi:10.1038/340215a0.

Dietrich, W. E., P. a. Nelson, E. Yager, J. G. Venditti, M. P. Lamb, and L. Collins (2005), Sediment patches, sediment supply, and channel morphology, in *4th IAHR Symposium on River*,

Coastal and Estuarine., edited by G. Parker and M. H. Garcia, pp. 79–90, Taylor & Francis Group, Urbana, Illinois, USA.

Egashira, S., and K. Ashida (1991), Flow resistance and sediment transportation in streams with step-pool bed morphology, in *Fluvial Hydraulics of Mountain Regions*, edited by A. Armanini and G. Di Silvio, pp. 45–58, Springer-Verlag.

Einstein, H. A. (1950), The Bed-Load Function for Sediment Transportation in Open Channel Flows, *Soil Conserv. Serv.*, (1026), 1–31.

Ferguson, R. (2007), Flow resistance equations for gravel- and boulder-bed streams, *Water Resour. Res.*, *43*(5), 1–12, doi:10.1029/2006WR005422.

Ferguson, R. I. (2003), The missing dimension: Effects of lateral variation on 1-D calculations of fluvial bedload transport, *Geomorphology*, *56*, 1–14, doi:10.1016/S0169-555X(03)00042-4.

Garcia, C., J. B. Laronne, and M. Sala (1999), Variable source areas of bedload in a gravel-bed stream, *J. Sediment. Res.*, *69*(1), 27–31, doi:10.2110/jsr.69.27.

Ghilardi, T., M. J. Franca, and a J. Schleiss (2014), Bulk velocity measurements by video analysis of dye tracer in a macro-rough channel, *Meas. Sci. Technol.*, *25*(3), 035003, doi:10.1088/0957-0233/25/3/035003.

Graf, W. H., and L. Suszka (1987), Sediment transport in steep channels, *J. Hydrosci. Hydraul. Eng.*, *5*, 11–26.

Hajimirzaie, S. M., A. G. Tsakiris, J. H. J. Buchholz, and A. N. Papanicolaou (2014), Flow characteristics around a wall-mounted spherical obstacle in a thin boundary layer, *Exp. Fluids*, *55*(6), 1–14, doi:10.1007/s00348-014-1762-0.

Hassan, M. A., D. Tonina, and T. H. Buxton (2015), Does small-bodied salmon spawning activity enhance streambed mobility?, *Water Resour. Res.*, *51*, 1–18, doi:10.1002/2015WR017079.

Jarrett, R. D. (1984), Hydraulics of high-gradient streams, *Jounral Hydraul. Eng.*, *110*(11), 1519–1539.

Kinzel, P. J., J. M. Nelson, and A. K. Heckman (2009), Response of sandhill crane (Grus canadensis) riverine roosting habitat to changes in stage and sandbar morphology, *River Res. Appl.*, *25*(2), 135–152, doi:10.1002/rra.1103.

Kleinhans, M. G., and L. C. van Rijn (2002), Stochastic Prediction of Sediment Transport in Sand-Gravel Bed Rivers, *J. Hydraul. Eng.*, *128*(4), 412–425, doi:10.1061/?ASCE?0733-9429?2002?128:4?412? CE.

Kondolf, G. M., and M. G. Wolman (1993), The sizes of salmonid spawning gravels, *Water Resour. Res.*, *29*(7), 2275–2285, doi:10.1029/93WR00402.

Lacey, R. W. J. W. J., and A. G. Roy (2008), The spatial characterization of turbulence around large roughness elements in a gravel-bed river, *Geomorphology*, *102*(3-4), 542–553, doi:10.1016/j.geomorph.2008.05.045.

Laronne, J. B., C. García, and I. Reid (2000), Mobility of patch sediment in gravel bed streams: patch character and its implications for bedload, in *Gravel-Bed Rivers V*, edited by M. P. Mosley, pp. 249–289, New Zealand Hydrological Society Inc., Wellington, New Zealand.

Lenzi, M. A., V. D'Agostino, and P. Billi (1999), Bedload transport in the instrumented catchment of the Rio Cordon PArt I: Analysis of bedload records, conditions and threshold of bedload entrainment, *Catena*, *36*, 171–190, doi:10.1016/S0341-8162(99)00017-X.

Lenzi M.A., and D'agostino V. (1999), Bedload transport in the instrumented catchment of the Rio Cordon Part II: Analysis of the bedload rate, *Catena*, *36*, 191–204.

Lisle, I. G., C. W. Rose, W. L. Hogarth, P. B. Hairsine, G. C. Sander, and J.-Y. Parlange (1998), Stochastic sediment transport in soil erosion, *J. Hydrol.*, *204*, 217–230, doi:10.1016/S0022-1694(97)00123-6.

Lisle, T. E., H. Ikeda, and F. Iseya (1991), Formation of stationary alternate bars in a steep channel with mixed-size sediment: A flume experiment, *Earth Surf. Process. Landforms*, *16*(5), 463–469, doi:10.1002/esp.3290160507.

Lisle, T. E., F. Iseya, and H. Ikeda (1993), Response of a channel with alternate bars to a decrease in supply of mixed-size bed load: A flume experiment, *Water Resour. Res.*, *29*(11), 3623–3629, doi:10.1029/93WR01673.

Lisle, T. E., J. M. Nelson, J. Pitlick, M. A. Madej, and B. L. Barkett (2000), Variability of bed mobility in natural, gravel-bed channels and adjustments to sediment load at local and reach scales, *Water Resour. Res.*, *36*(12), 3743–3755, doi:10.1029/2000WR900238.

Maturana, O., D. Tonina, J. A. McKean, J. M. Buffington, C. H. Luce, and D. Caamaño (2014), Modeling the effects of pulsed versus chronic sand inputs on salmonid spawning habitat in a low-gradient gravel-bed river, *Earth Surf. Process. Landforms*, *39*, 877–889, doi:10.1002/esp.3491.

Mcdonald, R. R., J. M. Nelson, and J. P. Bennett (2005), Multi-dimensional surface water modeling system user's guide. US Geological Survey online documentation. http://www.brr.cr.usgs.gov/projects/GEOMORPH_Lab/WebHelp_Pro/MD_SWMS.htm.,

Miller, A. J., and B. L. Cluer (1998), Modeling Considerations for Simulation of Flow in Bedrock Channels, in *Bedrock Channels, in Rivers Over Rock: Fluvial Processes in Bedrock Channels*, edited by K. J. Tinkler and E. E. Wohl, American Geophysical Union, Washington, D.C., USA.

Molnar, P., A. L. Densmore, B. W. McArdell, J. M. Turowski, and P. Burlando (2010), Analysis of changes in the step-pool morphology and channel profile of a steep mountain stream following a large flood, *Geomorphology*, *124*(1-2), 85–94, doi:10.1016/j.geomorph.2010.08.014.

Mueller, E., R. Batalla, C. Garcia, and A. Bronstert (2008), Modeling Bed-Load Rates from Fine Grain-Size Patches during Small Floods in a Gravel-Bed River, *J. Hydraul. Eng.*, *134*(10), 1430–1439, doi:10.1061/(ASCE)0733-9429(2008)134:10(1430).

Mueller, E. R., and J. Pitlick (2014), Sediment supply and channel morphology in mountain river systems: 2. Single thread to braided transitions, *J. Geophys. Res. Earth Surf.*, *119*, 1516–1541, doi:10.1002/2013JF002843.Sediment.

Nelson, J. M., and R. R. McDonald (1995), *Mechanics and modeling of flow and bed evolution in lateral separation eddies*, Flagstaff, Arizona.

Nelson, J. M., and J. D. Smith (1989), Evolution and stability of erodible channel beds, *River Meand. Am. Geophys. Union - Water Resour. Monogr.*

Nelson, J. M., J. P. Bennett, and S. M. Wiele (2003), Flow and Sediment-Transport Modeling, in *Tools in Fluvial Geomorphology*, pp. 539–576.

Nelson, P. A., J. G. Venditti, W. E. Dietrich, J. W. Kirchner, H. Ikeda, F. Iseya, and L. S. Sklar (2009), Response of bed surface patchiness to reductions in sediment supply, *J. Geophys. Res. Earth Surf.*, *114*(2), 1–18, doi:10.1029/2008JF001144.

Nelson, P. A., W. E. Dietrich, and J. G. Venditti (2010), Bed topography and the development of forced bed surface patches, *J. Geophys. Res. Earth Surf.*, *115*, F04024, doi:10.1029/2010JF001747.

Nelson, P. a., D. Bellugi, and W. E. Dietrich (2014), Delineation of river bed-surface patches by clustering high-resolution spatial grain size data, *Geomorphology*, *205*, 102–119, doi:10.1016/j.geomorph.2012.06.008.

Nicholas, A. P. (2000), Modelling bedload yield braided gravel bed rivers, *Geomorphology*, *36*, 89–106, doi:10.1016/S0169-555X(00)00050-7.

Nitsche, M., D. Rickenmann, J. M. Turowski, A. Badoux, and J. W. Kirchner (2011), Evaluation of bedload transport predictions using flow resistance equations to account for macro-roughness in steep mountain streams, *Water Resour. Res.*, *47*, W08513, doi:10.1029/2011WR010645.

Pagliara, S., and P. Chiavaccini (2006), Flow Resistance of Rock Chutes with Protruding Boulders, *J. Hydraul. Eng.*, *132*(6), 545–552, doi:10.1061/(ASCE)0733-9429(2006)132:6(545).

Paintal, a. S. (1971), A Stochastic Model Of Bed Load Transport, *J. Hydraul. Res.*, *9*(4), 527–554, doi:10.1080/00221687109500371.

Paola, C. (1996), Incoherent structure: Turbulence as a metaphor for stream braiding, in *Coherent Flow Structures in Open Channels*, edited by P. Ashworth, S. J. Bennett, J. L. Best, and S. McLelland, pp. 706–723, John Wiley, Chichester, UK.

Paola, C., and R. Seal (1995), Grain size patchiness as a cause of selective deposition and downstream fining, *Water Resour. Res.*, *31*(5), 1395–1407.

Papanicolaou, A. N., and C. Kramer (2005), The role of relative submergence on cluster microtopography and bedload predictions in mountain streams, in *River, Coastal and Estuarine Morphodynamics. Proceeding of the 4th IAHR conference*, edited by G. Parker and M. H. Garcia, pp. 1083–1086, Urbana, Illinois, USA.

Parker, G. (1990), Surface-based bedload transport relation for gravel rivers, *J. Hydraul. Res.*, *28*(4), 417–436, doi:10.1080/00221689009499058.

Parker, G., C. Paola, and S. Leclair (2000), Probabilistic Exner Sediment Continuity Equation for Mixtures with No Active Layer, *J. Hydraul. Eng.*, *126*(11), 818–826, doi:10.1061/(ASCE)0733-9429(2000)126:11(818).

Pasternack, G. B., A. T. Gilbert, J. M. Wheaton, and E. M. Buckland (2006), Error propagation for velocity and shear stress prediction using 2D models for environmental management, *J. Hydrol.*, *328*(1-2), 227–241, doi:10.1016/j.jhydrol.2005.12.003.

Rattray, M. J., and E. Mitsuda (1974), Theoretical analysis of conditions in a salt wedge, *Estuar. Coast. Mar. Sci., 2*, 375–394.

Recking, A. (2013), An analysis of nonlinearity effects on bed load transport prediction, *J. Geophys. Res. Earth Surf., 118*(3), 1264–1281, doi:10.1002/jgrf.20090.

Rickenmann, D. (1997), Sediment transport in Swiss torrents, *Earth Surf. Process. Landforms*, *22*(10), 937–951, doi:10.1002/(SICI)1096-9837(199710)22:10<937::AID-ESP786>3.0.CO;2-R.

Rickenmann, D. (2001), Comparison of bed load transport in torrents and gravel bed streams, *Water Resour. Res., 37*(12), 3295–3305, doi:10.1029/2001WR000319.

Rickenmann, D. (2005), Geschiebetransport bei steilen Gefällen, in *Festkolloquium, edited, Versuchsanstalt für Wasserbau, Hydrologie und Glaziologie.*

Rickenmann, D., and B. W. McArdell (2007), Continuous measurement of sediment transport in the Erlenbach stream using piezoelectric bedload impact sensors, *Earth Surf. Process. Landforms*, *32*(9), 1362–1378, doi:10.1002/esp.1478.

Rickenmann, D., and A. Recking (2011), Evaluation of flow resistance in gravel-bed rivers through a large field data set, *Water Resour. Res.*, *47*(7), doi:10.1029/2010WR009793.

Rickenmann, D., J. M. Turowski, B. Fritschi, A. Klaiber, and A. Ludwig (2012), Bedload transport measurements at the Erlenbach stream with geophones and automated basket samplers, *Earth Surf. Process. Landforms*, *37*(9), 1000–1011, doi:10.1002/esp.3225.

Scheingross, J. S., E. W. Winchell, M. P. Lamb, and W. E. Dietrich (2013), Influence of bed patchiness, slope, grain hiding, and form drag on gravel mobilization in very steep streams, *J. Geophys. Res. Earth Surf.*, *118*(2), 982–1001, doi:10.1002/jgrf.20067.

Schneider, J. M., D. Rickenmann, J. M. Turowski, K. Bunte, and J. W. Kirchner (2015), Applicability of bed load transport models for mixed-size sediments in steep streams considering macro-roughness, *Water Resour. Res.*, *51*, 5260–5283, doi:10.1002/2014WR016417.Received.

Segura, C., and J. Pitlick (2015), Coupling fluvial-hydraulic models to predict gravel transport in spatially variable flows, *J. Geophys. Res. Earth Surf.*, *120*, 834–855, doi:10.1002/2014JF003302.

Shamloo, H., N. Rajaratnam, and C. Katopodis (2001), Hydraulics of simple habitat structures, *J. Hydraul. Res.*, *39*(4), 351–366.

Shvidchenko, A. B., and G. Pender (2000), Flume study of the effect of relative depth on the incipient motion of coarse uniform sediments, *Water Resour. Res.*, *36*(2), 619–628.

Smart, G. (1984), Sediment Transport Formula for Steep Channels, *J. Hydraul. Eng.*, *110*(3), 267–276, doi:10.1061/(ASCE)0733-9429(1984)110:3(267).

Strom, K. B., and A. N. Papanicolaou (2007), ADV Measurements around a Cluster Microform in a Shallow Mountain Stream, *J. Hydraul. Eng.*, *133*(12), 1379–1389, doi:10.1061/(ASCE)0733-9429(2007)133:12(1379).

Sun, Z., and J. Donahue (2000), Statistically Derived Bedload Formula for Any Fraction of Nonuniform Sediment, *J. Hydraul. Eng.*, *126*(2), 105–111, doi:10.1061/(ASCE)0733-9429(2000)126:2(105).

Tritico, H. M., and R. H. Hotchkiss (2005), Unobstructed and Obstructed Turbulent Flow in Gravel Bed Rivers, *J. Hydraul. Eng.*, *131*(8), 635–645, doi:10.1061/(ASCE)0733-9429(2005)131:8(635).

Tsakiris, A. G., a. N. T. Papanicolaou, S. M. Hajimirzaie, and J. H. J. Buchholz (2014), Influence of collective boulder array on the surrounding time-averaged and turbulent flow fields, *J. Mt. Sci.*, *11*(6), 1420–1428, doi:10.1007/s11629-014-3055-8.

Turowski, J., and D. Rickenmann (2010), Measuring the Statistics of Bed-Load Transport Using Indirect Sensors, *J. Hydraul. Eng.*, *137*(1), 116–121, doi:10.1061/(ASCE)HY.1943-7900.0000277.

Turowski, J. M., E. M. Yager, A. Badoux, D. Rickenmann, and P. Molnar (2009), The impact of exceptional events on erosion, bedload transport and channel stability in a step-pool channel, *Earth Surf. Process. Landforms*, *34*(12), 1661–1673, doi:10.1002/esp.1855.

Turowski, J. M., A. Badoux, J. Leuzinger, and R. Hegglin (2013), Large floods, alluvial overprint, and bedrock erosion, *Earth Surf. Process. Landforms*, *38*(9), 947–958, doi:10.1002/esp.3341.

Vericat, D., R. J. Batalla, and C. N. Gibbins (2008), Sediment entrainment and depletion from patches of fine material in a gravel-bed river, *Water Resour. Res.*, *44*(11), W11415, doi:10.1029/2008WR007028.

Whittaker, J. G. (1986), An Equation for Predicting bedload transport in steep mountain Step-Pool Stream, in *9th Australasian Fluid Mechanics Conference*, pp. 358–361, Auckland.

Wu, F.-C., and K.-H. Yang (2004), A stochastic partial transport model for mixed-size sediment: Application to assessment of fractional mobility, *Water Resour. Res.*, *40*(4), 1–18, doi:10.1029/2003WR002256.

Yager, E. M., J. W. Kirchner, and W. E. Dietrich (2007), Calculating bed load transport in steep boulder bed channels, *Water Resour. Res.*, *43*(7), 1–24, doi:10.1029/2006WR005432.

Yager, E. M., W. E. Dietrich, J. W. Kirchner, and B. W. McArdell (2012a), Patch dynamics and stability in steep, rough streams, *J. Geophys. Res. Earth Surf.*, *117*(2), 1–16, doi:10.1029/2011JF002253.

Yager, E. M., W. E. Dietrich, J. W. Kirchner, and B. W. McArdell (2012b), Prediction of sediment transport in step-pool channels, *Water Resour. Res.*, *48*(1), 1–20, doi:10.1029/2011WR010829.

Yager, E. M., J. M. Turowski, D. Rickenman, and B. W. McArdell (2012c), Sediment supply, grain protrusion, and bedload transport in mountain streams, *Geophys. Res. Lett.*, *39*, L10402, doi:10.1029/2012GL051654.

Yuill, B., M. Nichols, and E. Yager (2010), Coarse bed material patch evolution in low-order, ephemeral channels, *Catena*, *81*(2), 126–136, doi:10.1016/j.catena.2010.02.002.

Table 2.1: Characteristics of patch classes for the 2010 and 2011 data sets

	2010			2011		
Class	D_{50} (mm)	D_{84} (mm)	A_F	D_{50} (mm)	D_{84} (mm)	A_F
B	522	813	0.25	449	717	0.27
cgB	225	499	0.02	n/p	n/p	n/p
gbC	183	474	0.01	n/p	n/p	n/p
bgC	137	278	0.19	159	291	0.1
C	133	198	0.08	96	142	0.06
bcG	71	268	0.05	n/a	n/a	n/a
gC	64	123	0.21	57	108	0.29
cG	52	103	0.14	50	112	0.18
G	16	29	0.06	20	41	0.10
< 2 mm	n/a	n/a	0.01	n/p	n/p	n/p
Mobile	74	181	0.70	58	141	0.74
Total	117	472	1.00	84	396	1.00

D_{50} and D_{84} are the median and 84th percentile grain size for each patch class. A_F is the ratio of the area of each patch class to the entire bed area. “Mobile” represents the bed excluding the immobile steps, “Total” is the entire bed. “n/a” denotes not available and “n/p” is not present. See Figure 2.2 for patch class definitions and complete GSD.

Table 2.2: Prediction errors in sediment flux calculations

	Patch Mean	Variable distribution	Shear stress Grain size relation	Yager et al. [2012c]
RMSE (m^3)	40	51	47	99
Within a factor of 2 (%)	53	51	53	51
Greater than 2 (%)	35	40	28	47
Less than 0.5 (%)	12	9	19	2
Overpredicted (%)	58	65	47	63
Underpredicted (%)	19	19	37	9

"Within a factor of 2" denotes the percent of predicted sediment volumes that were within the range 0.5-2 of the measured values. "Greater than 2" and "Less than 0.5" denote the percent of predictions that were greater or less than a factor of 2, respectively. "Overpredicted" and "Underpredicted" denote predictions that were greater than 1.25 or lower than 0.75 times the measured transported volumes. We considered predictions within a ratio of 1 ± 0.25 as "successfully predicted". Shear stress – Grain size relation uses the $\overline{\tau}_j - \overline{\tau} - D_{50j}$ relations.

Table 2.3: Prediction errors for sediment flux calculations using the shear-stress grain size relation and 2004 sediment transport data

	2010	2011	Egashira and Ashida [1991]	Rickenmann and Recking [2011]	Yager et al. [2012b] Total	Yager et al. [2012c]
RMSE (m^3)	33	40	36	40	52	42
Within a factor of 2 (%)	27	53	20	53	60	27
Greater than 2 (%)	33	40	20	40	40	47
Less than 0.5 (%)	40	7	60	7	0	27
Overpredicted (%)	33	40	33	40	53	47
Underpredicted (%)	40	27	60	27	7	27

See Table 2.2 for definitions. Each method is defined in the text. Yager et al. [2012c] uses their full equations whereas all other methods are just different ways to calculate the reach-averaged shear stress for use in our $\overline{\tau}_j - \overline{\tau} - D_{50j}$ relations and sediment transport equations.

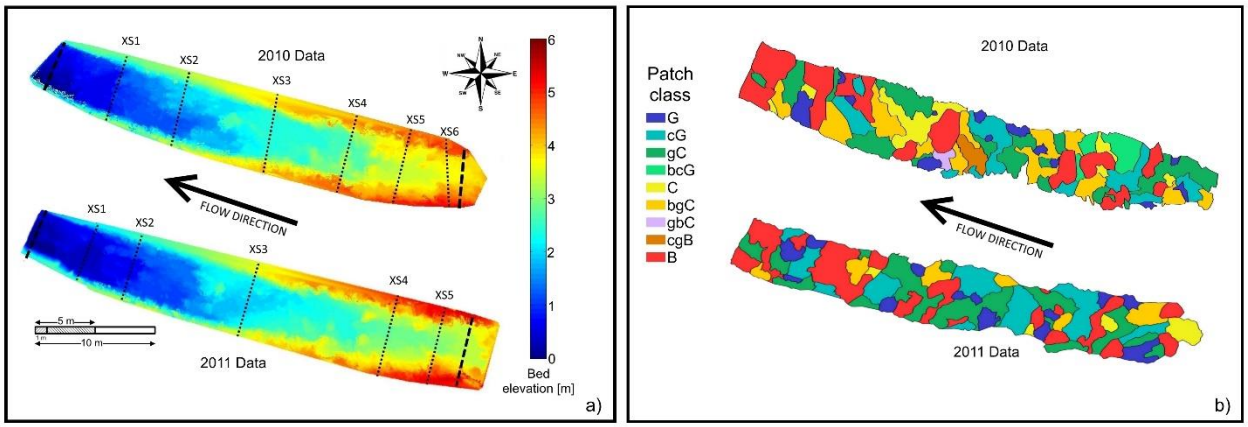

Figure 2.1: a) Bed elevation measured before (2010 data) and after (2011 data) the extreme event of August 1, 2010. Bed elevation values were normalized to the lowest elevation at the end of our study reach. The symbol “XS” indicates the locations of the cross sections where WSE were measured. Thick segmented lines indicate the upstream and downstream boundaries of the numerical model. An approach channel (straight trapezoidal channel with a constant streamwise slope) at the upstream boundary was included in the numerical simulations to account for transverse velocity distributions at most-upstream patches. b) Map of patches within the Erlenbach for the 2010 and 2011 data sets

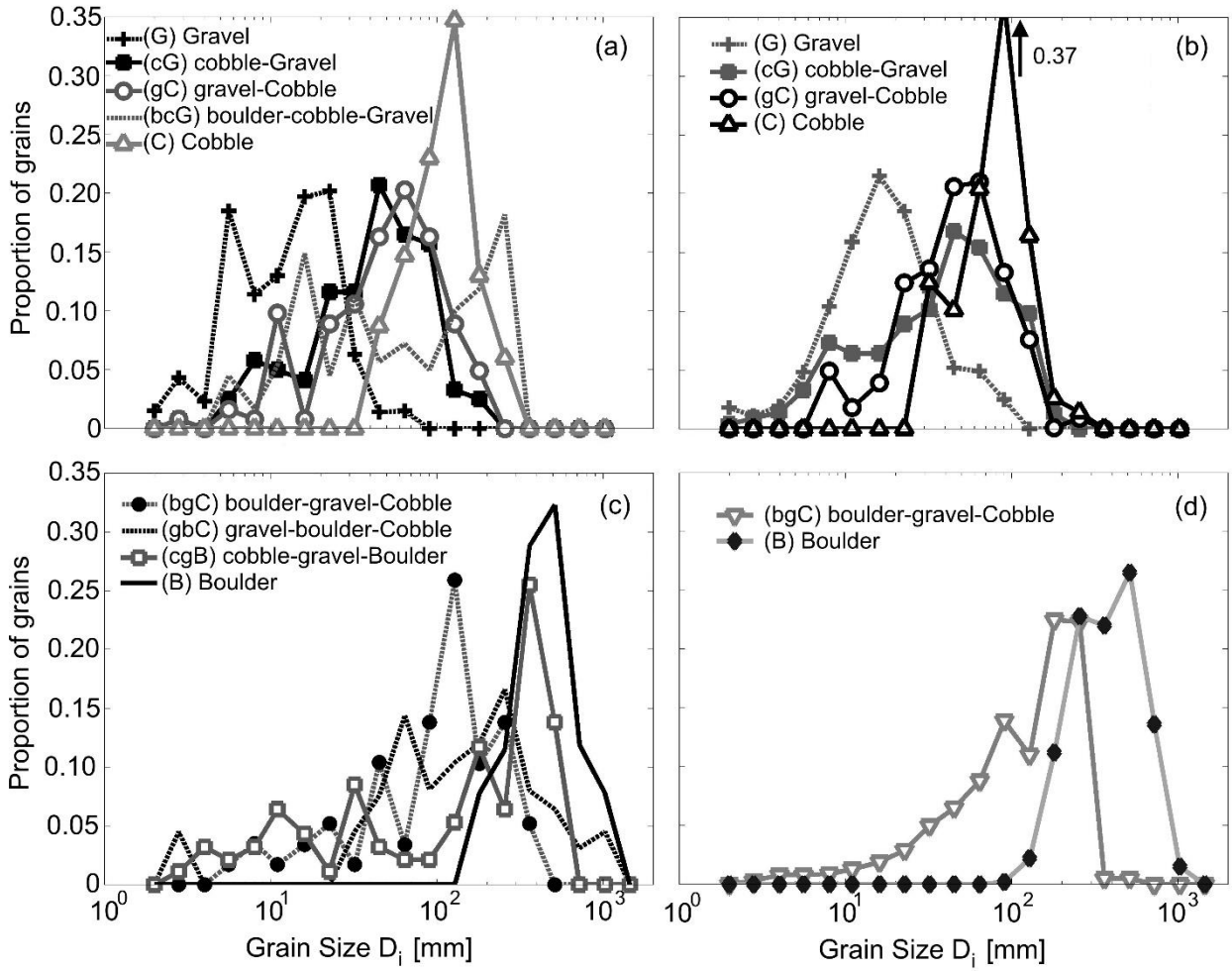

Figure 2.2: Grain size distributions for each patch class for the two data sets. (a), (c) 2010 data and (b), (d) 2011 data.

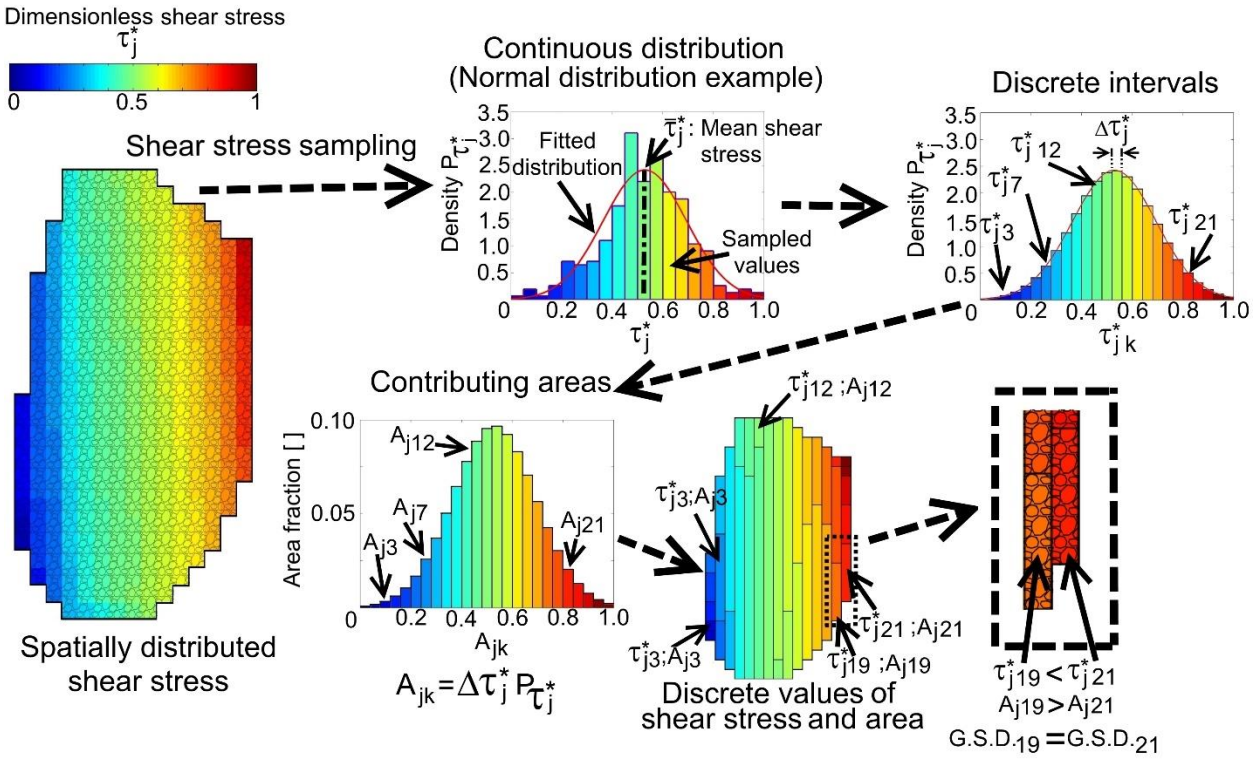

Figure 2.3: Diagram of the process to calculate discrete shear stresses from spatially distributed values. The process starts with sampling the spatial variations of shear stresses over a patch class (first figure at left) and then the observed shear stress distribution is simplified assuming that it comes from a probability distribution. For simplicity a single patch is shown in the figure although in our analysis we used patch classes. The process is repeated for each patch class and every given discharge. Definitions used in equations (2.5) and (2.6) are graphically represented.

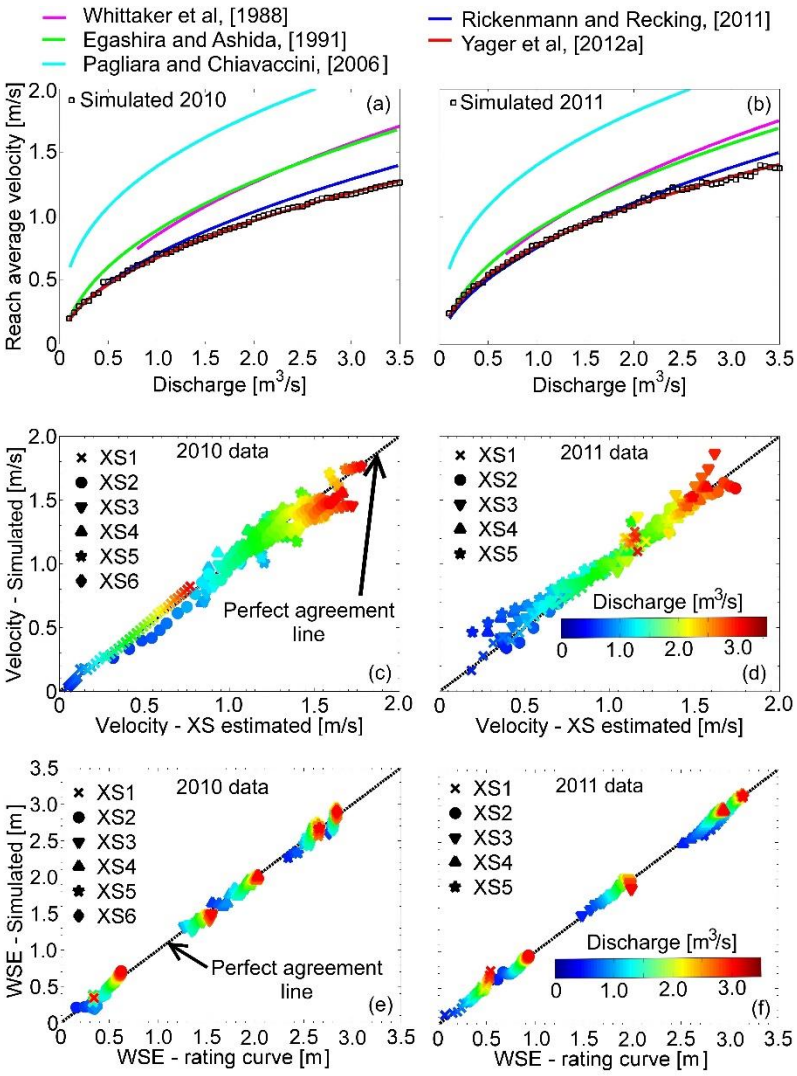

Figure 2.4: Reach averaged velocities for the (a) 2010 and (b) 2011 data sets predicted by the hydrodynamic model compared to those predicted by *Yager et al.* [2012b] as functions of discharge. Predictions from the resistance equations of *Whittaker* [1986], *Egashira and Ashida* [1991], *Pagliara and Chiavaccini* [2006], and *Rickenmann and Recking* [2011] (see text for details and description) are shown for comparison. Cross sectional averaged velocities for the (c) 2010 and (d) 2011 data sets predicted by the hydrodynamic model compared to those from our field measurements, where XS means cross section. Each velocity point is colored by its corresponding discharge.

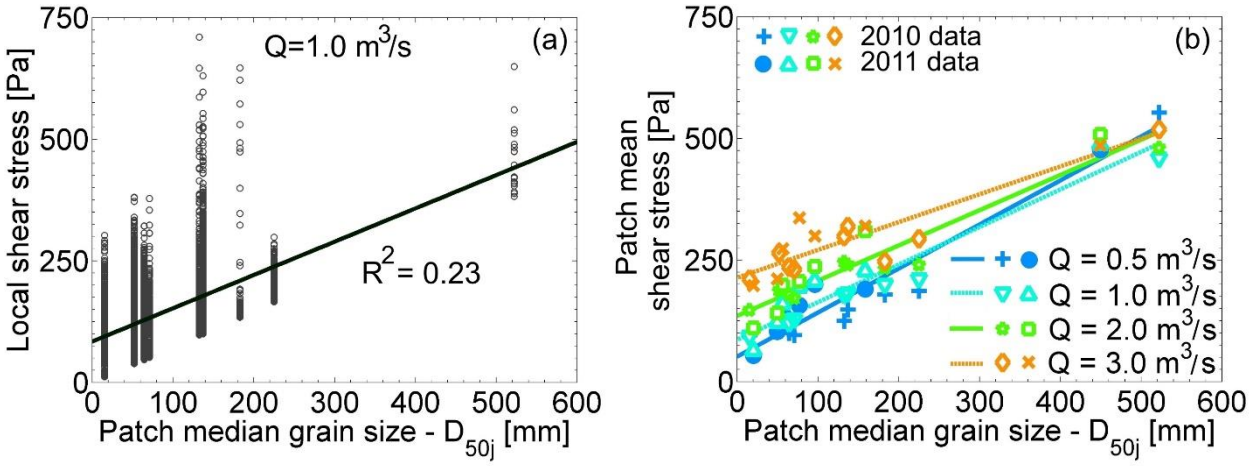

Figure 2.5: (a) Local boundary shear stress versus patch median grain size for a discharge of 1 m^3/s for the 2010 data set. The same results were found for discharges of 0.5, 2.0 and 3.0 m^3/s, which cover most of our studied discharge range. Each circle represents a wetted node in the numerical model. (b) Patch class averaged shear stress as a function of the patch class median grain size for different discharges. Linear fits are included to help visualize the trend, but they do not necessarily represent the best possible fit.

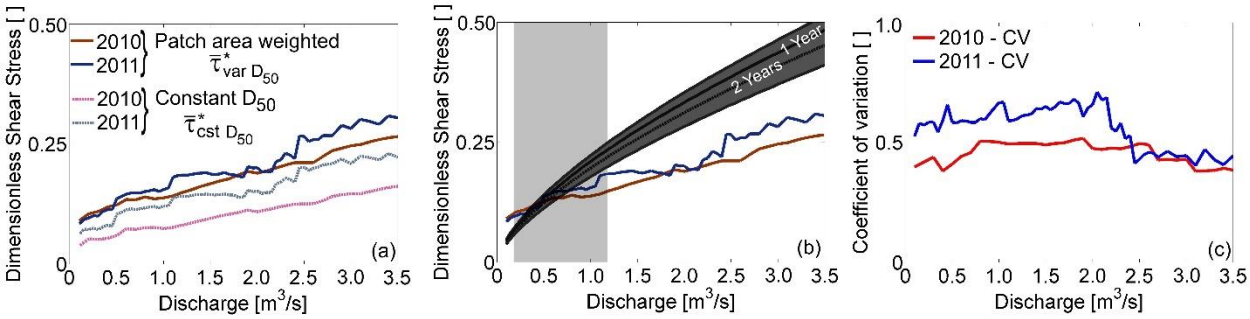

Figure 2.6: (a) Dimensionless reach averaged shear stresses dependence on what median grain size was used for normalization ($\overline{\tau}^*_{var\ D_{50}}$ and $\overline{\tau}^*_{cst\ D_{50}}$ methods). (b) Reach averaged dimensionless shear stresses predicted by the hydrodynamic model ($\overline{\tau}^*_{var\ D_{50}}$) for both data sets as functions of discharge compared to those predicted by the shear stress partitioning method of *Yager et al.* [2012b]. The dark grey area represents four different step protrusions calculated at 0.5, 1, 2, and 5 years since an extreme event. Upper and lower limits correspond to 0.5 and 5 years respectively, whereas 1 and 2 years are labeled directly. The light grey area shows the discharges where 90% of the sediment transport occurred for our events, calculated using a magnitude frequency analysis based on the sediment transport events from June 2007 until September 2010 using a total of 4494 individual discharges. (c) The coefficient of variation of the dimensionless reach averaged shear stress ($\overline{\tau}^*_{var\ D_{50}}$) as a function of discharge.

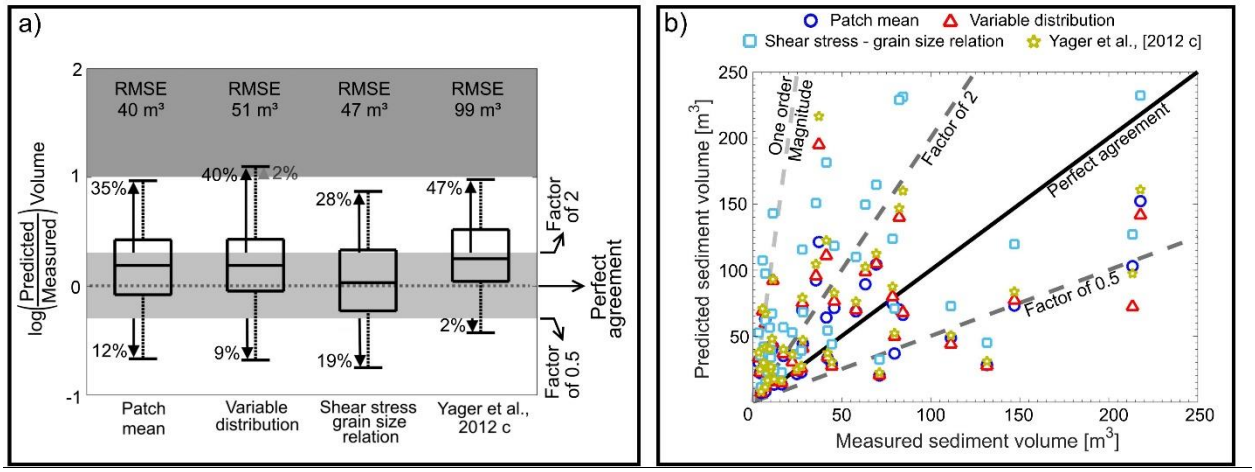

Figure 2.7: a) The log of the ratio of the predicted to measured sediment volumes. Predicted bed load volumes by the Patch mean, Variable distribution and shear stress - grain size relation are compared to those of *Yager et al.* [2012c]. In the Figure Shear stress - grain size relation is our $\overline{\tau}_j - \overline{\tau} - D_{50\,j}$ relation, see text for other definitions. The line of perfect agreement denotes the measured volume was predicted exactly. The top and bottom of each box are the 25th and 75th percentiles and the middle line inside the box is the median value. Lines extending out of the box correspond to the maximum and minimum predicted volume ratios. Arrows and corresponding text denote the percent of the sediment volume predictions that are greater or less than a factor of 2 (black) and greater than a factor of 10 (grey). The light gray shaded area represents predictions within a factor of 2 of the measured values. The dark grey shaded area represent over predictions by more than an order magnitude. The volume at the top of each box corresponds to the RMSE of the predicted bed load volume. b) Comparison of the measured and predicted sediment transport volumes for the same equations. Some predicted sediment volumes by *Yager et al.* [2012c] fall outside the box (6 sediment transport events, higher than 250 m^3).

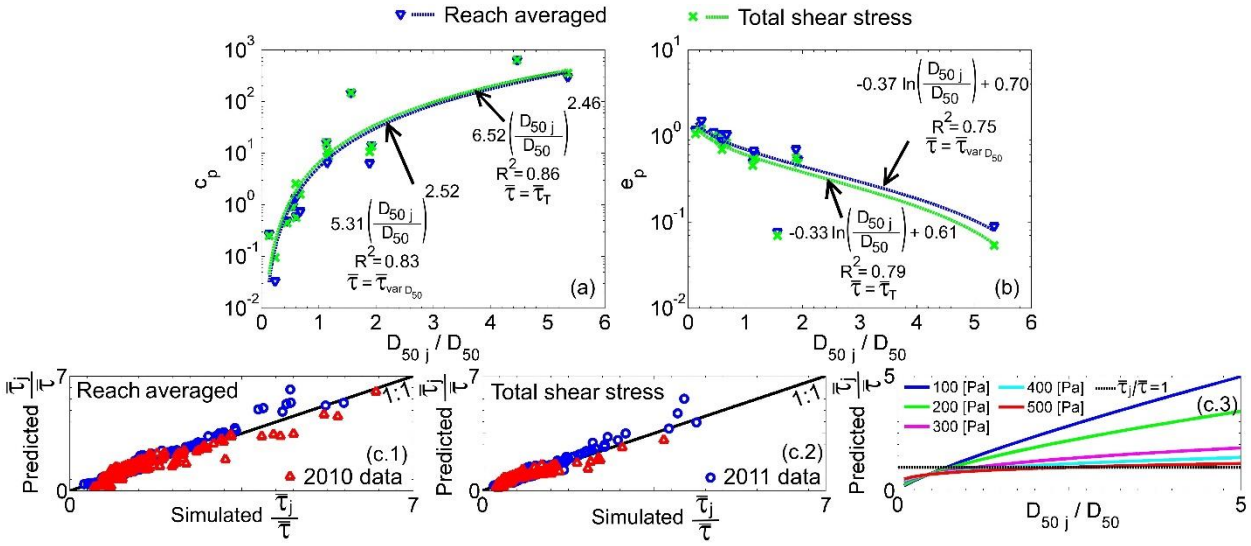

Figure 2.8: (a) Relations for the coefficient and (b) exponent of equation (2.17) as functions of the normalized patch class median grain size. (c.1) and (c.2) A comparison of the hydrodynamic model's prediction the for patch class shear stress ratio ($\bar{\tau}_j / \bar{\tau}$) and those predicted by equations (18) and (19). (c.3) The predicted $\bar{\tau}_j / \bar{\tau}$ ratio as a function of the relative patch class grain size for a range of shear stresses. Continuous black lines in Figures (c.1) and (c.2) represents a 1:1 relation.

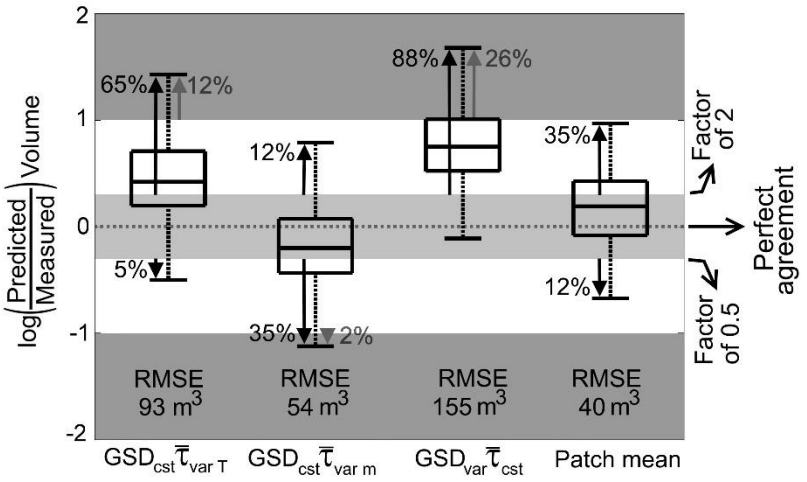

Figure 2.9: The log of the ratio of the predicted to measured sediment volumes when either the GSD or the distribution of shear stress was held constant (see text for definitions). The patch mean approach (see section 2.4.3) is included for comparison. See Figure 2.7 for an explanation of other figure properties.

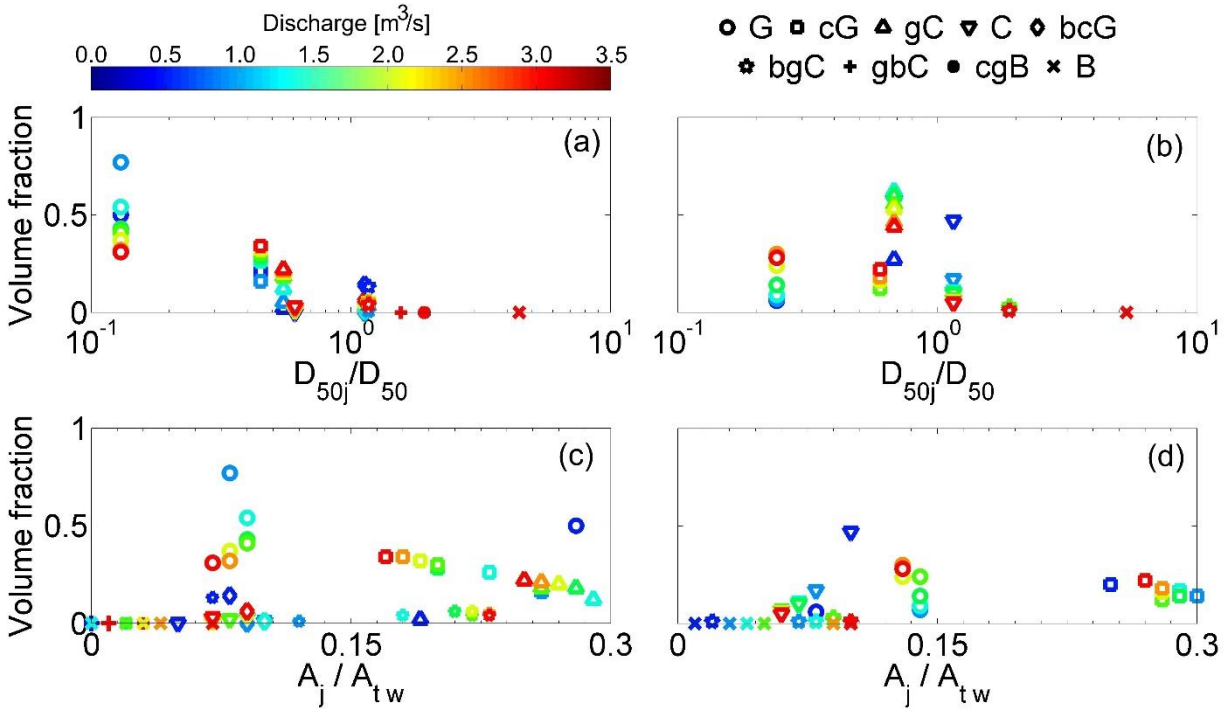

Figure 2.10: The volume fraction that each patch class contributes to the total transported volume as functions of (a and b) the normalized patch median grain size and (c and d) the relative area that each patch class occupied at each discharge. 2010 data are shown in (a) and (c), and 2011 are shown in (b) and (d).

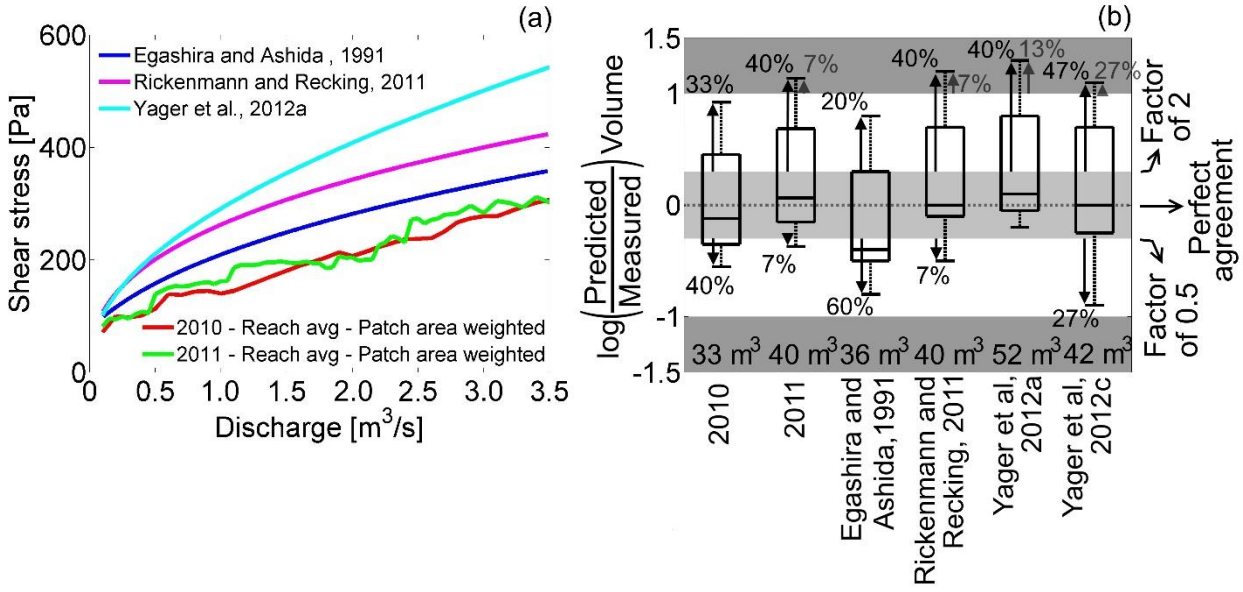

Figure 2.11: (a) Reach-averaged shear stress as a function of discharge. The shear stress for 2010 and 2011 used the $\tau_{var\ D_{50}}$ method, the total shear stress was calculated using resistance equations of *Egashira and Ashida* [1991], *Rickenmann and Recking* [2011], and *Yager et al.* [2012b]. (b) The log of the ratio of the predicted to measured sediment volume for sediment transport events during 2002-2006 at the Erlenbach. The results of *Yager et al.* [2012c] were included only as a reference and the volumes predicted in the original study are shown here. All other predictions used our $\tau_j - \tau - D_{50j}$ relations and sediment transport equation. See Figure 2.7 for an explanation of other figure properties.

Chapter 3: Effects of bedforms and large protruding grains on near-bed flow hydraulics in low relative submergence conditions

3.1 Abstract

In mountain rivers, bedforms, large relatively immobile grains, and bed texture and topographic variability can significantly alter local and reach-averaged flow characteristics. Low relative submergence regimes caused by large immobile grains can have highly three dimensional flow fields plunging flow. To explore the influence of large protruding grains and bedforms on flow properties, we conducted a set of experiments in which we varied the relative submergence while holding the average sediment transport capacity and upstream sediment supply constant. Flow and bed measurements were conducted at the beginning and end of each experiment to account for the absence or presence of bedforms, respectively. Detailed information on the flow was obtained by combining our measurements with a 3D numerical model. Commonly used theoretical velocity profiles only performed correctly at the reach scale when shallow flow effects and the roughness length of the relatively mobile sediment were considered. However, at the local scale large deviations from these profiles were observed and simple methods to estimate the near-bed shear stress may not perform well at this scale. Large roughness elements altered the spatial distribution of boundary shear stresses and caused significant deviations from hydrostatic pressure. Zones of high turbulent kinetic energy occurred near the water surface and were largely controlled by the immobile grains and plunging flow. For accurate flow predictions the effect of bedforms and large boulders must be explicitly considered in mountain rivers. The reach-averaged shear stress was not controlled by depth or slope, as commonly assumed, but by the relative boulder submergence and degree of plunging flow.

3.1.1 Key points

Velocity profile equations perform well at reach scale only if the roughness length uses mobile grains

Spatial distribution of shear stress is controlled by presence of bedforms and their shape

Zones of high turbulent kinetic energy are near the water surface when plunging flow occurs

3.2 Introduction

In mountainous rivers bedforms, large relatively immobile (during most floods) boulders, and bed texture and topographic variability affect turbulence intensities and induce flow unsteadiness and spatial gradients of flow velocity. For instance, local changes in the cross sectional area caused by obstructions, abrupt changes in bed elevation or channel expansions/contractions result in convective accelerations and modifications of velocity profiles [*Jarrett*, 1985, 1990; *Mclean and Smith*, 1986; *Ye and Mccorquodale*, 1998; *Olsen*, 2003; *Sukhodolov et al.*, 2006; *Blanckaert*, 2010; *Constantinescu et al.*, 2011; *Hajimirzaie et al.*, 2014] and magnitudes [*Bathurst*, 1985, 2002; *Marcus et al.*, 1992; *Katul*, 2002; *Wilcox et al.*, 2006]. Changes in turbulence intensities [*Bathurst*, 1978; *Nelson et al.*, 1993; *Papanicolaou et al.*, 2001, 2004; *Canovaro et al.*, 2007; *Thompson*, 2007; *Yager and Schmeeckle*, 2013], local pressure distributions [*Zeng et al.*, 2005, 2008; *Pournazeri et al.*, 2014] and water surface elevation [*Vallé and Pasternack*, 2006; *Yager et al.*, 2012] also can occur. Flow variability has important consequences for the spatial distribution of shear stresses [*Ferguson*, 2003; *Maddux et al.*, 2003a; *Clayton and Pitlick*, 2007; *Afzalimehr and Rennie*, 2009; *Papanicolaou et al.*, 2010; *Clayton*, 2012; *Cooper et al.*, 2013], water aeration [*Straub et al.*, 1954; *Straub and Lamb*, 1956; *Chanson*, 1997, 2004], mixing [*Chanson*, 1997; *Claxton et al.*, 2003; *Tonina and Buffington*, 2009], and transport of scalar properties such as water temperature and dissolved oxygen, all of which are key factors for aquatic habitat quality and riverine ecosystems [*Cienciala and Hassan*, 2013; *Ouellet et al.*, 2014].

A key control on the spatial variability in shear stress and therefore on sediment depositional patterns is the relative submergence, which is the ratio of the flow depth (h_a) to a characteristic grain size (D_I) [e.g. *Shamloo et al.*, 2001; *Papanicolaou et al.*, 2010; *Cooper et al.*, 2013]. At high relative submergences (HRS, where $h_a / D_I > 3.5$ *Papanicolaou and Kramer* [2005]) the bed shear stress depends on the Reynolds number and sediment accumulation tends to occur downstream of large roughness elements [*Papanicolaou and Kramer*, 2005], whereas in low relative submergence regimes (LRS) the bed shear stress may depend on the Froude

number and the sediment is typically deposited upstream of large immobile grains [*Papanicolaou et al.*, 2011]. However, little is known about the effects of LRS on erosion patterns and bedform formation because laboratory experiments in this flow regime have been conducted for non-erodible beds [*Papanicolaou and Kramer*, 2005; *Papanicolaou et al.*, 2010, 2011] without an upstream sediment supply [*Shamloo et al.*, 2001].

Another critical control on the spatial variability in shear stress is the presence of bedforms [*Einstein*, 1950; *Einstein and Barbarosa*, 1952; *Smith and McLean*, 1977; *Nelson et al.*, 1993; *Sukhodolov et al.*, 2006]. Studies on dunes (e.g. *Smith and McLean* [1977]; *Mclean and Smith* [1986]; *Nelson et al.* [1993]; *Bennett and Best* [1995]; *McLean et al.* [1999]; *Venditti and Bennett* [2000]; *Maddux et al.* [2003a, 2003b]; *McLean and Nikora* [2006]; *Sukhodolov et al.* [2006]; *Keylock et al.* [2014]) have shown that bedforms generate flow separation, near-bed accelerations at the downstream dune face, secondary currents, velocity intermittency [*Keylock et al.*, 2014] and control turbulence kinetic energy [*Sukhodolov et al.*, 2006] and intensity [*Bennett and Best*, 1995]. Other types of bedforms such as step-pool sequences [*Bathurst*, 1985; *Wohl and Thompson*, 2000; *Wilcox and Wohl*, 2007], grains clusters [*Buffin-Bélanger and Roy*, 1998; *Lawless and Robert*, 2001; *Tritico and Hotchkiss*, 2005; *Strom and Papanicolaou*, 2007; *Ozgoren et al.*, 2011] and pool-riffle sequences [*Clifford and French*, 1993] influence local velocity and turbulence characteristics, for instance turbulence kinetic energy (k). The maximum value of k is typically near the bed surface [*Nezu and Nakagawa*, 1993; *Nikora and Goring*, 2000], but models to predict k were derived for high relative submergence conditions and their accuracy in the presence of large protruding grains is not clear. Turbulence kinetic energy is important because it plays a key role in the transport of nutrients [*Webel and Schatzmann*, 1984], plant growth [*Sutcliffe*, 2014] and salmonid migration [*Tritico and Hotchkiss*, 2005].

Bedforms and large roughness elements also significantly affect the reach-averaged shear stress [*Sukhodolov et al.*, 2006] and cause local deviations from commonly assumed velocity profiles [*Lawless and Robert*, 2001; *Shamloo et al.*, 2001; *Strom and Papanicolaou*, 2007; *Afzalimehr and Rennie*, 2009; *Papanicolaou et al.*, 2012; *Hajimirzaie et al.*, 2014; *Tsakiris et al.*, 2014]. Such velocity profiles are often used to determine boundary shear stresses, which are subsequently used in sediment transport calculations. Velocity profiles within the

roughness layer have been assumed to be linear [*Nikora et al.*, 2001], nearly constant [*Recking*, 2009], or quadratic [*Wiberg and Smith*, 1991; *Lamb et al.*, 2008]. The testing of these velocity profile equations has been limited to relatively simple bed geometries that may not be representative of many mountain streams. An assessment is needed of the accuracy of these velocity models at local and reach scale for flows subject to bedforms and large immobile elements.

Few measurements of the temporal and spatial flow variability exist for beds with bedforms and large immobile grains, therefore three-dimensional (3D) flow models are a potential alternative to test common assumptions and equations for shear stresses and turbulent kinetic energy. Although the computational loads and input requirements are significantly larger than other models (e.g. resistance equations, see *Nitsche et al.* [2011] and references therein, FastMECH [*Nelson and McDonald*, 1995], or Nays2DH [*Nelson et al.*, 2015]), 3D models implicitly include non-hydrostatic effects [*Wu et al.*, 2000; *Zeng et al.*, 2005, 2008], secondary currents [*Pezzinga*, 1994; *Ye and Mccorquodale*, 1998; *Olsen*, 2003; *Wilson et al.*, 2003; *Khosronejad et al.*, 2007; *Constantinescu et al.*, 2011], and vertical accelerations induced by obstructions [*Liu and García*, 2008; *Esmaeili et al.*, 2009; *Aghaee and Hakimzadeh*, 2010; *Pournazeri et al.*, 2014]. This presents an important advantage over 2D models when flow variables (e.g. boundary shear stress) are required where the hydrostatic pressure assumption fails, for example in the wake of a step. It is not always clear if the hydrostatic pressure assumption approximates the vertical pressure distribution in highly irregular channels especially those with bedforms and roughness elements that disrupt the flow. If the hydrostatic pressure assumption is valid far from areas where vertical velocities and accelerations are considerable, 2D models may still be used to obtain spatially distributed flow variables such as shear stress.

In this study we analyze the spatial variability of the flow in a series of flume experiments that featured a staggered configuration of immobile hemispheres, which mimics some characteristics of steep mountain rivers. We combine our flume experiments with 3D Reynolds Averaged Navier-Stokes (RANS) – Volume of Fluid (VOF) simulations. The objectives of this study are to: (i) determine the changes in velocity profiles, bed shear stresses, turbulent kinetic energies and pressure distributions that are induced by bedform formation

around the hemispheres, (ii) test the performance of reach-averaged velocity and turbulent kinetic energy profiles equations in LRS conditions,(iii) analyze where the hydrostatic pressure distribution assumption is valid, and (iv) compare the flow properties described in (i) between different experiments that have the same sediment transport capacity but dissimilar relative submergences and bed surface bathymetries.

3.3 Methods

3.3.1 Experiment design

All experiments were conducted at the Mountain StreamLab at the University of Idaho [*Budwig and Goodwin*, 2012], which is a 0.76 m wide 20 m long (10 m long test section) channel (Figure 3.1 a). Simulated boulders (23 – 28 cm diameter) were randomly placed in the 3 m between the inlet flow straighteners and our test section ($X = 0$ m; X , Y , and Z are the streamwise, cross-stream and vertical directions, respectively) to ensure well-developed turbulent flow. An adjustable gate at the downstream end of the flume was used to control the water depth and make it on average parallel to the flume bottom.

The test-section contained staggered hemispheres to simulate large roughness elements, which consisted of 15.24 cm diameter concrete hemispheres mounted over 10 cm high foam cylinders that were glued to the flume's bottom (Figure 3.1 a, Table 3.1). We verified that a particle of this size would not be mobile under our flow conditions theoretically (*Lamb et al.* [2008]; *Parker* [1990] and *Yager et al.* [2007, 2012b] sediment transport equations) and empirically by placing loose hemispheres (without the foam base) on the bed. At the beginning of each experiment the intervening flume bed consisted of a 10 cm thick sediment layer whose grain size distribution (GSD) was downscaled by a factor of 4.3 from samples collected at Reynolds Creek (Figure 3.1b), a 3% slope river located in Idaho, USA. The scaling factor was chosen so the ratio D_I / D_{50m} were within the observed values by *Nitsche et al.* [2011] (ranged between 8.83 and 25, $D_I / D_{50m} = 15.2$ in our case), where D_I is the diameter of the immobile grains (hemispheres in our case) and D_{50m} the median grain size of the bed sediment (subscript m indicates that only the potentially mobile bed sediment [*Yager et al.*, 2007] is being considered). The lower portion of the GSD was truncated at 2 mm to avoid the use of sand or finer particles.

The Reynolds number (Re) and particle Reynolds number for all of our experiments were within the typical range of steep mountain rivers [*Buffington and Montgomery*, 1997; *Lenzi et al.*, 2006; *Yager et al.*, 2007] and ensured fully developed turbulent and hydraulically rough flow (Table 3.1). The Froude numbers were sub-critical ($Fr < 1$) [*Lepp et al.*, 1993; *Adenlof and Wohl*, 1994; *Lenzi*, 2001; *Yager et al.*, 2007] although locally, and especially around the immobile hemispheres, zones with $Fr \geq 1$ were present.

We varied the relative submergence between experiments to generate different shear stress divergences fields around the immobile hemispheres. Since the flow responds in diverse ways to changes in h_a / D_I [*Lacey and Roy*, 2008; *Lacey and Rennie*, 2012; *Moustakidis et al.*, 2012] we expected that this would produce different bedforms. We limited our experiments to fully submerged hemispheres in the LRS regimes and defined the relative submergence was defined as $h_{au} / (0.5 D_I)$, where h_{au} is the average water depth just upstream face of the hemispheres and $0.5 D_I$ is the initial protrusion of each hemisphere (Table 3.1). The effect of relative submergence were isolated by keeping a constant total transport capacity ($q_b = 0.06$ kg/s) and upstream sediment supply rate (q_s), which was equal to q_b, between experiments. The GSD of the bed sediment and that of the upstream sediment supply were identical in all runs. The same sediment transport capacity with different slopes (ranged between 0.0215 and 0.027, Table 3.1) was obtained by varying the flow discharge. For each experiment we let the bed to adjust to the imposed flow and upstream sediment supply until equilibrium conditions were reached. Equilibrium was defined as when the mean bed and water slopes were no longer changing, reach-averaged velocity was constant, $q_s = q_b$, and the upstream supply GSD was identical to that exiting the flume.

3.3.2 Experimental measurements

Our data collection plan had two purposes: a) to verify that equilibrium conditions were reached and b) to validate a 3D flow model. For a) we measured the reach-averaged velocity, bed load transport rates and GSD of sediment exiting the flume, and bed and water surface elevations. For the flow model validation we measured the three velocity components using an

acoustic doppler velocimeter (ADV) at different locations around an immobile hemisphere (Figure 3.2 a), which were complemented with bed and water surface elevations.

We monitored the WSE at the beginning and end of each experiment along three longitudinal profiles (at 5 cm intervals from $X = 1$ to 9 m) using an ultrasonic water level sensor (Massa M-300, accuracy of about 0.1 mm) mounted on a motorized cart that traversed the bed. One profile was located along the channel center ($Y = 0$ m), while the other two were aligned with the center of each row of hemispheres ($Y = \pm 0.152$ m). At the beginning and end of each experiment we surveyed the bed (dry) using a high-speed (50 kHz sampling rate), high accuracy (about 0.1 mm) charge-coupled device (CCD), laser displacement sensor that was mounted on the same cart. All of our scans had a resolution of 5 mm × 5 mm and covered the same 8 m test section. Reach-averaged velocity in our test section was measured using the tracer dilution method [*MacMurray*, 1985; *Kilpatrick and Wilson*, 1989; *Leibundgut et al.*, 2009] at intervals of 20 min using sodium chloride and conductivity measurements (every 1 s, Campbell Scientific® CS547A-L). Tracer concentration curves, corrected by water temperature (17.5±1 °C), were used to estimate the harmonic mean travel time [*Waldon*, 2004].

An overhead sediment conveyor (Figure 3.1 a) evenly fed sediment across the flume width. Sediment leaving the flume was deposited in a 0.85 m^3 submerged bag held by an overhead crane and measured at intervals of 3 s using a calibrated load cell. If the bag filled to about 80% of its capacity, it was replaced and the time spent during that process was discarded from our bed load rate calculations. We averaged q_b over one hour periods (simple moving average) and allowed 5% variability in the outflux ($q_b = 0.06 \pm 0.003$ kg/s) to establish that transport was in equilibrium. We then collected sediment samples for 120 s directly from the pipe that conducts sediment to the bulk bag. To reduce the processing time the GSD was measured using a gravelometer (≥ 100 random sampled grains, no correction factor is required to convert to volume by weight method [*Kellerhals and Bray*, 1971; *Bunte and Abt*, 2001]). Equilibrium occurred when all fed grain sizes were present in the bed load and the differences in feed and outflux D_{50m} and D_{84m} were within 10 %.

The ADV (SonTek® 16-MHZ MicroADV, 50 Hz, Figure 3.2 a) measurements were conducted at different elevations (Figure 3.3 a) for periods of 80 s after equilibrium was

reached. Velocity profile measurements were not conducted because the water depth was too shallow or air entrainment made accurate readings impossible. The despiking algorithm of *Islam and Zhu* [2013] was used with our ADV data where spikes were removed and replaced by linearly interpolated values.

3.3.3 Fluid flow model

The volume of fluid method (VOF) of *Hirt and Nichols* [1981] was used to capture the air-water interface. An indicator function (γ), known as phase fraction, defines the portion of a cell that is occupied by one phase (e.g. air or water). The transport equation for the indicator function is solved simultaneously with the Reynolds-averaged Navier-Stokes equations,

$$\nabla \cdot U = 0, \tag{2.1}$$

$$\frac{\partial(\rho U)}{\partial t} + \nabla \cdot (\rho U U) = -\nabla p + \nabla \cdot \tau + \rho f_b, \tag{2.2}$$

$$\frac{\partial \gamma}{\partial t} + \nabla \cdot (U\gamma) + \nabla \cdot \left(U_r \gamma (1-\gamma)\right) = 0, \tag{2.3}$$

where equations (2.1) and (2.2) represent the conservation of mass and momentum, respectively, and equation (2.3) gives the transport of the indicator function, which incorporates the artificial compression term of *Weller* [2005] (last term on left side of equation 3) to account for the high density ratio between fluids. U is the velocity field, ρ the fluid density, t the time, p the pressure, $\tau = 2\mu S_\tau - 2\mu(\nabla \cdot U) I/3$ is the deviatoric viscous stress tensor with $S_\tau = 0.5\left[\nabla U + (\nabla U)^T\right]$ the mean rate of strain tensor (T denotes the transpose of the matrix), $I \equiv \delta_{ij}$ the identity tensor (δ_{ij} is Kronecker's delta), μ the dynamic viscosity and f_b the body forces per unit mass, which include gravity and surface tension effects at the interface. Under our experimental conditions both air and water phases were assumed to be Newtonian and incompressible, which implies that $\tau = 2\mu S_\tau$ since $\nabla \cdot U = 0$. In addition the rate of strain tensor was considered to be a linear function of the stress tensor as:

$$\nabla \cdot \tau = \nabla \cdot \left(\mu \left[\nabla U + \left(\nabla U \right)^T \right] \right) = \nabla \cdot \left(\mu \nabla U \right) + \left(\nabla U \right) \cdot \nabla \mu, \tag{2.4}$$

which is also a more convenient form to be used in the numerical discretization.

The wall pressure boundary conditions were simplified following *Rusche*'s [2002] approach, in which a modified pressure (p_d) was used,

$$p_d = p - \rho g \cdot x, \tag{2.5}$$

$$\nabla p_d = \nabla p - \rho g - g \cdot x \nabla \rho, \tag{2.6}$$

where x is the three-dimensional vector position, g the acceleration due to the gravity, and ρ the fluid density. The modified pressure includes the static pressure gradient, gravity effects as body forces, and the pressure due to a density gradient. The advantage of using this formulation is that allowed us to specify a single boundary condition at the walls when two fluids are present (air-water phases, see section 3.3.4).

The phase fraction γ was solved using the Multidimensional Universal Limiter with Explicit Solution (MULES), based on *Zalesak* [1979]. Its use guarantees a strictly bounded solution between $0 \le \gamma \le 1$, where $\gamma = 0$ or $\gamma = 1$ indicates that exclusively air or water, respectively, is inside a cell and any other value denotes the presence of an interface. In all our experiments the WSE was defined as the isosurface $\gamma = 0.5$, which was approximately in the middle of the cell that contains the phase change (water to air). In this VOF formulation the two immiscible fluids were treated as a single fluid (also known as effective fluid), where its physical properties (ρ and μ) are a weighted average that accounts for γ ,

$$\rho = \rho_w \gamma + \rho_a \left(1 - \gamma \right), \tag{2.7}$$

$$\mu = \mu_w \gamma + \mu_a \left(1 - \gamma \right), \tag{2.8}$$

where the subscripts a and w stands for air and water phases, respectively.

The vector of relative velocity between phases U_r (in equation (2.3)), usually called the compression velocity, was calculated as:

$$U_r = \min\left[C_\gamma \frac{|\phi_f|}{|S_f|}, \max\left(\frac{|\phi_f|}{|S_f|}\right)\right] n_f, \tag{2.9}$$

where C_γ is a constant that usually ranges from 0 to 4 and is used to restrict interface smearing. We used $C_\gamma = 1$ because other values can exacerbate errors in the interfacial curvature and smearing [*Deshpande et al.*, 2012]. Definitions of ϕ_f, S_f, and n_f require the use of a discrete domain, which in our case was based on the finite volume technique (Figure 3.2 b). In the discretized domain ϕ_f is the volume flux ($\phi_f = U_f \cdot S_f$), S_f is the product of the unit normal outward vector corresponding to the owner cell and the surface area of the face, n_f is the face centered interface normal vector, and U_f the face velocity, which is estimated through a point-to-point interpolation between cells P and N, the owner and neighbor of a cell, respectively (Figure 3.2 b). Details of the equation discretization can be found in *Berberović et al.* [2009] and *Rusche* [2002]. Advantages of using the artificial compression term in equation (2.3) include the resolution of sharp interfaces and the reduction of numerical diffusion [*Weller*, 2005; *Deshpande et al.*, 2012; *Nieves-Remacha et al.*, 2015].

The body forces (f_b in equation (2.2)) were evaluated using the continuum surface force (CSF) model of [*Shevchuk et al.*, 2012], where the two-dimensional pressure gradients (resulting in a net force) were converted into a three-dimensional volume effect that accounts for the surface tension (σ = 0.07 N m^{-1}) and mean curvature of the free surface (K),

$$f_b = \sigma K \nabla\gamma, \tag{2.10}$$

$$K = -\nabla\left(\frac{\nabla\gamma}{|\nabla\gamma|}\right). \tag{2.11}$$

Combining equations (2.2), (2.4), (2.6), (2.10) and (2.11), the momentum equations results in:

$$\frac{\partial(\rho U)}{\partial t} + \nabla\cdot(\rho UU) - \nabla\cdot(\mu\nabla U) - (\nabla U)\cdot\nabla\mu = -\nabla p_d - g\cdot x\nabla\rho + \sigma K\nabla\gamma, \tag{2.12}$$

To estimate turbulence effects we used the two equation $k-\omega$ SST model of *Menter* [1994] and *Menter and Esch* [2001] that applies the $k-\omega$ (k is the kinetic energy of turbulent fluctuations per unit mass and ω the specific dissipation rate) and $k-\varepsilon$ models (where ε is the dissipation rate) near the wall and in the free-stream flow, respectively. Although other turbulence models such as $k-\varepsilon$ [*Ye and Mccorquodale*, 1998; *Wilson et al.*, 2003; *Nagata et al.*, 2005; *Kuzmin and Mierka*, 2006; *Liu and García*, 2008; *Aghaee and Hakimzadeh*, 2010] or different versions of *Wilcox's* [1988] $k-\omega$ [*Li and Zhang*, 1998; *Ye and Mccorquodale*, 1998; *Roulund et al.*, 2005; *Zeng et al.*, 2005; *Khosronejad et al.*, 2007; *Esmaeili et al.*, 2009] have been satisfactorily applied in open channel applications, *Menter's* [1994] $k-\omega$ SST model presents some critical advantages for our simulations. For instance, it performs better than the $k-\varepsilon$ model in the presence of adverse pressure gradients [*Hellsten*, 1998], which are expected in our simulations due to the immobile elements. It also provides more accurate predictions of wall shear stress [*Rodi and Scheuerer*, 1986], which is key for sediment transport applications. The SST formulation also overcomes the strong sensitivity of the $k-\omega$ model to free stream values for ω while maintaining robustness [*Menter*, 1992; *Menter and Esch*, 2001].

We used the near-wall formulation of *Grotjans and Menter* [1998] (also described in *Menter and Esch* [2001] and *Menter et al.* [2003]), for the bed boundary conditions because it can gradually switch from a wall function to a low-Re formulation based on the grid density. This allowed us to consider the highly complex bed geometry of our experiments without needing locally excessive cell aspect ratios or an extremely fine mesh to solve the viscous sub-layer.

3.3.4 Numerical implementation and boundary conditions

We used the flow solver interFoam, which is part of the open source software OpenFOAM® (www.openfoam.org) that uses the tensorial approach and object oriented techniques to closely resemble the mathematical expressions of the governing equations of fluid dynamics (section 2.3) [*Weller et al.*, 1998]. We first used a coarse mesh (average cell volume ~ 1.25 cm^3), let the model run for 90 s, and then mapped the calculated flow variables (U, p, p_d, μ_T, ω, k, where μ_T is the turbulent dynamic viscosity or eddy viscosity) and indicator function (γ) from the final time step to a new fine mesh. The pressure-velocity coupling was

solved using the PISO algorithm [*Issa*, 1986] and identical conditions for the solvers and numerical schemes were used for both meshes. The fine mesh had an average cell volume of ~ 0.15 cm^3 between the bed and water surface and had a similar resolution to the coarse mesh in the air-phase (Figure 3.2 b). The fine mesh allowed us to capture the bed topography in great detail while being suitable for application of the near-wall formulation for ω of *Grotjans and Menter* [1998]. We specified the flow discharge at the upstream boundary and let the WSE to adjust itself. The modified pressure (p_d) of *Rusche*'s [2002] (equation (2.6)) allowed us to specify a single boundary condition for both phases at the side walls when the WSE varied in time and space. We checked that water ($\gamma = 1$) never reached the upper boundary so that only air flow was allowed.

3.3.5 Analysis of model parameters

We ran the model for 70 s (using the fine mesh), discarded the first 10 s and used the remaining 60 s to compute the time averaged flow velocity and WSE, both based on data recorded every 0.05 s. We tested the performance of the velocity profile equations of *Lamb et al.* [2008] and *Recking* [2009] by averaging the downstream velocities at a given distance from the bed [*Smith and McLean*, 1977; *McLean et al.*, 1999] (samples were extracted at: 1, 1.25, 1.5, 2, and 2.5 mm, then from 2.5 to 20 mm at intervals of 2.5 mm). The shear velocity ($u^* = \sqrt{\overline{\tau}_m / \rho_w}$, where $\overline{\tau}_m$ is the reach averaged shear stress acting on the mobile grains [*Yager et al.*, 2007]), was calculated using the bed shear stress in the X direction ($\overline{\tau}_X$) at $Z = 1.0$ cm, which was also double averaged (time and space). The near-bed (1.0 cm from bed) shear stress field was calculated from velocity gradients using the Boussinesq hypothesis. We chose 1.0 cm because maximum shear stress values occurred very close to this elevation and the shear stress gradients became less pronounced at higher elevations.

Lamb et al. [2008] assumed deep flow ($h \gg k_s$, where h is the local water depth and k_s the roughness length scale) which yielded a constant mixing length coefficient ($\alpha_1 = 0.12$) that is independent of the water depth. However, in their unsimplified formulation α_1 can be a function of k_s and h and therefore we did not assume deep flow and let α_1 vary with h.

Assuming the roughness height as $z_0 = k_s / 30$ and matching *Lamb et al's.* [2008] near-bed velocity profile with the logarithmic zone at the transition between profiles ($z = k_s$) results in:

$$\alpha_1 = \frac{\kappa}{\ln(30)}\left(1 - \frac{k_s}{2h}\right) \tag{2.13}$$

where κ is von Karman's constant of 0.41. To evaluate the equations of *Lamb et al.* [2008] and *Recking* [2009] at the reach scale we used the reach-averaged water depth from the flow model and the median grain size of the mobile sediment (D_{50m}) for each experiment to estimate k_s . In all initial bed conditions D_{50m} was 1 cm and it was 0.95, 1.17 and 1.06 cm for the S2.15%, S2.40%, and S2.70%, respectively. Typically k_s is a function of a representative bed grain size (e.g $k_s = 3.5 D_{84}$ or $6.8 D_{50}$, Figure 3.4 a), but if numerical modelling with adequate mesh resolution is used, k_s can be almost an order magnitude lower [*Tonina and Jorde*, 2013] and can range between $0.3 D_{50}$ to $0.5 D_{50}$ using the expressions of *Clifford et al.* [1992].

3.4 Results

3.4.1 Bed surface elevation changes

In general all experiments had sediment deposition upstream of the hemispheres, whereas scour occurred in only one experiment (S2.15%). All experiments had sediment accumulation on average, the magnitude of which increased with higher slope (8.1, 9.2, and $12.5 \cdot 10^{-3}$ m^3/m for the 2.15%, 2.40% and 2.70% experiments, respectively. Figure 3.2 a). Most sediment deposited near the walls and switched from the right to left wall moving downstream. This tendency was clearer in experiments S2.15% and S2.40%, while experiment S2.70% had a relatively more homogeneous bed. Only experiment S2.15% developed large 7 cm deep (~3/4 of the original bed thickness) elongated pool-like areas downstream the hemispheres. Different bedforms were likely due to the different hydraulic conditions between experiments, in particular the relative submergence, shear stresses, recirculation areas and mixing zones [*Shamloo et al.*, 2001; *Papanicolaou and Kramer*, 2006; *Papanicolaou et al.*, 2010]. In this study we are do not propose a mechanism for bedform development, but rather analyze the influence of the topography on the flow field by comparing the initial and final bed conditions.

3.4.2 Flow model validation

The flow model accurately reproduced the local velocity in all three directions, especially the downstream velocity (RMSE = 0.054 m/s) where almost all data points were within 10% of the measured values (Figure 3.3 a). The accuracies of the cross-stream and vertical (RMSE 0.059 and 0.065 m/s) velocities (Y and Z directions, respectively) were lower than in the downstream direction, although the general magnitude was captured in both cases. Experiments S2.15% and S2.40% had the largest differences between predicted and measured values for the cross-stream and vertical directions, respectively. These deviations were likely due to the simplifications in our numerical simulations, such as assuming that the final bed state had the same bathymetry as when the ADV measurements took place and that the effects of a moving sediment bed on the flow were negligible despite evidence that mobile bedforms affect the flow structure [*Sukhodolov et al.*, 2004; *Keylock et al.*, 2014]. Uncertainties in ADV measurements associated with the effects of turbulent structures smaller than the size of the sampling volume [*Peltier et al.*, 2013] and increased noise in the vertical velocity component due to the presence of bubbles [*Frizell*, 2002; *Liu et al.*, 2002; *Cea et al.*, 2007] could also have introduced some errors. Some discrepancies may also be caused by the use of discrete elements to represent the bed topography, which although they are very fine, cannot capture all of the bed details.

In general the model accurately predicted the location and magnitude of the WSE (RMSE on average 6 mm, max 1 cm. Figure 3.3). Furthermore, the model nicely reproduced the plunging flow over the hemispheres, as well as the wave location. Water surface slope was well captured by the model with percent differences between predicted and measured values ranging from 0.2% to 8.6% for S2.40% and S2.70%, respectively, for final bed conditions (Table 3.2). Locally, the major differences between the modeled and the measured WSE were downstream of the hemispheres where the model sometimes predicted shallower flows. These differences could be partly result from simplifications in the VOF method, in particular the solution is adjusted to maintain the boundedness in the γ equation (Equation (2.3)). The accuracy of the ultrasonic water level sensor can be affected when WSE fluctuations exist [*Aguilar et al.*, 2016] and may also explain some discrepancies. The results of local velocity

and WSE predictions suggest that the model accuracy is adequate to describe the spatial flow field in our study.

3.4.3 Velocity profiles

The relation of *Recking* [2009] was not very accurate and overpredicted the velocity immediately above the bed and underpredicted the velocity in the region outside the roughness layer in all experiments. The choice of k_s did not affect the predictions of *Recking* [2009] because it uses $k_s = D_{50m}$ in all cases. Varying α_1 with h gave us a lower α_1 than that suggested by *Lamb et al.* [2008] (if $D_{50m} = 1$ cm, $\alpha_1 = 0.053$ and 0.115 for $k_s = 6.8\,D_{50m}$ and $0.5\,D_{50m}$ respectively). The use of $\alpha_1 = 0.12$ can led to significant errors and cause a discontinuity in the velocity profile when transitioning from the roughness layer to the logarithmic region (Figure 3.4 a and b). An appropriate k_s was also key to capture the velocity profile shape when using *Lamb et al.* [2008] (Figure 3.4 b); when $k_s = 6.8\,D_{50m}$ the roughness layer extended too far into the flow column and resulted in under-predicted velocities. The expressions of *Clifford et al.* [1992] and a variable α_1 allowed the *Lamb et al.* [2008] equations to predict the reach-averaged velocity profile fairly well for all experiments except the final bed condition in S2.40%, which was systematically underpredicted (Figure 3.4 c).

The 3D model's local velocity profiles depended on the proximity to a hemisphere or a side wall (Figure 3.5). Near the bed ($z/h \leq 0.10$), the velocity profiles were always affected by changes in bed topography between initial and final conditions. The surrounding topography also influenced profiles for which the local topography was static. For example a velocity profile over the hemisphere (Figure 3.5 location 8) shifted from only positive velocities to having some negative values in the final bed condition. The equations of *Lamb et al.* [2008] and *Recking* [2009] did not always perform well (Figure 3.5) when applied locally in that they generally underpredicted the velocity in profiles relatively far from the hemispheres (Figure 3.5, profiles 1-6) and incorrectly predicted the profile shape above the hemispheres.

3.4.4 Hydrostatic pressure

We tested the hydrostatic pressure assumption in several locations using the calculated static pressure averaged over 60 s at the same locations as the velocity profiles (Figure 3.5). The slope of the hydrostatic pressure assumption (9810 Pa m^{-1}) was compared to that obtained by fitting a linear regression to our model's predicted pressure profile. We then used the z-test [*Cohen et al.*, 2003] (95% confidence) to test if the slopes were statistically different. Here only the final bed conditions in experiment S2.70% are discussed but we observed similar results in all cases.

In general the pressure had a linear distribution, which was confirmed by the high coefficient of determination (R^2) obtained for the linear regressions of the model's static pressure profile (Figure 3.6). Deviations from linearity were observed at the hemisphere (Figure 3.6 at locations 8 and 9) and in its wake (locations 10 - 11). The hydrostatic assumption performed better at profiles that were relatively distant from the hemisphere (locations 1 and 6), based on R^2, than those near and over the hemisphere (locations 2 and 7 to 11). Based on the z-test only four locations (1, 2, 5 and 6) had a static pressure distribution slope that was not statistically different than the hydrostatic pressure slope.

3.4.5 Near-bed shear stress

In all experiments the reach-averaged near-bed shear stress changed between the initial and final bed conditions (Figure 3.7 a). The average shear stress magnitude ($\overline{\tau}$, averaged in time and space) and streamwise component ($\overline{\tau}_X$) in experiments S2.40% and S2.70% decreased more than 10% and 15%, respectively, from initial to final bed conditions but the changes in experiment S2.15% were relatively small ((Figure 3.8 a). Given that the hemispheres configuration, discharge and sediment supply did not vary between the initial and final bed conditions we attribute the differences in $\overline{\tau}$ and $\overline{\tau}_X$ in a given run to bed topography changes. To further understand how bed evolution affected the shear stress field we split the bed into two components, the immobile hemispheres and the rest of the bed, which was defined as mobile. The mean immobile τ_X (hereinafter $\overline{\tau}_{XI}$) increased in each experiment, especially in S2.70% where it changed from -1.46 to 3.11 Pa (negative value is upstream). These changes in $\overline{\tau}_{XI}$ were

not reflected in $\overline{\tau}_X$ due to the relatively small area that the immobile hemispheres occupied. A reduction in the mean mobile τ_X ($\overline{\tau}_{Xm}$) of 11 and 16 % in experiments S2.40% and 2.70%, respectively, can be attributed to the self-formed bedforms, whereas experiment S2.15% had almost no change in $\overline{\tau}_{Xm}$. No exact relation between $\overline{\tau}$, $\overline{\tau}_X$ or $\overline{\tau}_{Xm}$ and relative submergence was observed, however in general the shear stress decreased with increased relative submergence for given bed condition (initial or final, $R^2 = 0.62$) (Figure 3.8 b). No relation between $\overline{\tau}_{XI}$ and slope or relative submergence was observed in the initial or final bed conditions.

The distributions of τ_X had similar shapes in all experiments (Figure 3.7 b), and were generally normally distributed. Deviations from Gaussian were observed in the distribution tails, especially for lower τ_X values. Considering that the coefficient of variation (ratio of the standard deviation to the mean value) was relatively constant (ranged from 1.57 to 1.87), and that the tails of the shear stress distribution only occupied a small area of the bed (see Chapter 1), the normal distribution could be used as a first approximation.

3.4.6 Turbulent kinetic energy

The turbulent kinetic energy was calculated based on our closure method ($k-\omega$ SST model) and we limited our analysis to the near-bed region using the same elevations as those for the velocity (see section 3.4.3). The reach averaged dimensionless k profile ($\overline{k}' = \overline{k}/u_*^2$, where $\overline{k}$ is the reach-averaged k) had two well defined zones, one within the roughness layer where the $\overline{k}'$ gradients were higher and an outer layer with relatively smooth changes in $\overline{k}'$ (Figure 3.9 a). By comparing initial and final bed conditions it is clear that the extent of these zones and the average profile shapes were generally not affected by the presence of bedforms. Contrary to the profiles predicted by *Nezu and Nakagawa* [1993] and *Nikora and Goring* [2000] we observed that in general $\overline{k}'$ increased with greater distance from the bed.

Locally the dimensionless k (k') profiles were closer to those described by *Nezu and Nakagawa* [1993], *Nikora and Goring* [2000], *Biron et al.* [2004], and *Sukhodolov et al.* [2006]. The elevations of peak k' varied with the location relative to the hemisphere; the

maximum k' was close the bed and near the water surface upstream and downstream of the hemispheres, respectively. Variations in local k' profiles caused by bed topography were only significant near the bed and upstream of the hemispheres (Figure 3.9 d, locations 1 to 6). In the final bed conditions an increase in peak k' occurred upstream the hemispheres (locations 1, 3 and 4), while a systematic increase in k' (comparing initial and final bed conditions) was observed in profiles located locations 5 and 6.

The reach-averaged near-bed k ($\overline{k}$) changed with bedforms presence (initial vs final bed conditions) in a similar way as shear stress (Figure 3.8 a and c); practically no change occurred for S2.15% and a reduction of 12 and 18% occurred for S2.40% and S2.70%, respectively. In general $\overline{k}$ also decreased with increased relative submergence, although not when initial and final beds were combined (Figure 3.8 c). For a given relative submergence, the k on the hemispheres ($\overline{k}_I$) was always higher than k on the mobile sediment ($\overline{k}_m$) and $\overline{k}_I$ and $\overline{k}_m$ generally decreased with increasing relative submergence, in particular for the final bed conditions (Figure 3.8 d).

The local near-bed k was highest immediately downstream of the hemispheres (Figure 3.9 c). In the initial bed conditions k decaed along the centerline of the wakes downstream of the immobile hemispheres. However, the high k areas were significant and extended for roughly half the distance between hemispheres. The spatial distribution of k was affected by the development of bedforms; the maximum k areas occupied most of the hemispheres' wakes at the experiment beginning and at the end they were reduced to small regions downstream of the hemispheres.

3.5 Discussion

The same imposed bed load flux was transported at different mean shear stresses (Figure 3.8 a); had S2.70% had nearly twice the magnitude of $\overline{\tau}_m$ as experiments S2.15% and S2.40%. Bed load transport is typically assumed to be a deterministic process [*Gomez and Church*, 1989; *Gomez and Phillips*, 1999] that is a function of the available mean shear stress and the grain size distribution of the bed material [e.g. *Parker et al.*, 1982; *Parker*, 1990; *Wilcock and Crowe*, 2003]. If sediment fluxes were estimated based only in $\overline{\tau}_m$, different transport capacities

between experiments may have been predicted. However, despite different reach-averaged shear stresses similar bedload transport rates can be caused by bedform migration processes [*Gomez et al.*, 1989; *Gomez and Phillips*, 1999; *Lisle et al.*, 2001; *Recking et al.*, 2009], spatially and temporally varying grain arrangement and sorting [*Raudkivi and Ettema*, 1982; *Kirchner et al.*, 1990; *Gomez*, 1993; *Laronne et al.*, 2000; *Chen and Stone*, 2008], and different distributions of shear stresses [*Dietrich and Whiting*, 1989; *Smart*, 1999; *Clayton*, 2012b; *Cienciala and Hassan*, 2013]. Accounting for the spatial variability in shear stress is key for accurate sediment transport predictions (see Chapter 1).

3.5.1 Numerical modeling

Compared to other 3D models (naysCUBE and those that use the rigid lid assumption, see for example [*Ouillon and Dartus*, 1997; *Casulli and Stelling*, 1998; *Rodríguez et al.*, 2004; *Khosronejad et al.*, 2007]) we found that the VOF method, in particular its implementation in interFoam, has two critical advantages. First, our fine grid has no need for roughness calibration, which means that roughness parametrization become less important than numerical boundary conditions [*Lane and Richards*, 1998; *Lane et al.*, 1999; *Tonina and Jorde*, 2013]. Second, the interface capturing method allowed us to include skimming or plunging flow induced by the hemispheres. Other numerical techniques to solve for the WSE such as the interface-tracking method (see for example NaysCube [*Nelson et al.*, 2015]) are prone to diverge into plunging flow conditions because the mesh has to collapse in a very narrow area, which considerably increases the Courant number. When 3D flow models are required and obstructions significantly affect the WSE or flow routing, we recommend the use of interFoam or other models based on VOF. 3D models that use the rigid lid approximation or a dry/wet strategy are likely to have significant errors in local velocity and pressure distributions, especially where the water surface fluctuates in time (even for a steady discharge) or has sharp gradients.

3.5.2 Velocity and pressure profiles and implications for shear stress prediction

Our results suggest that the velocity profiles of *Lamb et al.* [2008], only when combined with a variable α_1 and the equation of *Clifford et al.* [1992], can accurately predict the reach-averaged near-bed velocity in the presence of bedforms and large immobile elements. The use

of a constant α_1 (deep flow assumption) can result in a discontinuity in the velocity profile for the LRS observed in our experiments and in many mountain streams. Following *Yager et al.* [2007, 2012] we used the mobile median grain size (D_{50m}) to define k_s and excluded the hemispheres. Including hemispheres in estimates of k_s would increase the roughness layer thickness ($D_{50} > D_{50m}$) and underpredict the velocities throughout the flow depth. Therefore, in field applications large, relatively immobile roughness elements should not be included in estimates of k_s. Care must be taken when k_s is specified; only when a topographic survey captures all of the surface irregularities can a low grain roughness length be used ($k_s = 0.5D_{50m}$). In our experiments the hemispheres did not influence k_s because they occupied a relatively low portion of the total bed area, in cases where the large roughness elements occupy a larger fraction of the bed our assumption may not be valid. Further research is needed to establish a threshold, in terms of immobile grains density, where k_s can be accurately estimated using only the mobile grains.

Local velocity profiles and near-bed shear stresses varied significantly (Figure 3.5 and Figure 3.7) mainly as a response to the bed topography and hemispheres. The *Lamb et al.* [2008] equations were not often accurate locally and should not be used to estimate local boundary shear stresses under highly spatially variable conditions in most mountain streams. Other simple techniques to estimate local shear stresses such as the single velocity method [*Dietrich and Whiting*, 1989], in which the shear stress is estimated considering only one measurement of the near-bed velocity, may also be ineffective because it is not always clear where the transition from the roughness layer to the logarithmic region occurs.

We observed a linear pressure profile in most cases (Figure 3.6), despite it being statistically different from the hydrostatic pressure. Flow models that assume a hydrostatic pressure distribution should be used with caution, especially if estimates of local flow variables are required. For these models, more reliable flow results will be obtained far from local sources of vertical velocity divergences such as roughness elements. In particular, 2D model predictions of shear stresses and sediment fluxes near obstructions are likely to have errors because of significant deviations from hydrostatic pressure. Additional safety design factor must be considered when this type of model is used to analyze the effects of local sediment deposition

and scour on bridge pier stability or the potential addition of large boulders and woody debris in restoration projects. In particular for predictions of sediment fluxes, gradients stronger than hydrostatic enhance the buoyant force on a grain and therefore make grains apparently lighter and more mobile, conversely gradients weaker than hydrostatic result in the same grain being apparently heavier [*Francalanci et al.*, 2005, 2008].

Our experimental conditions to test velocity profile and pressure equations were limited to a single hemisphere configuration and low relative submergence regimes. Future studies should consider variations in the large roughness configuration (e.g. distance and density, steps and pools) and a wider range of relative submergences (e.g. one to four after *Shamloo et al.* [2001]). In addition, other flow modelling techniques (e.g. Large Eddy Simulation) could be used to further quantify velocity profile equation performance compared to our flow model (RANS). However, given that our model did not use a specific velocity profile and actually solved for the three dimensional velocity and pressure field the reach-averaged velocity profiles are unlikely to be caused by the model choice.

3.5.3 Controls on reach-averaged shear stress

Most estimates of reach-averaged shear stress use the depth-slope product ($\rho_w g h_a S_{bed}$) and therefore it is expected that the shear stress increases with higher depths and slopes and that these are the important parameters to measure in the field. No systematic relation between reach-averaged shear stresses (i.e. $\overline{\tau}$, $\overline{\tau}_X$, $\overline{\tau}_{Xm}$, and $\overline{\tau}_{XI}$) and slope or relative submergence occurred (Figure 3.8 and b). Exclusively considering the initial conditions $\overline{\tau}$, $\overline{\tau}_X$, and $\overline{\tau}_{Xm}$ increased with higher slope and decreased with greater relative submergence (higher flow depth), whereas in presence of bedforms (final bed condition) the trend with slope was lost. The ratio $h_a / \left(0.5 D_I\right)$, which is how relative submergence is usually defined, did not correlate to $\overline{\tau}$, $\overline{\tau}_X$, and $\overline{\tau}_{Xm}$ in the final bed conditions. These results combined suggest that water depth and slope are not the main controls in reach-averaged shear stresses ($\overline{\tau}$, $\overline{\tau}_X$, and $\overline{\tau}_{Xm}$) in LRS. In steep, rough channels that are dominated by plunging flow and topographic variability (i.e. bedforms) estimates of near-bed shear stress should account for a measure of boulders (or large roughness elements) submergence. The derivation of the total shear stress based on the depth-

slope product relies on numerous assumptions including the fact that convective accelerations can be neglected. Our results imply that in LRS regimes with plunging flow, these accelerations are very important and influence the reach-averaged shear stress in ways that the simple depth-slope product approximation does not include. Sediment transport equations for steep rough channels have indirectly account for such effects, using the total shear stress (depth-slope product) can overestimate bed load transport by orders of magnitude (see discussion by *Yager et al.* [2007, 2012] and *Nitsche et al.* [2011]) and flow resistance partitioning techniques are used to account for only the shear stress acting on the mobile grains. Some flow partitioning techniques account for the presence of large roughness elements [*Whittaker*, 1986; *Egashira and Ashida*, 1991; *Pagliara and Chiavaccini*, 2006; *Ferguson*, 2007; *Yager et al.*, 2007, 2012; *Rickenmann and Recking*, 2011] but not for irregular bedforms or the hydraulics of plunging flow and more research is needed to incorporate these effect reach-averaged shear stress predictions.

In contrast to other shear stresses, $\overline{\tau}_{XI}$ increases with greater slope sin the final but not initial bed condition. In particular, the negative $\overline{\tau}_{XI}$ for the initial condition in S2.15% was caused by negative velocity gradients (decrease in velocity away from the bed) that occupied most of the hemisphere surface (Figure 3.10). The occurrence of negative shear stresses on relatively immobile grains has, to the best of our knowledge, not been addressed in the literature. The stability of artificial structures used to improve fish habitat, such as large boulders [*Shamloo et al.*, 2001; *Papanicolaou et al.*, 2011] could be compromised if they are not designed to tolerate shear stresses in the upstream direction.

3.5.4 Turbulent kinetic energy

Our reach-averaged dimensionless k ($\overline{k}'$) profiles did not have the typical shape observed in the literature [*Nezu and Nakagawa*, 1993; *Nikora and Goring*, 2000; *Tritico and Hotchkiss*, 2005; *Sukhodolov et al.*, 2006]; the turbulent kinetic energy continuously decreased towards the bed, with a low gradient in most of the water column and a sharp gradient within the roughness layer (Figure 3.9 b). Similar k profiles have also been reported for flow through fully emergent vegetation [*Nepf*, 1999; *Nepf and Vivoni*, 2000]. Our profiles shapes were likely caused by the low relative submergence of our experiments, which is why k production

affected the entire water column even near the WSE (Figure 3.9 d). The effects of the large immobile elements on k can observed in Figure 3.9 c and d, in which the maximum values of k are found downstream of the hemispheres and are also pronounced at the WSE. The longitudinal distribution of k was similar to that reported by *Tritico and Hotchkiss* [2005] and *Lacey and Roy* [2008] who studied flow around obstructions and found that k appears to develop at obstructions and decay downstream. Our results are not dependent on our chosen flow model because *Stoesser et al.* [2006] compared the results of RANS and LES simulations at low relative submergence ratios and found that the $k-\omega$ turbulence model yields the correct shape and magnitude of k profiles.

The spatial distribution of k has important implications for fish habitat and behavior [*Tritico and Hotchkiss*, 2005; *Harrison et al.*, 2011; *Bretón et al.*, 2013; *Baki et al.*, 2015] and for the establishment and stability of instream and bank vegetation [*Nepf*, 1999; *Nepf and Vivoni*, 2000; *White and Nepf*, 2007; *Hopkinson and Wynn*, 2009; *Zong and Nepf*, 2011]. For example, cyprinid [*Silva et al.*, 2012] and trout [*Smith et al.*, 2005] prefer zones with low turbulent kinetic energy because turbulence increases the energetic cost of swimming [*Lupandin*, 2005]. However, zones of turbulence production, such as downstream of a boulder, are used by fish to rest, feed and defend territory because of the presence of low velocities [*Fausch*, 1993; *Griffith*, 1993]. Our spatial k distributions (Figure 3.9) are in agreement with those of *Baki et al.* [2015] who studied turbulence characteristics in fish passage designs with staggered boulders arrangements. The degree of plunging flow over our hemispheres played a significant role in the production and distribution of k and habitat enhancement projects may need to account for different potential submergence conditions. Very different flow patterns and therefore distributions of k may be obtained if large roughness elements are partly or fully submerged [*Ozgoren et al.*, 2011]. Care must also be taken if habitat enhancement projects include a potentially mobile bed bedforms can significantly affect the spatial distribution of k, especially downstream of the large roughness elements (Figure 3.9 c). Locations near large roughness elements will also create zones of high k, which will enhances nutrient and gas exchange but could decrease organic matter deposition and promote bed scour.

The magnitude of k also has important consequences for sediment mobility [*Grass*, 1970; *Best*, 1992; *Papanicolaou et al.*, 2002; *Schmeeckle and Nelson*, 2003; *Zanke*, 2003; *Wu*

and Yang, 2004; *Cheng*, 2006; *Vollmer and Kleinhans*, 2007; *Lamb et al.*, 2008]. For example, the normalized streamwise turbulence intensity (σ_{uX}/u_*, where σ_u is the root-mean square of streamwise turbulent fluctuations) decreases with increasing relative roughness (k_s/h_a) [e.g. *Lamb et al.*, 2008]. To evaluate if this occurs in our experiments, we approximated σ_u as $\sigma_u = \sqrt{2/3k}$ and assumed that σ_u is a good estimate for σ_{uX}. Although our experiments covered only a small range of relative roughnesses (0.061 to 0.082) they had the same trend described by *Lamb et al.* [2008] and fell very close to the experiments of *Kironoto and Graf* [1994] (Figure 3.11). Notice that we defined the roughness length as $k_s = 0.5D_{50m}$, which did not include the hemispheres. Including the hemispheres would shift the points to higher k_s / h but the observed trend would remain. Our study demonstrates that the changes in turbulence intensity with relative roughness that have developed for very simple bed topographies still hold for highly complex beds (i.e. presence of irregular bedforms) with plunging flow.

3.6 Conclusions

A series of laboratory experiments were conducted to study the influence of large roughness elements and bedforms on near-bed and spatial distribution of flow hydraulics in low relative submergence regimes. We used a 3D model with free surface calculations based on the VOF method that accurately captured the spatial variability in WSE and local velocity, which allowed us to explore the detailed flow characteristics. The bed evolution in each experiment was caused by different hydraulic conditions, in particular the relative submergence and spatial distribution of shear stresses. Zones of scour and deposition created bedforms that had a significant impact on flow properties at both local and reach-averaged scales. At the reach scale the velocity profile of *Lamb et al.* [2008] agreed well with our model's predicted velocities. However, two modifications needed to obtain accurate results, the roughness length was based only on the mobile grains and a mixing length coefficient varied with the flow depth. At a local scale the accuracy of the *Lamb et al.* [2008] velocity profile was lower and significantly deviated from modeled values. The reach-averaged shear stresses varied inversely with relative submergence but not consistently with slope. This implies that flow depth and bed slope may not be the appropriate parameters to compute reach-averaged shear stresses for complex bed topographies with plunging flow. The reach-average turbulent kinetic energy also decreased

with increasing relative submergence and was also controlled by the degree of plunging flow. For low relative submergence flows, especially if plunging flow occurs, a spatial distribution of shear stresses may be needed to accurately predict morphological changes. Additional research on the combined effects of immobile elements (e.g. density and location) and different relative submergences is needed to better understand bedform evolution and sedimentation patterns. A better understanding of these combined effects is key to improve river restoration and aquatic habitat enhancement projects.

3.7 Acknowledgements

Funding for this research was provided by an NSF Career award to E.M. Yager (0847799) and the Chilean Government - CONICYT “Becas de Doctorado en el Extranjero – Becas Chile”. Invaluable laboratory assistance was provided by Bob Basham and Christina Beeson. Thoughtful discussions with Megan Kenworthy helped in the planning and execution of the laboratory experiments.

3.8 References

Adenlof, K. A., and E. E. Wohl (1994), Controls on Bedload Movement in a SubAlpine Stream of the Colorado Rocky-Mountains, U.S.A., *Arct. Alp. Res.*, *26*(1), 77–85, doi:10.2307/1551881.

Afzalimehr, H., and C. D. Rennie (2009), Determination of bed shear stress in gravel-bed rivers using boundary-layer parameters, *Hydrol. Sci. J.*, *54*(1), 147–159, doi:10.1623/hysj.54.1.147.

Aghaee, Y., and H. Hakimzadeh (2010), Three Dimensional Numerical Modeling of Flow around Bridge Piers Using LES and RANS, in *International Conference on Fluvial Hydraulics (River Flow 2010)*, edited by Dittrich, Koll, Aberle, and Geisenhainer, pp. 211–218.

Aguilar, M. F., W. M. McDonald, and R. L. Dymond (2016), Benchmarking laboratory observation uncertainty for in-pipe storm sewer discharge measurements, *J. Hydrol.*, *534*, 73–86, doi:10.1016/j.jhydrol.2015.12.052.

Baki, A. B. M., D. Z. Zhu, and N. Rajaratnam (2015), Turbulence Characteristics in a Rock-Ramp-Type Fish Pass, *J. Hydraul. Eng.*, *141*(2), 4014075, doi:doi:10.1061/(ASCE)HY.1943-7900.0000962.

Bathurst, J. C. (1978), Flow resistance of large-scale roughness, *J. Hydraul. Div.*, *104*(12), 1587–1603.

Bathurst, J. C. (1985), Flow resistance estimation in mountain rivers, *J. Hydraul. Eng.*, *111*(4), 625–643.

Bathurst, J. C. (2002), At-a-site variation and minimum flow resistance for mountain rivers, *J. Hydrol.*, *269*(1-2), 11–26, doi:10.1016/S0022-1694(02)00191-9.

Bennett, S. J., and J. L. Best (1995), Mean flow and turbulence structure over fixed, two-dimensional dunes implications for sediment transport and bedform stability, *Sedimentology*, *42*, 491–513.

Berberović, E., N. P. Van Hinsberg, S. Jakirlić, I. V. Roisman, and C. Tropea (2009), Drop impact onto a liquid layer of finite thickness: Dynamics of the cavity evolution, *Phys. Rev. E*, *79*(3), 036306, doi:10.1103/PhysRevE.79.036306.

Best, J. (1992), On the entrainment of sediment and initiation of bed defects: insights from recent developments within turbulent boundary layer research, *Sedimentology*, *39*(5), 797–811, doi:10.1111/j.1365-3091.1992.tb02154.x.

Biron, P. M., C. Robson, M. F. Lapointe, and S. J. Gaskin (2004), Comparing different methods of bed shear stress estimates in simple and complex flow fields, *Earth Surf. Process. Landforms*, *29*(11), 1403–1415, doi:10.1002/esp.1111.

Blanckaert, K. (2010), Topographic steering, flow recirculation, velocity redistribution, and bed topography in sharp meander bends, *Water Resour. Res.*, *46*(9), 1–23, doi:10.1029/2009WR008303.

Bretón, F., A. B. M. Baki, O. Link, D. Z. Zhu, and N. Rajaratnam (2013), Flow in nature-like fishway and its relation to fish behaviour, *Can. J. Civ. Eng.*, *40*(July 2012), 567–573, doi:10.1139/cjce-2012-0311.

Budwig, R. S., and P. Goodwin (2012), The Center for Ecohydraulics Research Mountain Stream Lab – a facility for collaborative research and education, in *Innovations 2012: world innovations in engineering education and research*, edited by W. Aung, V. Ilic, O. Mertanen, J. Moscinski, and J. Uhomoibhi, pp. 17–28, iNEER, Potomac, Maryland, USA.

Buffin-Bélanger, T., and A. G. Roy (1998), Effects of a pebble cluster on the turbulent structure of a depth-limited flow in a gravel-bed river, *Geomorphology*, *25*(3-4), 249–267, doi:10.1016/S0169-555X(98)00062-2.

Buffington, J. M., and D. R. Montgomery (1997), A systematic analysis of eight decades of incipient motion studies, with special reference to gravel-bedded rivers, *Water Resour. Res.*, *33*(8), 1993–2029, doi:10.1029/97WR03138.

Bunte, K., and S. R. Abt (2001), *Sampling Surface and Subsurface Particle-Size Distributions in Wadable Gravel- and Cobble-Bed Streams for Analyses in Sediment Transport, Hydraulics, and Streambed Monitoring*, General Technical Report RMRS-GTR-74, U.S. Dept. of Agriculture, Forest Service, Rocky Mountain Research Station, Fort Collins, CO.

Canovaro, F., E. Paris, and L. Solari (2007), Effects of macro-scale bed roughness geometry on flow resistance, *Water Resour. Res.*, *43*(10), 1–17, doi:10.1029/2006WR005727.

Casulli, V., and G. S. Stelling (1998), Numerical simulation of 3D quasi-hydrostatic, free-surface flows, *J. Hydraul. Eng.*, *124*(7), 678–686.

Cea, L., J. Puertas, and L. Pena (2007), Velocity measurements on highly turbulent free surface flow using ADV, *Exp. Fluids*, *42*, 333–348, doi:10.1007/s00348-006-0237-3.

Chanson, H. (1997), Air Bubble Entrainment in Open Channels. Flow structure and bubble size distribution, *Int. J. Multiph. Flow*, *23*(1), 193–203.

Chanson, H. (2004), Drag reduction in skimming flow on stepped spillways by aeration, *J. Hydraul. Res.*, *42*(3), 316–322, doi:10.1080/00221686.2004.9728397.

Chen, L., and M. C. Stone (2008), Influence of bed material size heterogeneity on bedload transport uncertainty, *Water Resour. Res.*, *44*(1), 1–11, doi:10.1029/2006WR005483.

Cheng, N. S. (2006), Influence of shear stress fluctuation on bed particle mobility, *Phys. Fluids*, *18*, 096602, doi:10.1063/1.2354434.

Cienciala, P., and M. A. Hassan (2013), Linking spatial patterns of bed surface texture, bed mobility, and channel hydraulics in a mountain stream to potential spawning substrate for small resident trout, *Geomorphology*, *197*, 96–107, doi:10.1016/j.geomorph.2013.04.041.

Claxton, A. J., P. D. Bates, and H. L. Cloke (2003), Mixing of Hillslope, River, and Alluvial Ground Waters in Lowland Floodplains, *GroundWater*, *41*(7), 926–936, doi:10.1111/j.1745-6584.2003.tb02435.x.

Clayton, J. A. (2012), Spatial Variations in Excess Shear Stress in a Gravel-Bed River Bend, *Phys. Geogr.*, *33*(1), 68–85, doi:10.2747/0272-3646.33.1.68.

Clayton, J. A., and J. Pitlick (2007), Spatial and temporal variations in bed load transport intensity in a gravel bed river bend, *Water Resour. Res.*, *43*, W02426, doi:10.1029/2006WR005253.

Clifford, N. J., and J. R. French (1993), Monitoring and analysis of turbulence in geophysical boundaries: some analytical and conceptual issues, in *Turbulence: Perspectives on Flow and Sediment Transport*, edited by N. J. Clifford, J. R. French, and J. Hardisty, pp. 93–120, John Wiley & Sons, Chichester, UK.

Clifford, N. J., A. Robert, and K. S. Richards (1992), Estimation of flow resistance in gravel-bedded rivers: A physical explanation of the multiplier of roughness length, *Earth Surf. Process. Landforms*, *17*(2), 111–126, doi:10.1002/esp.3290170202.

Cohen, J., P. Cohen, S. G. West, and L. Aiken (2003), *Applied Multiple Regression / Correlation Analysis for the Behavioral Sciences*, 3rd ed., Lawrence Erlbaum Associates, Inc., Publishers, Mahwah, New Jersey.

Constantinescu, G., M. Koken, and J. Zeng (2011), The structure of turbulent flow in an open channel bend of strong curvature with deformed bed: Insight provided by detached eddy simulation, *Water Resour. Res.*, *47*(5), 1–17, doi:10.1029/2010WR010114.

Cooper, J. R., J. Aberle, K. Koll, and S. J. Tait (2013), Influence of relative submergence on spatial variance and form-induced stress of gravel-bed flows, *Water Resour. Res.*, *49*(9), 5765–5777, doi:10.1002/wrcr.20464.

Deshpande, S. S., L. Anumolu, and M. F. Trujillo (2012), Evaluating the performance of the two-phase flow solver interFoam, *Comput. Sci. Discov.*, *5*(1), 014016, doi:10.1088/1749-4699/5/1/014016.

Dietrich, W. E., and P. Whiting (1989), Boundary Shear Stress and Sediment Transport In River Meanders of Sand and Gravel, in *River Meandering*, *American Geophysical Union - Water Resources. Monographs*, vol. 12, edited by S. Ikeda and G. Parker, pp. 1–50, American Geophysical Union, Washington, D.C., USA.

Egashira, S., and K. Ashida (1991), Flow resistance and sediment transportation in streams with step-pool bed morphology, in *Fluvial Hydraulics of Mountain Regions*, edited by A. Armanini and G. Di Silvio, pp. 45–58, Springer-Verlag.

Einstein, H. A. (1950), The Bed-Load Function for Sediment Transportation in Open Channel Flows, *Soil Conserv. Serv.*, (1026), 1–31.

Einstein, H. A., and N. L. Barbarosa (1952), River Channel Roughness, *Trans. Am. Soc. Civ. Eng.*, *117*(1), 1121–1132.

Esmaeili, T., A. A. Dehghani, A. R. Zahiri, and K. Suzuki (2009), 3D Numerical simulation of scouring around bridge piers (case study: bridge 524 crosses the Tanana River), *World Acad. Sci. Eng. Technol.*, *58*, 1028–1032.

Fausch, K. D. (1993), Experimental analysis of microhabitat selection by juvenile steelhead (Oncorhynchus mykiss) and coho salmon (O. kisutch) in a British Columbia stream, *Can. J. Fish. Aquat. Sci.*, *50*(6), 1198–1207, doi:10.1139/f93-136.

Ferguson, R. (2007), Flow resistance equations for gravel- and boulder-bed streams, *Water Resour. Res.*, *43*(5), 1–12, doi:10.1029/2006WR005422.

Ferguson, R. I. (2003), The missing dimension: Effects of lateral variation on 1-D calculations of fluvial bedload transport, *Geomorphology*, *56*, 1–14, doi:10.1016/S0169-555X(03)00042-4.

Francalanci, S., G. Parker, and E. Paris (2005), Effects of non-hydrostatic pressure distribution on bedload transport, in *4th IAHR Symposium on River, Estuarine, and Coastal Morphodynamics*, edited by G. Parker and M. H. Garcia, pp. 13–21, Taylor & Francis.

Francalanci, S., G. Parker, and L. Solari (2008), Effect of seepage-induced nonhydrostatic pressure distribution on bed-load transport and bed morphodynamics, *J. Hydraul. Eng.*, *134*(4), 378–389.

Frizell, K. W. (2002), Effects of Aeraton on the Performance of an ADV, in *2000 joint conference on water resources engineering and water resources planning and management. ASCE*, Minneapolis.

Gomez, B. (1993), Roughness of stable, armored gravel beds, *Water Resour. Res.*, *29*(11), 3631–3642, doi:10.1029/93WR01490.

Gomez, B., and M. Church (1989), An assessment of bed load sediment transport formulae for gravel bed rivers, *Water Resour. Res.*, *25*(6), 1161–1186, doi:10.1029/WR025i006p01161.

Gomez, B., and J. D. Phillips (1999), Deterministic uncertainty in bed load transport, *J. Hydraul. Eng.*, *125*(3), 305–308.

Gomez, B., R. Naff, and D. W. Hubbell (1989), Temporal variations in bedload transport rates associated with the migration of bedforms, *Earth Surf. Process. Landforms*, *14*(2), 135–156.

Grass, A. J. (1970), Initial instability of fine sand, *J. Hydraul. Div. Am. Soc. Civ. Eng.*, *96*, 19–632.

Griffith, J. S. (1993), Coldwater streams, in *Inland fisheries management in North America*, edited by C. C. Kohler and W. A. Hulbert, pp. 405–425, American Fisheries Society, Bethesda, Maryland.

Grotjans, H., and F. R. Menter (1998), Wall functions for industrial applications, in *Computational Fluid Dynamics' 98*, edited by K. D. Papailiou, D. Tsahalis, J. Périaux, C. Hirsch, and M. Pandolfi, pp. 1112–1117, John Wiley Sons, Chichester, UK.

Hajimirzaie, S. M., A. G. Tsakiris, J. H. J. Buchholz, and A. N. Papanicolaou (2014), Flow characteristics around a wall-mounted spherical obstacle in a thin boundary layer, *Exp. Fluids*, *55*(6), 1–14, doi:10.1007/s00348-014-1762-0.

Harrison, L. R., C. J. Legleiter, M. A. Wydzga, and T. Dunne (2011), Channel dynamics and habitat development in a meandering, gravel bed river, *Water Resour. Res.*, *47*(4), W04513, doi:10.1029/2009WR008926.

Hellsten, A. (1998), Some improvements in Menter's k-omega SST turbulence model, *29th AIAA, Fluid Dyn. Conf.*, 1–11, doi:10.2514/6.1998-2554.

Hirt, C. W., and B. D. Nichols (1981), Volume of fluid (VOF) method for the dynamics of free boundaries, *J. Comput. Phys.*, *39*(1), 201–225, doi:10.1016/0021-9991(81)90145-5.

Hopkinson, L., and T. Wynn (2009), Vegetation impacts on near bank flo, *Ecohydrology*, *2*, 404–418, doi:10.1002/eco.

Islam, M. R., and D. Z. Zhu (2013), Kernel Density–Based Algorithm for Despiking ADV Data, *J. Hydraul. Eng.*, *139*(7), 785–739, doi:10.1061/(ASCE)HY .1943-7900.0000734.

Issa, R. I. (1986), Solution of the implicitly discretised fluid flow equations by operator-splitting, *J. Comput. Phys.*, *62*(1), 40–65.

Jarrett, R. D. (1985), *Determination of Roughness Coefficients for Streams in Colorado*.

Jarrett, R. D. (1990), Hydrologic and hydraulic research in mountain rivers, *J. Am. Water Resour. Assoc.*, *26*(3), 419–429, doi:10.1111/j.1752-1688.1990.tb01381.x.

Katul, G. (2002), A mixing layer theory for flow resistance in shallow streams, *Water Resour. Res.*, *38*(11), 1–8, doi:10.1029/2001WR000817.

Kellerhals, R., and D. I. Bray (1971), Sampling procedures for coarse fluvial sediments, *J. Hydraul. Div. ASCE*, *97*, 1165–1180.

Keylock, C. J., A. Singh, J. G. Venditti, and E. Foufoula-Georgiou (2014), Robust classification for the joint velocity-intermittency structure of turbulent flow over fixed and mobile bedforms, *Earth Surf. Process. Landforms*, *39*(13), 1717–1728, doi:10.1002/esp.3550.

Khosronejad, A., C. D. Rennie, S. A. A. Salehi Neyshabouri, and R. D. Townsend (2007), 3D numerical modeling of flow and sediment transport in laboratory channel bends, *J. Hydraul. Eng.*, *133*(10), 1123–1134, doi:10.1061/(ASCE)0733-9429(2007)133:10(1123).

Kilpatrick, F. A., and J. F. Wilson (1989), Measurement of time of travel in streams by dye tracing, in *Techniques of water-resources investigations of the United States Geological Survey - Applications of Hydraulic*, pp. 1–27, U.S. Geological Survey, Water Resources Division, Reston, VA.

Kirchner, J. W., W. E. Dietrich, F. Iseya, and H. Ikeda (1990), The variability of critical shear stress, friction angle, and grain protrusion in water worked sediments, *Sedimentology*, *37*, 647–672.

Kironoto, B. A., and W. H. Graf (1994), Turbulence characteristics in rough uniform open-channel flow, *Proc. Inst. Civ. Eng. - Water Marit. Eng.*, *106*(4), 334–344, doi:http://dx.doi.org/10.1680/iwtme.1994.27234.

Kuzmin, D., and O. Mierka (2006), On the implementation of the κ-ε turbulence model in incompressible flow solvers based on a finite element discretisation, *Int. J. Comput. Sci. Math.*, *1*(2), 1–8, doi:10.1504/IJCSM.2007.016531.

Lacey, R. W. J., and C. D. Rennie (2012), Laboratory Investigation of Turbulent Flow Structure around a Bed-Mounted Cube at Multiple Flow Stages, *J. Hydraul. Eng.*, *138*(1), 71–84, doi:10.1061/(ASCE)HY.1943-7900.0000476.

Lacey, R. W. J. W. J., and A. G. Roy (2008), The spatial characterization of turbulence around large roughness elements in a gravel-bed river, *Geomorphology*, *102*(3-4), 542–553, doi:10.1016/j.geomorph.2008.05.045.

Lamb, M. P., W. E. Dietrich, and J. G. Venditti (2008), Is the critical shields stress for incipient sediment motion dependent on channel-bed slope?, *J. Geophys. Res. Earth Surf.*, *113*(2), 1–20, doi:10.1029/2007JF000831.

Lane, S. N., and K. S. Richards (1998), High resolution, two-dimensional spatial modelling of flow processes in a multi-thread channel, *Hydrol. Process.*, *12*(8), 1279–1298, doi:10.1002/(SICI)1099-1085(19980630)12:8<1279::AID-HYP615>3.0.CO;2-E.

Lane, S. N., K. F. Bradbrook, K. S. Richards, P. a. Biron, and a. G. Roy (1999), The application of computational fluid dynamics to natural river channels: Three-dimensional versus two-dimensional approaches, *Geomorphology*, *29*(1-2), 1–20, doi:10.1016/S0169-555X(99)00003-3.

Laronne, J. B., C. García, and I. Reid (2000), Mobility of patch sediment in gravel bed streams: patch character and its implications for bedload, in *Gravel-Bed Rivers V*, edited by M. P. Mosley, pp. 249–289, New Zealand Hydrological Society Inc., Wellington, New Zealand.

Lawless, M., and A. Robert (2001), Three dimensional flow structure around small-scale bedforms in a simulated gravel bed environment, *Earth Surf. Process. Landforms*, *26*, 507–522.

Leibundgut, C., P. Maloszewski, and C. Külls (2009), *Tracers in Hydrology*, John Wiley & Sons, Ltd.

Lenzi, M. A. (2001), Step-pool evolution in the Rio Cordon, Northeastern Italy, *Earth Surf. Process. Landforms*, *26*(9), 991–1008, doi:10.1002/esp.239.

Lenzi, M. A., L. Mao, and F. Comiti (2006), When does bedload transport begin in steep boulder-bed streams?, *Hydrol. Process.*, *20*(16), 3517–3533, doi:10.1002/hyp.6168.

Lepp, L. R., C. J. Koger, and J. A. Wheeler (1993), Channel erosion in steep gradient, gravel-paved streams, *Bull. Assoc. Eng. Geol.*, *30*(4), 443–454.

Li, C. ., and Y. . Zhang (1998), Simulation of free surface recirculating flows in semi-enclosed water bodies by a k–ω model, *Appl. Math. Model.*, *22*(3), 153–164, doi:10.1016/S0307-904X(98)00014-6.

Lisle, T. E., Y. Cui, G. Parker, J. E. Pizzuto, and A. M. Dodd (2001), The dominance of dispersion in the evolution of bed material waves in gravel-bed rivers, *Earth Surf. Process. Landforms*, *26*(13), 1409–1420, doi:10.1002/esp.300.

Liu, M., D. Z. Zhu, and N. Rajaratnam (2002), Evaluation of ADV measurements in bubbly two-phase flows, in *Hydraulic measurement and experiment methods 2002, proceedings of the specialty conference*, ASCE, Estes Park.

Liu, X., and M. H. García (2008), Three-Dimensional Numerical Model with Free Water Surface and Mesh Deformation for Local Sediment Scour, *J. Waterw. Port, Coastal, Ocean Eng.*, *134*(4), 203–217, doi:10.1061/(ASCE)0733-950X(2008)134:4(203).

Lupandin, A. I. (2005), Effect of Flow Turbulence on Swimming Speed of Fish, *Biol. Bull.*, *32*(5), 558–565, doi:10.1007/s10525-005-0125-z.

MacMurray, H. L. (1985), The use of the salt-velocity method for the precise measurement of resistance to flow in rough-boundary open channels, PhD Thesis, Department of Environmental Management, University of Canterbury.

Maddux, T. B., J. M. Nelson, and S. R. McLean (2003a), Turbulent flow over three-dimensional dunes: 1. Free surface and flow response, *J. Geophys. Res. Surf.*, *108*(F1), F16009, doi:F16009\r10.1029/2003jf000017.

Maddux, T. B., S. R. McLean, and J. M. Nelson (2003b), Turbulent flow over three-dimensional dunes: 2. Fluid and bed stresses, *J. Geophys. Res. Surf.*, *108*(F1), F16010, doi:F16010\r10.1029/2003jf000018.

Marcus, W. A., K. Roberts, L. Harvey, and G. Tackman (1992), An Evaluation of Methods for Estimating Manning's n in Small Mountain Streams, *Mt. Res. Dev.*, *12*(3), 227–239, doi:10.2307/3673667.

McLean, S. R., and V. I. Nikora (2006), Characteristics of turbulent unidirectional flow over rough beds: Double-averaging perspective with particular focus on sand dunes and gravel beds, *Water Resour. Res.*, *42*(10), 1–19, doi:10.1029/2005WR004708.

Mclean, S. R., and J. D. Smith (1986), A model for flow over two-dimensional bed forms, *J. Hydraul. Eng.*, *112*(4), 300–317.

McLean, S. R., S. R. Wolfe, and J. M. Nelson (1999), Spatially averaged flow over a wavy surface revisited, *J. Geophys. Res.*, *104*(C7), 743–753, doi:10.1029/1999JC900116.

Menter, F. R. (1992), *Improved two-equation k-omega turbulence models for aerodynamic flows*, NASA Technical Memorandum 103975 - Ames Research Center, Moffett Field, California, USA.

Menter, F. R. (1994), Two-equation eddy-viscosity turbulence models for engineering applications, *AIAA J.*, *32*(8), 1598–1605.

Menter, F. R., and T. Esch (2001), Elements of Industrial Heat Transfer Predictions, in *16th Brazilian Congress of Mechanical Engineering*, pp. 117–127, COBEM.

Menter, F. R., J. C. Ferreira, and T. Esch (2003), The SST Turbulence Model with Improved Wall Treatment for Heat Transfer Predictions in Gas Turbines, *Int. Gas Turbine Congr. 2003*, (1992), 1–7.

Moghadam, M. K., and A. Keshavarzi (2007), Flow separation behind habitat structure in gravel bed rivers, *J. fsheries Aquat. Sci.*, *2*(4), 294–301.

Moustakidis, I., A. N. Papanicolaou, and A. G. Tsakiris (2012), The effect of boulder spacing on flow patterns around boulders under partial submergence, in *4th International Junior Researcher and Engineer Workshop on Hydraulic Structures*, pp. 74–82.

Nagata, N., T. Hosoda, T. Nakato, and Y. Muramoto (2005), Three-Dimensional Numerical Model for Flow and Bed Deformation around River Hydraulic Structures, *J. Hydraul. Eng.*, *131*(12), 1074–1087, doi:10.1061/(ASCE)0733-9429(2005)131:12(1074).

Nelson, J. M., and R. R. McDonald (1995), *Mechanics and modeling of flow and bed evolution in lateral separation eddies*, Flagstaff, Arizona.

Nelson, J. M., S. R. McLean, and S. R. Wolfe (1993), Mean flow and turbulence fields over two-dimensional bed forms, *Water Resour. Res.*, *29*(12), 3935, doi:10.1029/93WR01932.

Nelson, J. M. et al. (2015), The International River Interface Cooperative: Public Domain Flow and Morphodynamics Software for Education and Applications, *Adv. Water Resour.*, doi:10.1016/j.advwatres.2015.09.017.

Nepf, H. M. (1999), Drag, turbulence, and diffusion in flow through emergent vegetation, *Water Resour. Res.*, *35*(2), 479–489.

Nepf, H. M., and E. R. Vivoni (2000), Flow structure in depth-limited, vegetated flow, *J. Geophys. Res.*, *105*(12), 28547–28557, doi:doi:10.1029/2000JC900145.

Nezu, L., and H. Nakagawa (1993), *Turbulence in Open Channel Flows*, Taylor & Francis, Rotterdam, Netherlands.

Nieves-Remacha, M. J., L. Yang, and K. F. Jensen (2015), OpenFOAM Computational Fluid Dynamic Simulations of Two-Phase Flow and Mass Transfer in an Advanced-Flow Reactor, *Ind. Eng. Chem. Res.*, *54*, 6649–6659, doi:10.1021/acs.iecr.5b00480.

Nikora, V., and D. Goring (2000), Flow turbulence over fixed and weakly mobile gravel beds, *J. Hydraul. Eng.*, *126*(9), 679–690.

Nikora, V., D. Goring, I. McEwan, and G. Griffiths (2001), Spatially averaged open-channel flow over rough bed, *J. Hydraul. Eng.*, *127*(2), 123–133.

Nitsche, M., D. Rickenmann, J. M. Turowski, A. Badoux, and J. W. Kirchner (2011), Evaluation of bedload transport predictions using flow resistance equations to account for macro-roughness in steep mountain streams, *Water Resour. Res.*, *47*, W08513, doi:10.1029/2011WR010645.

Olsen, N. R. B. (2003), Three-Dimensional CFD Modeling of Self-Forming Meandering Channel, *J. Hydraul. Eng.*, *129*(5), 366–372.

Ouellet, V., Y. Secretan, and J. Morin (2014), Daily averaged 2D water temperature model for the St. Lawrence river, *River Res. Appl.*, *30*, 733–744, doi:10.1002/rra.

Ouillon, S., and D. Dartus (1997), Three-dimensional computation of flow around a groyne, *J. Hydraul. Eng.*, *123*(11), 962–970.

Ozgoren, M., E. Pinar, B. Sahin, and H. Akilli (2011), Comparison of flow structures in the downstream region of a cylinder and sphere, *Int. J. Heat Fluid Flow*, *32*(6), 1138–1146, doi:10.1016/j.ijheatfluidflow.2011.08.003.

Pagliara, S., and P. Chiavaccini (2006), Flow Resistance of Rock Chutes with Protruding Boulders, *J. Hydraul. Eng.*, *132*(6), 545–552, doi:10.1061/(ASCE)0733-9429(2006)132:6(545).

Papanicolaou, A., A. Tsakiris, and C. Kramer (2010), Effects of relative submergence on flow and sediment patterns around clasts, in *River flow 2010 : Proceedings of the International Conference on Fluvial Hydraulics*, edited by A. Dittrich, K. Koll, J. Aberle, and P. Geisenhainer, Braunschweig, Germany.

Papanicolaou, A. N., and C. Kramer (2005), The role of relative submergence on cluster microtopography and bedload predictions in mountain streams, in *River, Coastal and Estuarine Morphodynamics. Proceeding of the 4th IAHR conference*, edited by G. Parker and M. H. Garcia, pp. 1083–1086, Urbana, Illinois, USA.

Papanicolaou, A. N., and C. Kramer (2006), The role of relative submergence on cluster microtopography and bedload predictions in mountain streams, in *River, Coastal and Estuarine Morphodynamics*, Taylor & Francis.

Papanicolaou, A. N., P. Diplas, C. L. Dancey, and M. Balakrishnan (2001), Surface Roughness Effects in Near-Bed Turbulence: Implications to Sediment Entrainment, *J. Eng. Mech.*, *127*(3), 211–218, doi:10.1061/(ASCE)0733-9399(2001)127:3(211).

Papanicolaou, A. N., P. Diplas, N. Evaggelopoulos, and S. Fotopoulos (2002), Stochastic Incipient Motion Criterion for Spheres under Various Bed Packing Conditions, *J. Hydraul. Eng.*, *128*(4), 369–380, doi:10.1061/(ASCE)0733-9429(2002)128:4(369).

Papanicolaou, A. N., A. Bdour, and E. Wicklein (2004), One-dimensional hydrodynamic/sediment transport model applicable to steep mountain streams, *J. Hydraul. Res.*, *00*(0), 1–19, doi:10.1080/00221686.2004.9641204.

Papanicolaou, A. N., C. M. Kramer, A. G. Tsakiris, I. Moustakidis, and T. L. Huff (2011), Depositional patterns in steep mountainous streams under low relative submergence (LRS) regime, in *World Environmental and Water Resources Congress*, edited by R. E. Beighley and M. W. Kilgore, pp. 2379–2388, American Society of Civil Engineers, Palm Springs, CA, USA.

Papanicolaou, A. N., C. M. Kramer, A. G. Tsakiris, T. Stoesser, S. Bomminayuni, and Z. Chen (2012), Effects of a fully submerged boulder within a boulder array on the mean and turbulent flow fields: Implications to bedload transport, *Acta Geophys.*, *60*(6), 1502–1546, doi:10.2478/s11600-012-0044-6.

Parker, G. (1990), Surface-based bedload transport relation for gravel rivers, *J. Hydraul. Res.*, *28*(4), 417–436, doi:10.1080/00221689009499058.

Parker, G., P. C. Klingeman, and D. G. McLean (1982), bedload and size distribution in paved gravel-bed streams, *J. Hydraul. Div.*, *108*(4), 544–571.

Peltier, Y., N. Rivière, S. Proust, E. Mignot, a. Paquier, and K. Shiono (2013), Estimation of the error on the mean velocity and on the Reynolds stress due to a misoriented ADV probe in the horizontal plane: Case of experiments in a compound open-channel, *Flow Meas. Instrum.*, *34*, 34–41, doi:10.1016/j.flowmeasinst.2013.08.002.

Pezzinga, G. (1994), Velocity distribution in compound channel flows by numerical modeling, *J. Hydraul. Eng.*, *120*(10), 1176–1198.

Pournazeri, S., S. S. Li, and F. Haghighat (2014), Efficient non-hydrostatic modelling of flow and bed shear stress in a pier scour hole, *Can. J. Civ. Eng.*, *41*(5), 450–460, doi:10.1139/cjce-2013-0160.

Raudkivi, A. J., and R. Ettema (1982), Stability of Armour Layers in Rivers, *J. Hydraul. Div.*, *108*(9), 1047–1057.

Recking, A. (2009), Theoretical development on the effects of changing flow hydraulics on incipient bed load motion, *Water Resour. Res.*, *45*(4), 1–16, doi:10.1029/2008WR006826.

Recking, A., P. Frey, A. Paquier, and P. Belleudy (2009), An experimental investigation of mechanisms involved in bed load sheet production and migration, *J. Geophys. Res. Solid Earth*, *114*(3), 1–13, doi:10.1029/2008JF000990.

Rickenmann, D., and A. Recking (2011), Evaluation of flow resistance in gravel-bed rivers through a large field data set, *Water Resour. Res.*, *47*(7), doi:10.1029/2010WR009793.

Rodi, W., and G. Scheuerer (1986), Scrutinizing the k-ε Turbulence Model Under Adverse Pressure Gradient Conditions, *J. Fluids Eng.*, *108*(2), 174–179.

Rodríguez, J. F., F. A. Bombardelli, M. H. García, K. M. Frothingham, B. L. Rhoads, and J. D. Abad (2004), High-resolution numerical simulation of flow through a highly sinuous river reach, *Water Resour. Manag.*, *18*, 177–199.

Roulund, A., B. M. Sumer, J. Fredsoe, J. Michelsen, J. Fredsøe, and J. Michelsen (2005), Numerical and experimental investigation of flow and scour around a circular pile, *J. Fluid Mech.*, *534*, 351–401, doi:10.1017/S0022112005004507.

Rusche, H. (2002), Computational Fluid Dynamics of Dispersed Two-Phase Flows at High Phase Fractions, Imperial College Imperial College of Science, Technology and Medicine, London.

Schmeeckle, M. W., and J. M. Nelson (2003), Direct numerical simulation of bedload transport using a local , dynamic boundary condition, *Sedimentology.*, *50*, 279–301, doi:10.1046/j.1365-3091.2003.00555.x.

Segura, C., and J. Pitlick (2015), Coupling fluvial-hydraulic models to predict gravel transport in spatially variable flows, *J. Geophys. Res. Earth Surf.*, *120*, 834–855, doi:10.1002/2014JF003302.

Shamloo, H., N. Rajaratnam, and C. Katopodis (2001), Hydraulics of simple habitat structures, *J. Hydraul. Res.*, *39*(4), 351–366.

Shevchuk, I., P. Rauschenberger, and J. Janicka (2012), A VOF method for isobaric expandable flows, in *83rd Meeting of the Association of Applied Mathematics and Mechanics*, vol. 12, pp. 531–532.

Silva, A. T., C. Katopodis, J. M. Santos, M. T. Ferreira, and A. N. Pinheiro (2012), Cyprinid swimming behaviour in response to turbulent flow, *Ecol. Eng.*, *44*, 314–328, doi:10.1016/j.ecoleng.2012.04.015.

Smart, G. M. (1999), Turbulent velocity profiles and boundary shear in gravel bed rivers, *J. Hydraul. Eng.*, *125*(2), 106–116.

Smith, D. L., E. L. Brannon, and M. Odeh (2005), Response of Juvenile Rainbow Trout to Turbulence Produced by Prismatoidal Shapes, *Trans. Am. Fish. Soc.*, *134*(3), 741–753, doi:10.1577/T04-069.1.

Smith, J. D., and S. R. McLean (1977), Spatially averaged flow over a wavy surface, *J. Geophys. Res.*, *82*(12), 1735, doi:10.1029/JC082i012p01735.

Stoesser, T., D. von Terzi, W. Rodi, and N. R. B. Olsen (2006), RANS Simulation and LES of Flow Over Dunes at Low Relative Submergence Ratios, in *Proceedings of the 7th International Conference on HydroScience and Engineering (ICHE 2006)*, Philadelphia, USA.

Straub, L. G., and O. P. Lamb (1956), Studies of air entrainment in open-channel flows, *Trans. Am. Soc. Civ. Eng.*, *121*, 30–44.

Straub, L. G., J. M. Killen, and O. P. Lamb (1954), Velocity measurement of air-water mixtures, *Trans. Am. Soc. Civ. Eng.*, *119*, 207–220.

Strom, K. B., and A. N. Papanicolaou (2007), ADV Measurements around a Cluster Microform in a Shallow Mountain Stream, *J. Hydraul. Eng.*, *133*(12), 1379–1389, doi:10.1061/(ASCE)0733-9429(2007)133:12(1379).

Sukhodolov, A. N., J. J. Fedele, and B. L. Rhoads (2004), Turbulent flow over mobile and molded bedforms: a comparative field study, in *River Flow 2004. Proceedings of the Second International Conference on Fluvial Hydraulics*, edited by M. Greco, A. Carravetta, and R. Della Morte, pp. 317–325, CRC Press, Napoli, Italy.

Sukhodolov, A. N., J. J. Fedele, and B. L. Rhoads (2006), Structure of flow over alluvial bedforms: an experiment on linking field and laboratory methods, *Earth Surf. Process. Landforms*, *31*(10), 1292–1310, doi:10.1002/esp.1330.

Sutcliffe, A. G. (2014), Modelling the effects of aquatic plant growth and management on the hydraulics of a chalk stream, University of London.

Thompson, D. M. (2007), The characteristics of turbulence in a shear zone downstream of a channel constriction in a coarse-grained forced pool, *Geomorphology*, *83*(3-4), 199–214, doi:10.1016/j.geomorph.2006.05.001.

Tonina, D., and J. M. Buffington (2009), Hyporheic exchange in mountain rivers I: Mechanics and environmental effects, *Geogr. Compass*, *3*(3), 1063–1086, doi:10.1111/j.1749-8198.2009.00226.x.

Tonina, D., and K. Jorde (2013), Hydraulic modelling approaches for ecohydraulic studies: 3D, 2D, 1D and non-numerical models, in *Ecohydraulics: An Integrated Approach*, edited by I. Maddock, A. Harby, P. Kemp, and P. Wood, pp. 31–74, John Wiley & Sons, Ltd, Chichester, UK.

Tritico, H. M., and R. H. Hotchkiss (2005), Unobstructed and Obstructed Turbulent Flow in Gravel Bed Rivers, *J. Hydraul. Eng.*, *131*(8), 635–645, doi:10.1061/(ASCE)0733-9429(2005)131:8(635).

Tsakiris, A. G., a. N. T. Papanicolaou, S. M. Hajimirzaie, and J. H. J. Buchholz (2014), Influence of collective boulder array on the surrounding time-averaged and turbulent flow fields, *J. Mt. Sci.*, *11*(6), 1420–1428, doi:10.1007/s11629-014-3055-8.

Vallé, B. L., and G. B. Pasternack (2006), Submerged and unsubmerged natural hydraulic jumps in a bedrock step-pool mountain channel, *Geomorphology*, *82*(1-2), 146–159, doi:10.1016/j.geomorph.2005.09.024.

Venditti, J. G., and S. J. Bennett (2000), Spectral analysis of turbulent flow and suspended sediment transport over fixed dunes, *J. Geophys. Res.*, *105*(C9), 22,035–22,047.

Vollmer, S., and M. G. Kleinhans (2007), Predicting incipient motion, including the effect of turbulent pressure fluctuations in the bed, *Water Resour. Res.*, *43*(5), 1–16, doi:10.1029/2006WR004919.

Waldon, M. G. (2004), Estimation of Average Stream Velocity, *J. Hydraul. Eng.*, *130*(11), 1119–1122, doi:10.1061/(ASCE)0733-9429(2004)130:11(1119).

Webel, G., and M. Schatzmann (1984), Transverse Mixing in Open Channel Flow, *J. Hydraul. Eng.*, *110*(4), 423–435, doi:10.1061/(ASCE)0733-9429(1984)110:4(423).

Weller, H. G. (2005), *Derivation, modelling and solution of the conditionally averaged two-phase flow equations. Technical Report, OpenCFD Ltd.*, London, United Kingdom.

Weller, H. G., G. Tabor, H. Jasak, and C. Fureby (1998), A tensorial approach to computational continuum mechanics using object-oriented techniques, *Comput. Phys.*, *12*(6), 620–631, doi:10.1063/1.168744.

White, B. L., and H. M. Nepf (2007), Shear instability and coherent structures in shallow flow adjacent to a porous layer, *J. Fluid Mech.*, *593*, 1–32, doi:10.1017/S0022112007008415.

Whittaker, J. G. (1986), An Equation for Predicting bedload transport in steep mountain Step-Pool Stream, in *9th Australasian Fluid Mechanics Conference*, pp. 358–361, Auckland.

Wiberg, P. L., and J. D. Smith (1991), Velocity distribution and bed roughness in high-gradient streams, *Water Resour. Res.*, *27*(5), 825–838, doi:10.1029/90WR02770.

Wilcock, P. R., and J. C. Crowe (2003), Surface-based Transport Model for Mixed-Size Sediment, *J. Hydraul. Eng.*, *129*(2), 120–128, doi:10.1061/(ASCE)0733-9429(2003)129:2(120).

Wilcox, A. C., and E. E. Wohl (2007), Field measurements of three-dimensional hydraulics in a step-pool channel, *Geomorphology*, *83*(3-4), 215–231, doi:10.1016/j.geomorph.2006.02.017.

Wilcox, A. C., J. M. Nelson, and E. E. Wohl (2006), Flow resistance dynamics in step-pool channels: 2. Partitioning between grain, spill, and woody debris resistance, *Water Resour. Res.*, *42*(5), 1–14, doi:10.1029/2005WR004278.

Wilcox, D. C. (1988), Reassessment of the scale-determining equation for advanced turbulence models, *Am. Inst. Aeronaut. Astronaut.*, *26*(11), 1299–1310.

Wilson, C., J. Boxall, I. Guymer, and N. R. B. Olsen (2003), Validation of a three-dimensional numerical code in the simulation of pseudo-natural meandering flows, *J. Hydraul. Eng.*, *10*(10), 758–768, doi:10.1061/(ASCE)0733-9429(2003)129:10(758).

Wohl, E. E., and D. M. Thompson (2000), Velocity Characteristics Along a Small Step-Pool Channel, *Earth Surf. Process. Landforms*, *25*, 353–367.

Wu, F.-C., and K.-H. Yang (2004), Entrainment probabilities of mixed-size sediment incorporating near-bed coherent flow structures, *J. Hydraul. Eng.*, *130*(12), 1187–1197, doi:10.1061/(ASCE)0733-9429(2004)130:12(1187).

Wu, W., W. Rodi, and T. Wenka (2000), 3D numerical modeling of flow and sediment transport in open channels, *J. Hydraul. Eng.*, *126*(1), 4–15.

Yager, E. M., and M. W. Schmeeckle (2013), The influence of vegetation on turbulence and bed load transport, *J. Geophys. Res. Earth Surf.*, *118*(3), 1585–1601, doi:10.1002/jgrf.20085.

Yager, E. M., J. W. Kirchner, and W. E. Dietrich (2007), Calculating bed load transport in steep boulder bed channels, *Water Resour. Res.*, *43*(7), 1–24, doi:10.1029/2006WR005432.

Yager, E. M., W. E. Dietrich, J. W. Kirchner, and B. W. McArdell (2012), Prediction of sediment transport in step-pool channels, *Water Resour. Res.*, *48*(1), 1–20, doi:10.1029/2011WR010829.

Ye, J., and J. A. Mccorquodale (1998), Simulation of curved open channel flows by 3D hydrodynamic model, *J. oh Hydraul. Eng.*, *124*(7), 687–698.

Zalesak, S. T. (Naval R. L. (1979), Fully multidimensional flux-corrected transport algorithms for fluids, *J. Comput. Phys.*, *31*, 335–362.

Zanke, U. C. E. (2003), On the influence of turbulence on the initiation of sediment motion, *Int. J. Sediment Res.*, *18*(1), 17–31.

Zeng, J., G. Constantinescu, and L. Weber (2005), A fully 3D non-hydrostatic model for prediction of flow, sediment transport and bed morphology in open channels, in *31st International Association Hydraulic Research Congress*, pp. 554–560, Seoul, Korea.

Zeng, J., G. Constantinescu, and L. Weber (2008), A 3D non-hydrostatic model to predict flow and sediment transport in loose-bed channel bends, *J. Hydraul. Res.*, *46*(3), 356–372, doi:10.3826/jhr.2008.3328.

Zong, L., and H. Nepf (2011), Spatial distribution of deposition within a patch of vegetation, *Water Resour. Res.*, *47*(3), W03516, doi:10.1029/2010WR009516.

Table 2.1: Summary of the primary experiments details

Experiment	Channel slope	Flow discharge	Flow depth[b]	Flow depth Upstream of hemisphere[c]	Relative submergence	Flow velocity[b]	Reynolds Number[d]	Froude Number[d]	Reynolds Particle Number[d]
	S_{bed}	Q	h_a	h_{au}	$\frac{h_a}{D_I/2}$; $\frac{h_{au}}{D_I/2}$	U_a	Re	Fr	Re^*
	[m/m]	[m^3/s]	[m]	[ ]	[ ]	[m/s]	[]	[]	[]
S2.15%I[a]	0.0215	0.0596	0.082	0.113	1.08 ; 1.48	0.620	50879	0.690	337
S2.15%F[a]	0.0215	0.0596	0.077	0.114	1.01 ; 1.50	0.590	45112	0.680	324
S2.40%I	0.0240	0.0530	0.074	0.100	0.98 ; 1.31	0.620	45936	0.726	347
S2.40%F	0.0240	0.0530	0.066	0.123	0.86 ; 1.61	0.640	41973	0.796	382
S2.70%I	0.0270	0.0466	0.062	0.093	0.81 ; 1.22	0.520	32112	0.667	451
S2.70%F	0.0270	0.0466	0.061	0.105	0.80 ; 1.37	0.590	35841	0.763	438

a) The last letter I or F indicates the initial and final bed conditions, respectively.

b) Measured reach-averaged flow or velocity.

c) Flow depth measured just upstream of the hemisphere.

d) Reynolds and Froude number were based on U_a and h_a ; Reynolds particle number was based on bed surface grains

Table 2.2: RMSE of the predicted velocity and water surface elevation

	Velocity RMSE			Water Surface Elevation				
	U_X	U_Y	U_Z	Slope Measured[b]	Slope Predicted	RMSE [m]		
	[m/s]	[m/s]	[m/s]	[ ]	[ ]	Left	Center	Right
S2.15%I[a]				0.0271	0.0260	0.010	0.008	0.013
S2.15%F	0.057	0.066	0.069	0.0179	0.0191	0.006	0.006	0.009
S2.40%I[a]				0.0183	0.0172	0.008	0.003	0.006
S2.40%F	0.046	0.059	0.077	0.0226	0.0225	0.004	0.002	0.007
S2.70%I[a]				0.0290	0.0280	0.005	0.004	0.006
S2.70%F	0.057	0.045	0.039	0.0198	0.0215	0.010	0.005	0.007

a) No ADV measurement were collected for the initial bed conditions

b) WSE slopes shown here correspond to the section used in the numerical model along the center profile and do not necessarily represent the reach-averaged water surface slope (see Figure 3 b).

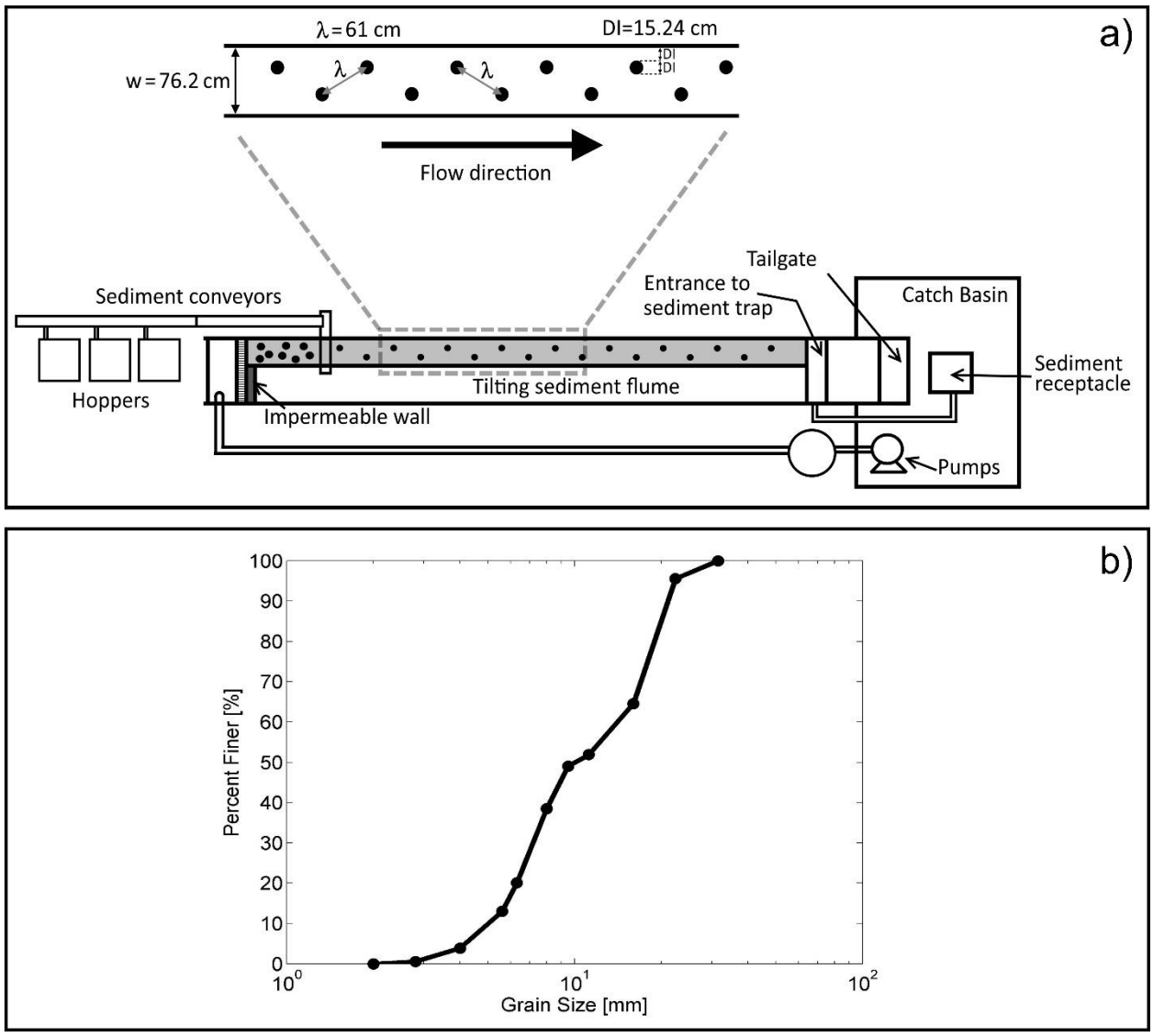

Figure 3.1: a) Plan view of the experiment setup. An impermeable wall was placed near the middle of the flume to reduce the width (b) Grain size distribution used for the sediment and the upstream sediment supply.

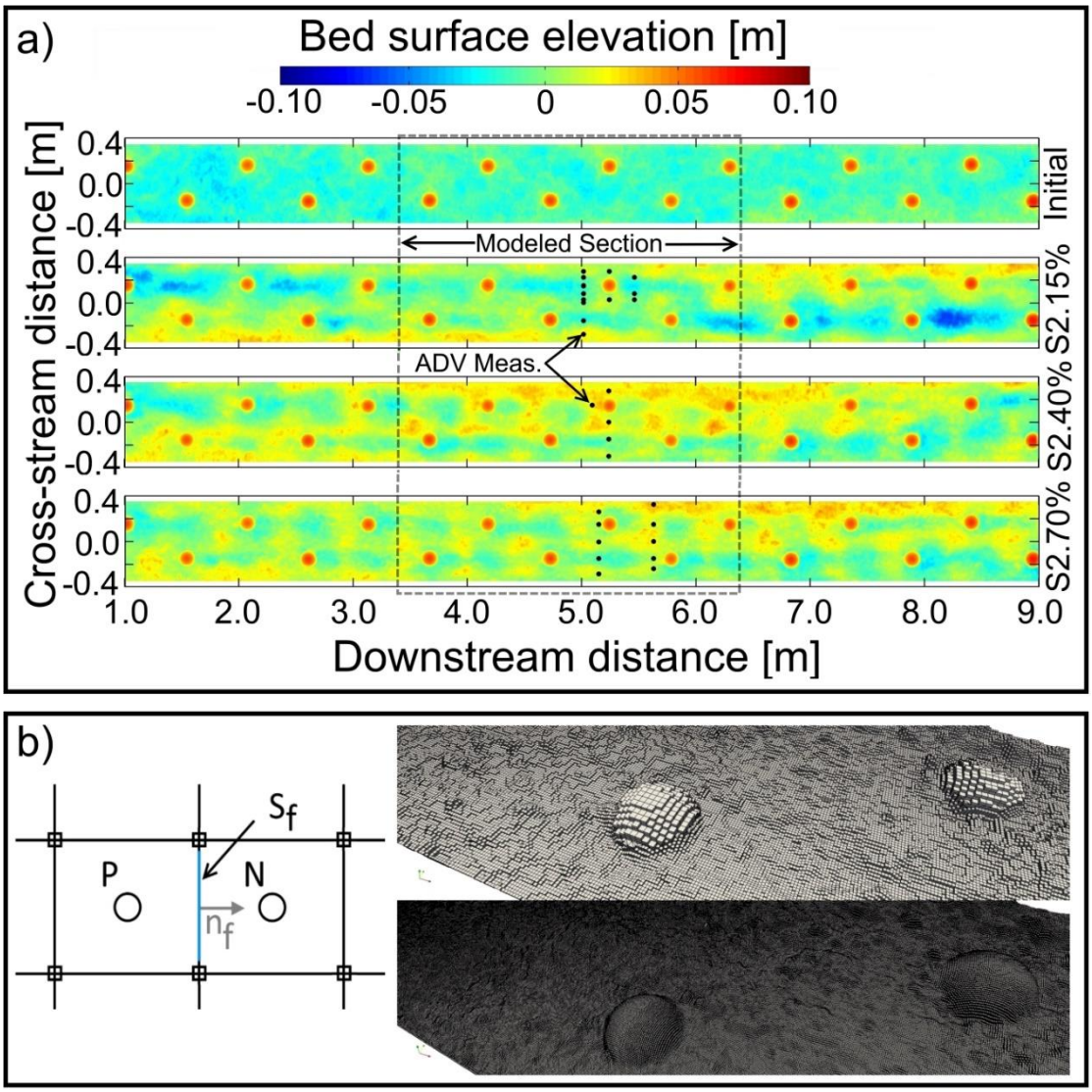

Figure 3.2: a) Topography (net bed slope removed) for the initial and final bed conditions for each experiment. The section (from 3.4 to 6.4 m) showed as a segmented line was used in the numerical flow model. ADV measurement locations (black dots) varied depending on the particular flow conditions of each experiment. b) On the left the definitions used in the discrete mesh for the finite volume technique are shown (see section 3.3.3), and on the right is a comparison of the initial coarse and final fine meshes. All results in this study are from the fine mesh.

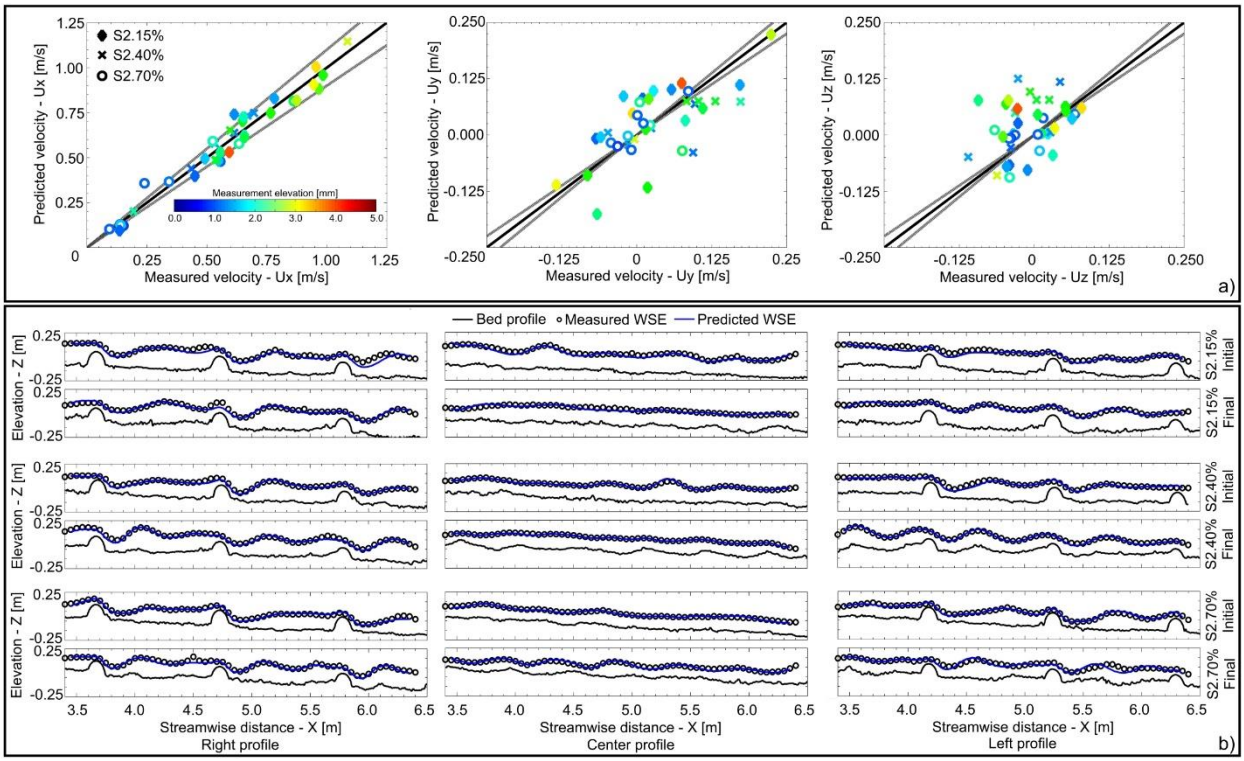

Figure 3.3: Measured and predicted values for: a) velocity in three directions (see Figure 3.2 a) colored by their elevation above to the bed (local elevation). All velocity data are for the final bed condition. Gray lines indicate a 10% deviation from the measured velocity b) Water surface elevations along three profiles (right, center and left). Initial and final bed conditions for all three profiles and experiments are shown.

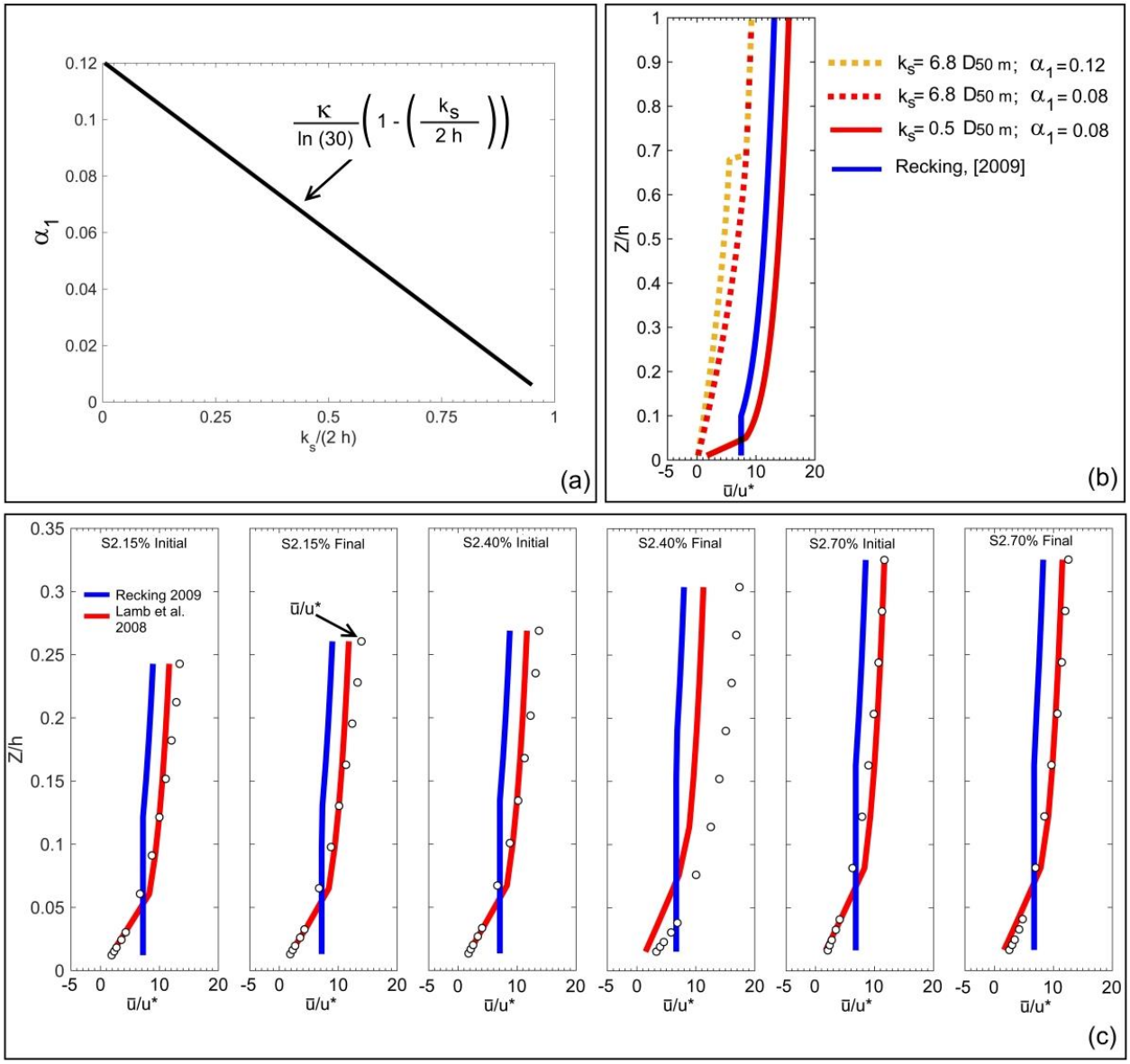

Figure 3.4: a) Variation of the α_1 coefficient as a function of k_s and h when deep flow is not assumed. b) Reach-averaged dimensionless velocity profiles ($\bar{u}/u*$) predicted by *Lamb et al.* [2008] for different definitions of k_s and α_1. c) Velocity profiles as a function of the dimensionless elevation (Z/h) for the initial and final bed conditions in all experiments. Black circles within the figures are the model's result, the velocity profiles of *Lamb et al.* [2008] and *Recking* [2009] with $k_s = 0.5\,D_{50m}$ and α_1 calculated with equation 3.13 are included for comparison. Standard error bars were not included because they fell within the symbol diameter.

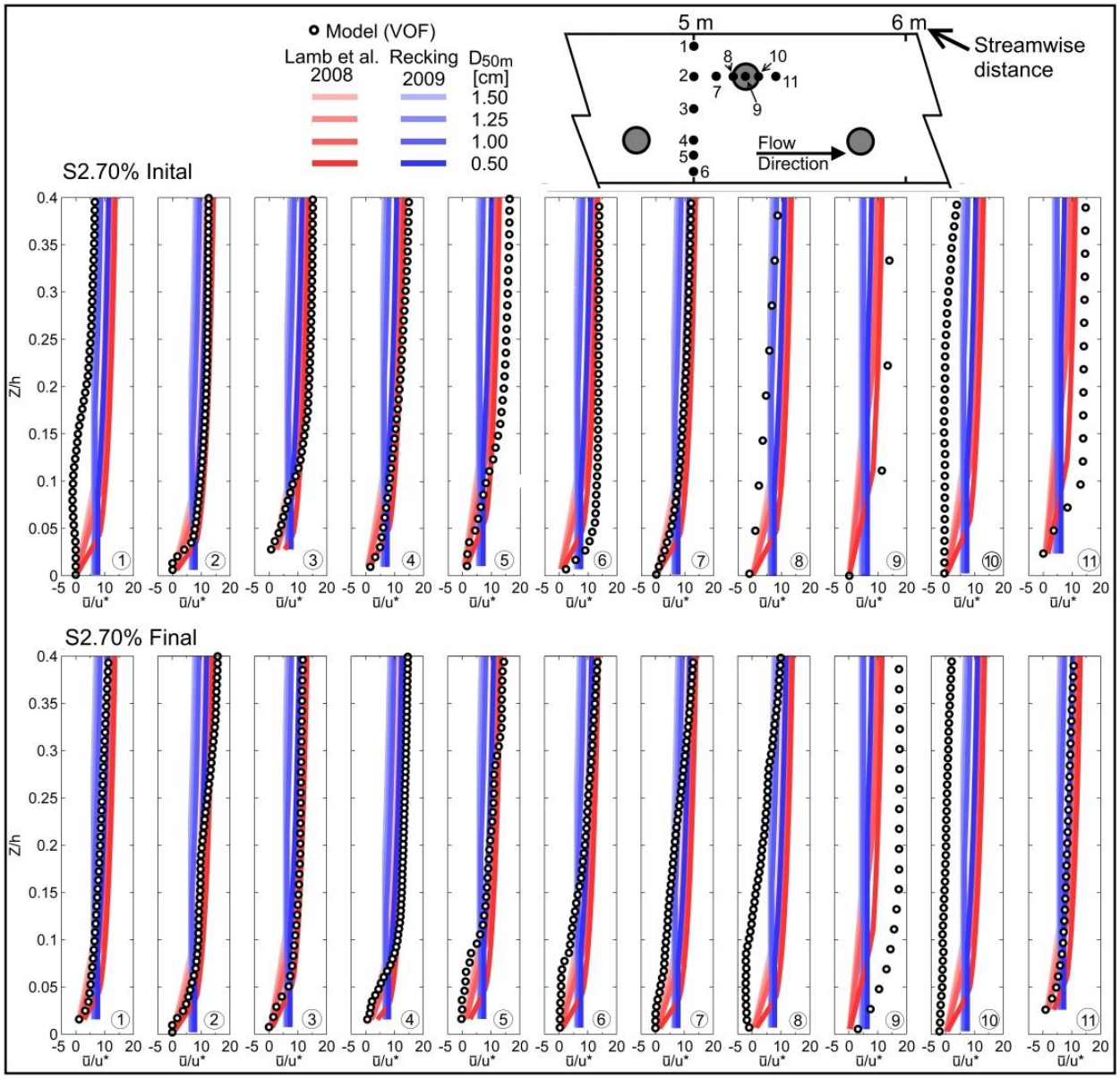

Figure 3.5: Local velocity profiles for the initial and final bed conditions in experiment S2.70%. Circled numbers in the lower right corner of each figure correspond to the sampling locations that are shown in the top cartoon. Velocity profiles of *Lamb et al.* [2008] and *Recking* [2009] were calculated for a range of D_{50m} to show the dependency on the local grain size distribution. The selected range correspond to observed values of D_{50m} in different bed areas of the experiments.

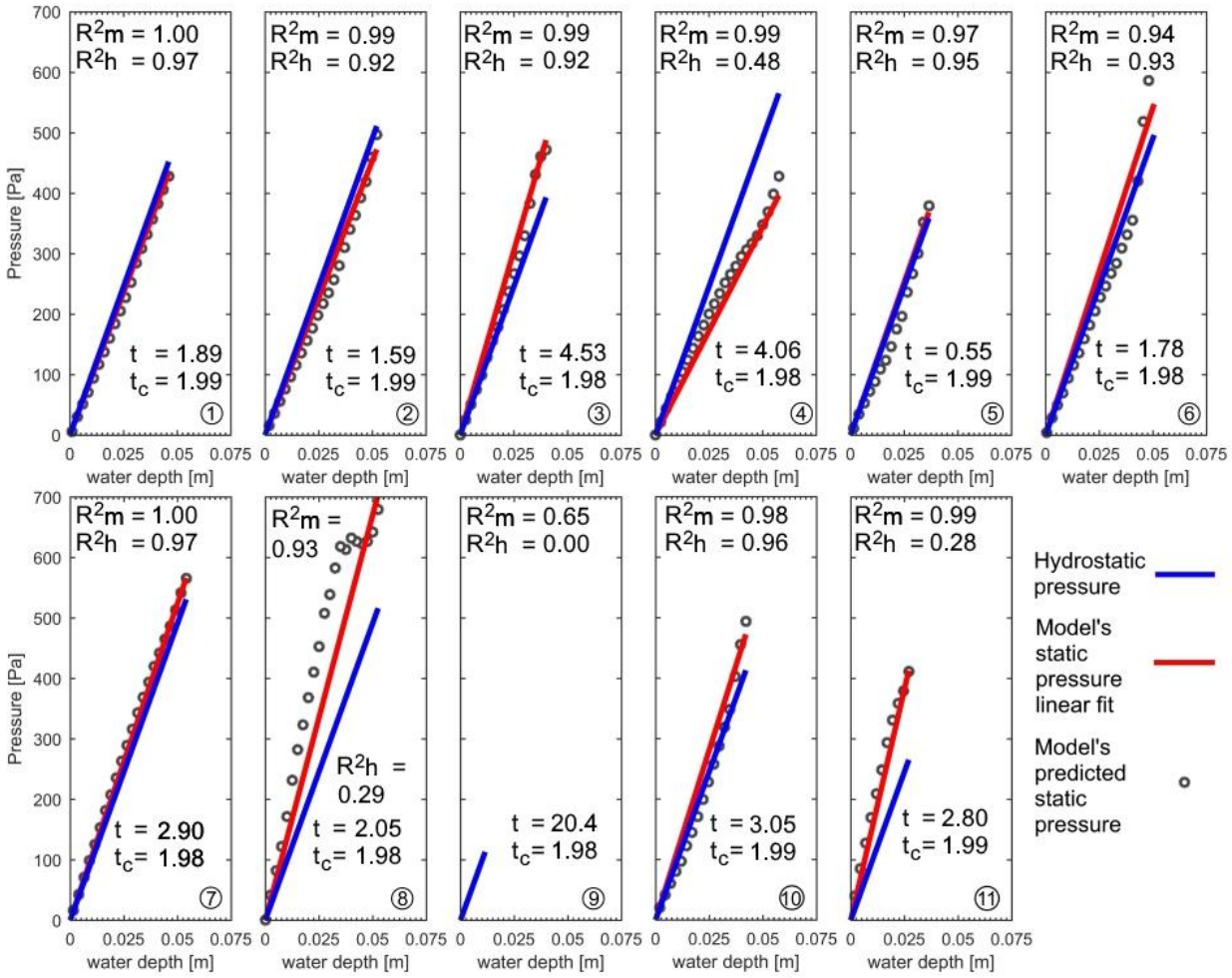

Figure 3.6: Comparisons of the static pressure profile to the hydrostatic pressure distribution for the final bed condition in experiment S2.70%. Sample locations are the same as in Figure 3.5. Within each figure two coefficients of determination (R^2) are shown; R^2m was obtained from a linear regression to the model's static pressure and R^2h indicates how well the hydrostatic pressure distribution fit the model's static pressure. In addition, t and t critical (t_c) are the scores for the z-test of *Cohen et al.* [2003]. If $t \leq t_c$ the slopes are not statistically different with 95% confidence.

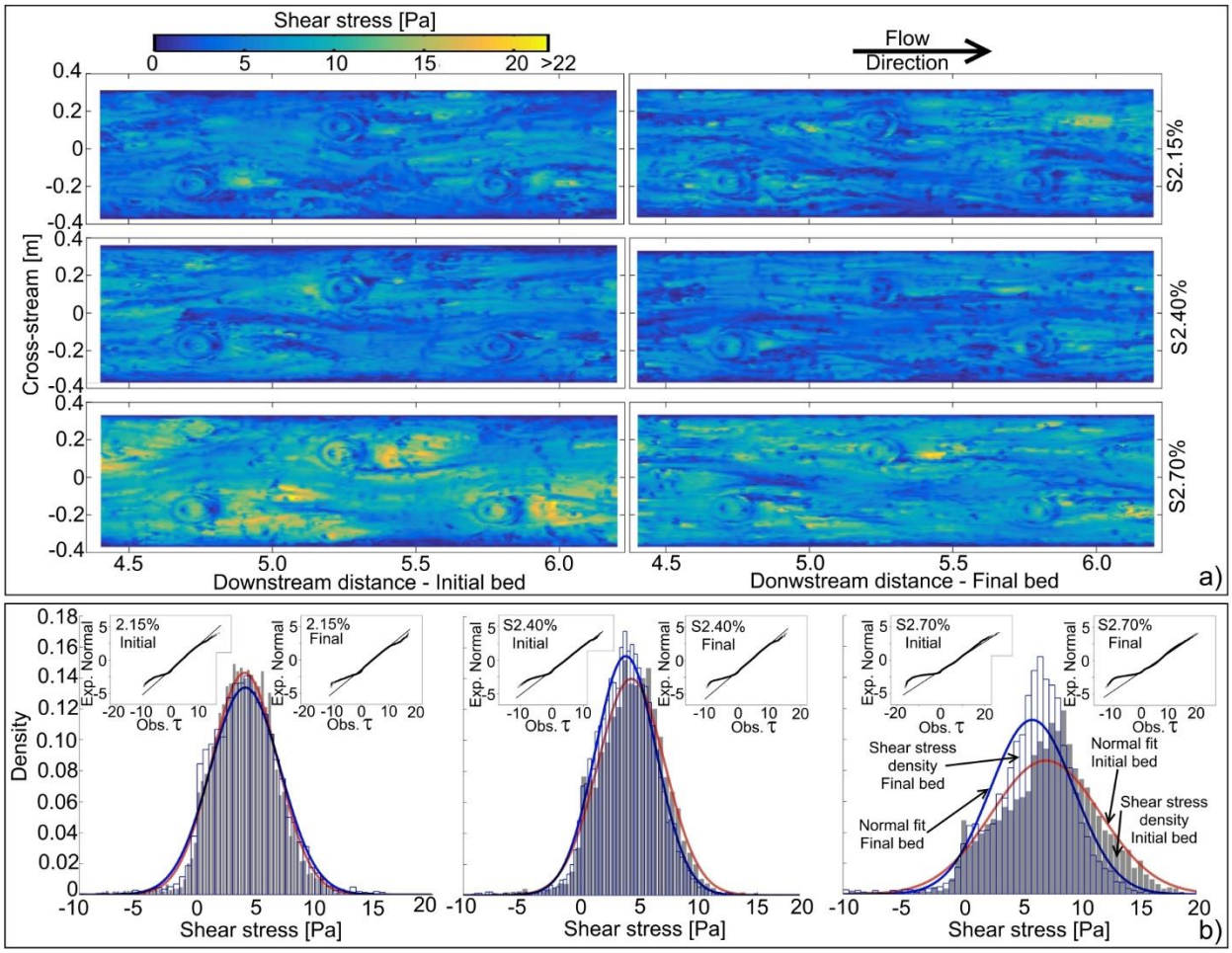

Figure 3.7: a) A comparison of the near-bed shear stress distribution between initial and final bed conditions (rows) and between experiments (columns). For clarity only a portion of the test section is shown. b) Histograms of near-bed streamwise shear stress distributions. Gray filled and transparent blue histograms correspond to the observed (from the model) shear stress densities for the initial and final bed conditions, respectively. Blue (initial bed) and red (final bed) thick lines are the normal distribution fits. Boxes inside each density plot are quantile-quantile plots for the normal distribution. The straight line indicates a match between the predicted (normal distribution) and observed shear stresses.

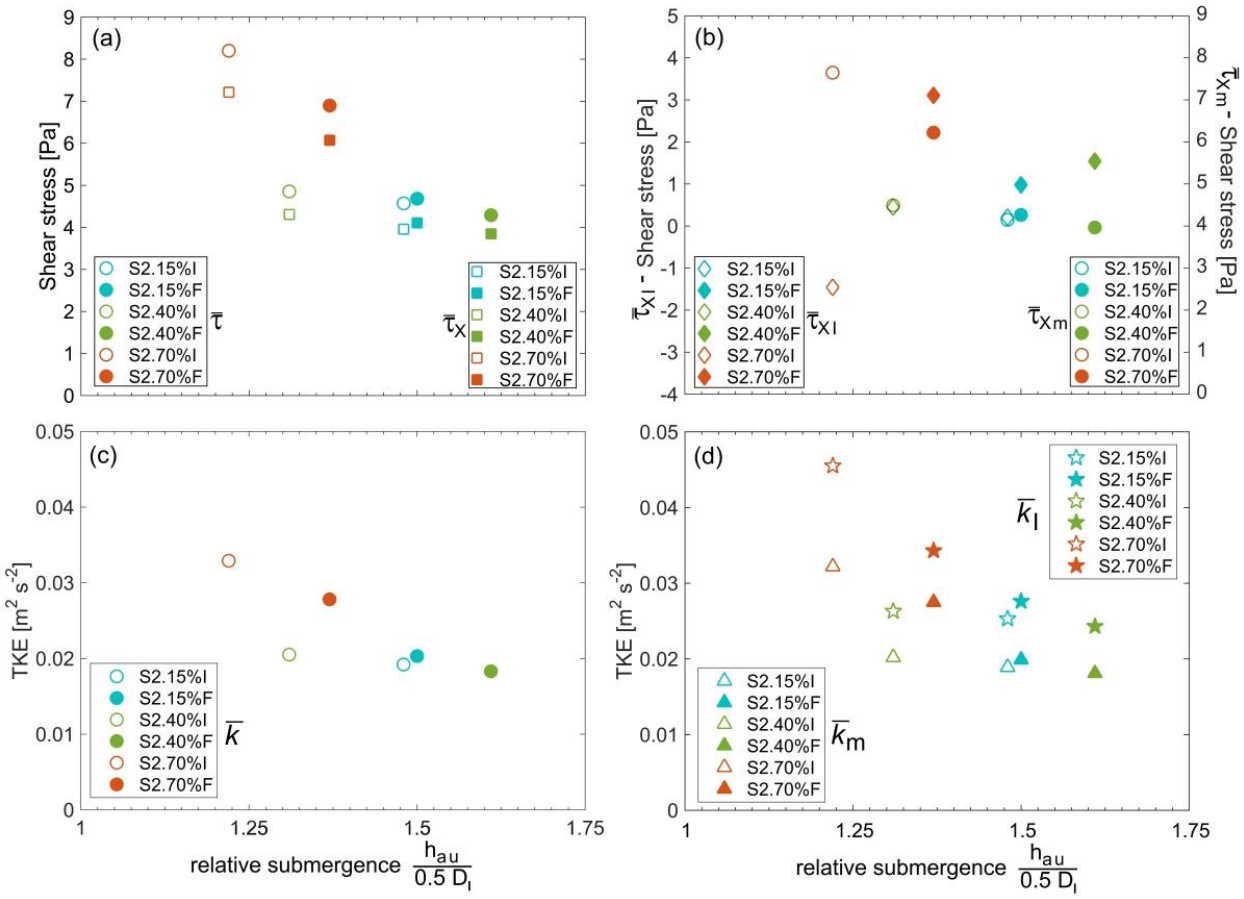

Figure 3.8 : Variation in the (a) reach-averaged, downstream, (b) mobile bed and immobile bed averaged shear stresses and (c) reach-averaged and (d) mobile and immobile bed averaged turbulent kinetic energies as a function of the relative submergence. Symbols are colored by experiment's slope.

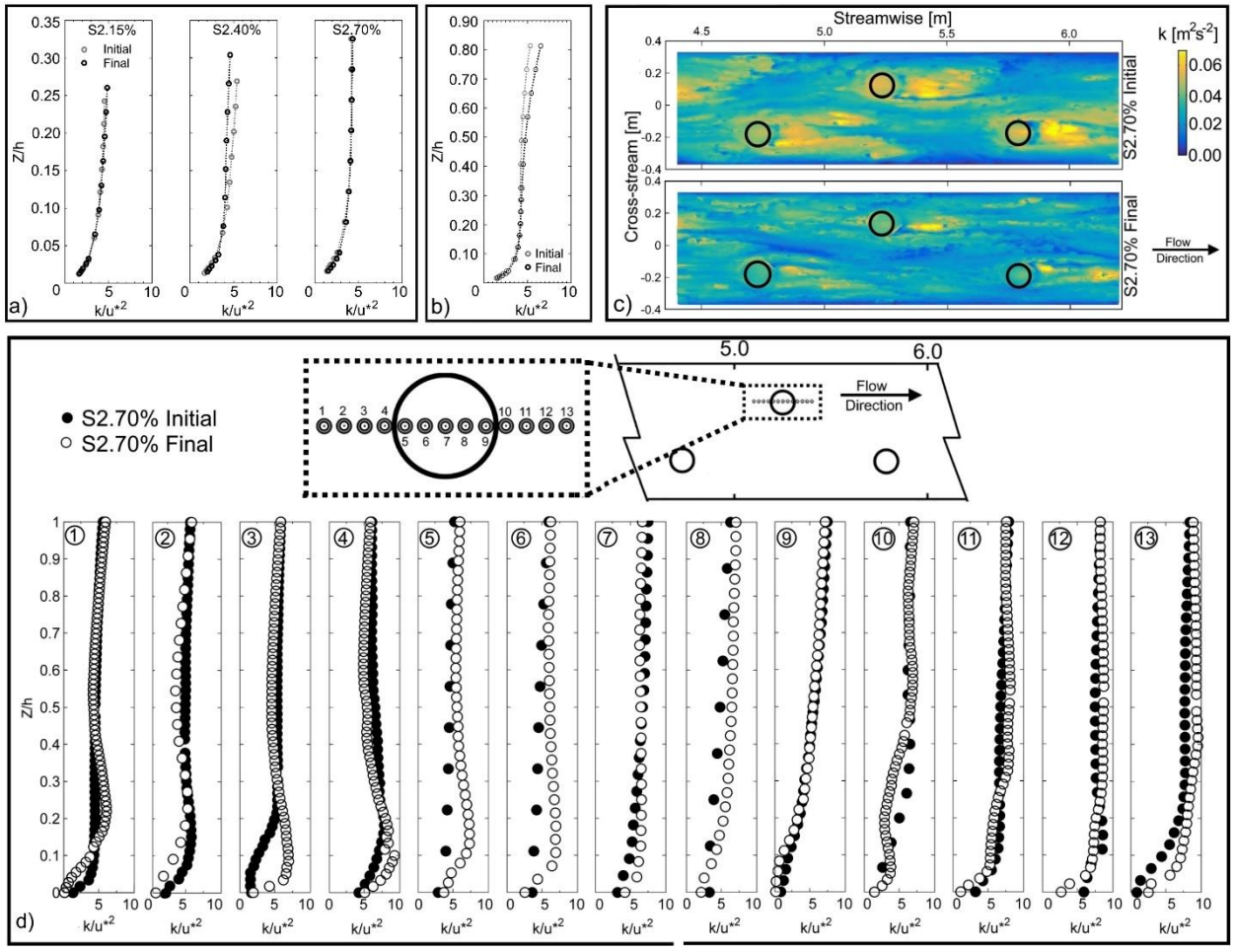

Figure 3.9: a) Dimensionless reach-averaged near-bed turbulent kinetic energies for initial and final bed conditions in all experiments as functions of the dimensionless elevation (Z / h). b) Dimensionless reach-averaged turbulent kinetic energy for initial (grey lines) and final (black lines) bed conditions of experiment S2.70% as a function of the dimensionless elevation. c) Near-bed turbulent kinetic energy distribution for experiment S2.70% for initial and final bed conditions. Only a portion of the test section is shown. d) Local near-bed turbulent kinetic energy profiles for experiment S2.70%. Locations of each profile are shown in the upper sketch.

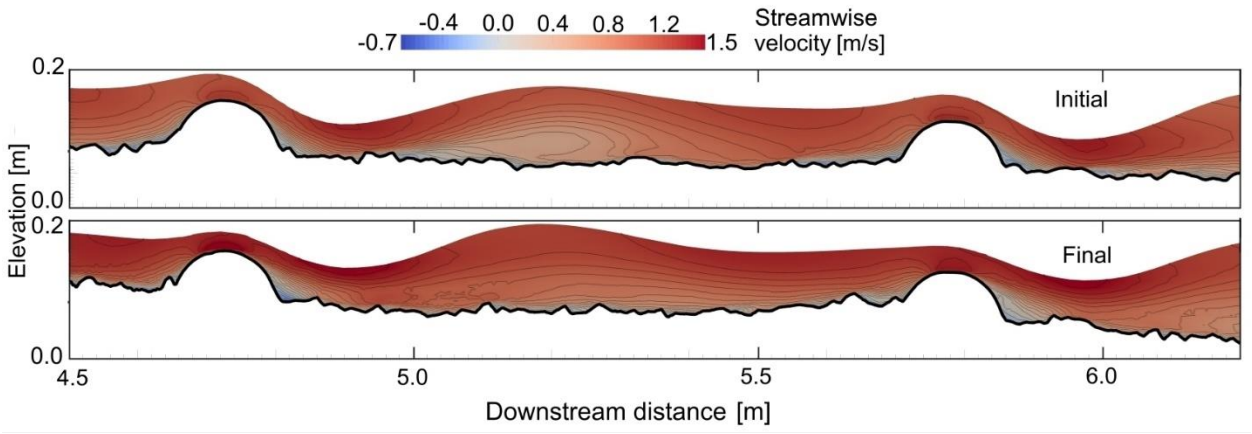

Figure 3.10: Water surface elevation and streamwise velocity contours for experiment S2.15% for the initial and final bed conditions. Flow is from left to right.

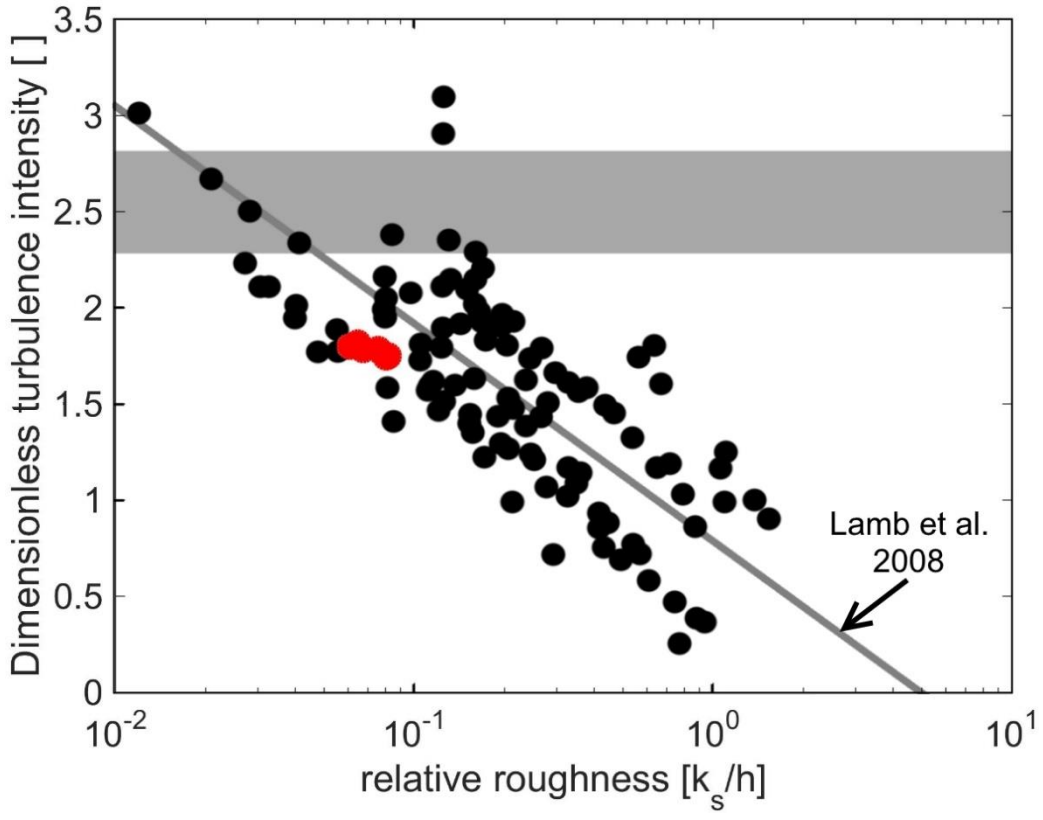

Figure 3.11: Near-bed dimensionless turbulence intensity (σ_{uX}/u_*) as a function of the relative roughness. Red and black dots correspond to our experiments and those from Figure 5 in *Lamb et al.* [2008], respectively. The equation of *Lamb et al.* [2008] is shown as a straight line and the grey filled area is the hydraulically smooth region.

Chapter 4: Bed surface adjustments to spatially variable flow induced by large immobile grains under low relative submergence regime

4.1 Abstract

In mountainous rivers, large relatively immobile grains partly control the local and reach-averaged flow hydraulics and sediment fluxes. When the flow depth is similar to the size of these large protruding grains (low relative submergence), highly three dimensional flow structures and plunging flow occur which affect the spatial distribution of the bed surface elevation, texture and sedimentation. To explore how the bed surface responds to these flow obstructions we conducted a set of experiments in which we varied the relative submergence while holding the average sediment transport capacity and upstream sediment supply constant. We used staggered hemispheres to simulate large boulders and at the beginning of each experiment the bed thickness and grain size distribution was identical. To obtain details on the flow structure around the hemispheres we combined our laboratory measurements with a 3D flow model. The divergence in shear stress caused by the hemispheres promoted size-selective bedload transport and formed a patch of coarse sediment in the hemisphere's upstream region. Changes in bed elevation caused a decrease in local shear stress, which combined with the increase in grain size enhanced the stability of this patch. The region downstream of the hemispheres was largely controlled by a recirculation zone and had little to no change in grain size. The formation, development and stability of sediment patches is controlled by spatial variability of shear stress, in particular to the combination of shear stress divergence and magnitude and direction of the local shear stress field.

4.1.1 Key points

Sediment deposition is controlled by the presence of an obstacle in low relative submergence

Upstream of an obstacle selective deposition of coarse particles occurred

Downstream of an obstacle little to no change in grain size distribution occurred

4.2 Introduction

Mountains rivers are characterized by highly three-dimensional flow, and large spatial variations in bed surface elevation and texture. Spatial changes in flow are a response to large immobile grains [*Bathurst*, 1978; *Lenzi*, 2004; *Yager et al.*, 2007, 2012b, 2012c; *Nitsche et al.*, 2011; *Wilcox et al.*, 2011], large woody debris [*Manga and Kirchner*, 2000; *Curran and Wohl*, 2003; *Faustini and Jones*, 2003; *Montgomery et al.*, 2003; *Hassan et al.*, 2005; *Wilcox and Wohl*, 2006], and cross sectional variations [*Thompson*, 2007]. The flow is controlled by local changes in bed surface texture and roughness, which in turn are a consequence of the variability in water depths [*Vallé and Pasternack*, 2006; *Yager et al.*, 2012b], velocities [*Bathurst*, 1985, 2002; *Jarrett*, 1985, 1990; *Mclean and Smith*, 1986; *Marcus et al.*, 1992; *Ye and Mccorquodale*, 1998; *Katul*, 2002; *Olsen*, 2003; *Sukhodolov et al.*, 2006; *Wilcox and Wohl*, 2006; *Blanckaert*, 2010; *Constantinescu et al.*, 2011; *Hajimirzaie et al.*, 2014] , shear stresses [*Shamloo et al.*, 2001; *Ferguson*, 2003; *Maddux et al.*, 2003; *Clayton and Pitlick*, 2007; *Afzalimehr and Rennie*, 2009; *Nelson et al.*, 2010; *Papanicolaou et al.*, 2010; *Clayton*, 2012; *Cooper et al.*, 2013], pressure gradients [*Francalanci et al.*, 2005; *Zeng et al.*, 2005, 2008; *Pournazeri et al.*, 2014], centrifugal forces [*Hooke*, 1975; *Nelson and Smith*, 1989; *Whiting and Dietrich*, 1991; *Legleiter et al.*, 2011], and fluid momentum exchange [*Nikora et al.*, 2001; *Thompson*, 2007; *Recking et al.*, 2008]. External conditions such as the upstream sediment supply [*Dietrich et al.*, 1989, 2005; *Lisle and Madej*, 1992; *Lisle et al.*, 1993, 2000; *Buffington and Montgomery*, 1999b; *Schuerch et al.*, 2006; *Yager et al.*, 2007, 2012b, 2012c; *Yu et al.*, 2009; *Madej et al.*, 2009; *Nelson et al.*, 2009; *Recking et al.*, 2012; *Pitlick et al.*, 2012; *Mueller and Pitlick*, 2014] can also affect the bed surface elevation and texture and hence the spatial flow distribution.

Relative submergence (h_a / D_I, where h_a is the average flow depth and D_I is the characteristic grain size) is a key control on sediment deposition patterns in mountainous rivers. In low h_a / D_I regimes ($h_a / D_I \leq 3.5$ *Papanicolaou and Kramer* [2005], hereinafter LRS) sediment tends to accumulate upstream of large protruding grains [*Papanicolaou and Kramer*, 2005; *Papanicolaou et al.*, 2010, 2011] while in high h_a / D_I (HRS) sediment accumulates downstream [*Papanicolaou et al.*, 2010, 2012]. However, these experiments used non-erodible beds composed of glass spheres, and therefore did not include the effects of vertical accelerations and plunging flow over woody debris, immobile grains and steps [*Shamloo et al.*,

2001]. Many mountain rivers have pool morphologies that result from erosion and these pools have an important influence on flow hydraulics [*Thompson et al.*, 1998; *Buffington et al.*, 2002; *Harrison and Keller*, 2007; *Thompson*, 2007]. Thus, accounting for sediment erosion under the conditions of plunging flow could result in more broadly applicable results.

A particular case of selective sediment deposition is the formation of sediment patches, which are distinct areas of the bed with a relatively narrow grain size distribution (GSD) compared to that of the entire reach [*Laronne et al.*, 2000; *Dietrich et al.*, 2005]. Sediment patches creates areas of different roughness and affect the local hydraulics but are commonly omitted from flow and sediment transport models [*Lisle et al.*, 2000; *Nicholas*, 2000; *Ferguson*, 2003; *Ferguson and Church*, 2009] and consequently the model's performance is reduced [*Clayton*, 2012]. The mechanism controlling patch formation, evolution, and characteristics (i.e. area, grain size distribution, location) is also unclear. It has been hypothesized that patches arise from a local sediment transport capacity – sediment supply imbalance [*Dietrich et al.*, 1989; *Kinerson*, 1990; *Lisle et al.*, 1991, 1993; *Yarnell et al.*, 2006; *Nelson et al.*, 2009], grain to grain interactions [*Lisle et al.*, 1991; *Nelson et al.*, 2009; *Nelson*, 2010] or size-selective cross-stream transport in topographically forced heterogeneous flow fields [*Dietrich and Whiting*, 1989; *Lisle et al.*, 1991; *Nelson et al.*, 2010], but in reality all of these processes interact and their relatively importance may vary. Recently, *Nelson et al.* [2015a, 2015b] used numerical simulations to confirm the importance of cross-stream sediment fluxes on grain size sorting, bar development and persistence, and morphologic evolution. However, it is not clear if cross-stream sediment fluxes will have the same importance when the flow is mostly controlled by large immobile grains in LRS, which is common in mountain rivers. Predicting the location and characteristics of patches in natural rivers is also challenging because of the lack of correlation between local hydraulics (e.g. shear stress) and surface grain texture [*Lisle et al.*, 2000; *Nelson et al.*, 2010] and because sediment erosion and deposition patterns are stage-dependent [*Shamloo et al.*, 2001; *Papanicolaou et al.*, 2011].

Sediment patch location and characteristics have very important implications for riverine habitat availability, for instance salmonid spawning can occur in local zones of gravel textures that are finer than the entire reach [*Kondolf and Wolman*, 1993; *Buffington and Montgomery*, 1999a; *Buxton et al.*, 2015a, 2015b; *Hassan et al.*, 2015]. The spatial variability

of sediment texture in natural rivers is negatively affected by human activities [*Montgomery et al.*, 1996; *Jones et al.*, 2000; *Bunte*, 2004; *Downs et al.*, 2011]. For example, dams largely reduce the sediment supply and therefore modify bed characteristics in downstream reaches [*Dietrich et al.*, 1989; *Lisle et al.*, 1993; *Power et al.*, 1996; *Buffington and Montgomery*, 1999a; *Pitlick and Wilcock*, 2001; *Yarnell et al.*, 2006], and logging operations significantly impact the bedload transport capacity [*Johnson*, 1993; *Smith et al.*, 1993; *Assani and Petit*, 1995; *Imaizumi and Sidle*, 2012; *Hiraoka et al.*, 2015], routing of sediment through a reach [*Swanson and Lienkaemper*, 1978], and bed surface texture [*Buffington and Montgomery*, 1999a]. One solution to restore and improve degraded fish habitat is the in-stream placement of large rocks [*Shamloo et al.*, 2001; *Papanicolaou et al.*, 2010], which provide zones of low velocities [*Papanicolaou et al.*, 2011], and reduced turbulence intensities [*Tritico and Hotchkiss*, 2005] for resting and feeding [*Nowell and Jumars*, 1984]. However, the effects of these large rocks on flow [*Wohl and Thompson*, 2000; *Shamloo et al.*, 2001; *Lin et al.*, 2002; *Dey and Raikar*, 2007; *Strom and Papanicolaou*, 2007; *Lacey and Roy*, 2008; *Palau-Salvador et al.*, 2008; *Hajimirzaie et al.*, 2014; *Tsakiris et al.*, 2014] sediment transport rates [*Yager et al.*, 2007, 2012a, 2012b; *Nitsche et al.*, 2012]), and bed surface texture [*Strom et al.*, 2004; *Papanicolaou and Kramer*, 2005; *Papanicolaou et al.*, 2010, 2011, 2012] are difficult to predict.

We analyze how the bed surface adjusts to spatially variable flow caused by large (relative to the flow depth) simulated boulders, specifically in LRS regimes. We conducted a series of laboratory experiments that featured a staggered configuration of immobile hemispheres and combined our measurements with a 3D Reynolds Averaged Navier-Stokes (RANS) – Volume of Fluid (VOF) model to obtain the spatial distribution of flow characteristics. The questions that motivate this study are: what are patterns of GSD, deposition and erosion around large immobile grains in LRS? Do sediment patches form around these immobile grains? What causes the formation of these patches? How do patches become relatively stable? And, is there any systematic change in bed surface elevation and grain size distribution, reach-averaged velocity and near-bed shear stress with different LRS conditions?

4.3 Methods

4.3.1 Experiment setup and methodological considerations

We conducted our laboratory experiments at the Mountain StreamLab, University of Idaho [*Budwig and Goodwin*, 2012]. The flume is 0.76 m wide and 20 m long (10 m long test section) (Figure 4.1a). At the upstream end, water passes through a panel of flow straighteners. To ensure fully developed turbulent and mixed flow, simulated boulders (23-28 cm diameter) were randomly placed upstream of the test section. Water depth was controlled using an adjustable tail gate and was parallel to the flume bottom on average.

The experiment configuration (Figure 4.1 a, Table 4.1) simplified the characteristics of a typical mountain river, where large roughness elements were represented by staggered concrete hemispheres. The hemispheres were 15.24 cm in diameter (D_I) mounted over 10 cm high foam cylinders and glued to the flume's bottom with a uniform spacing of $\lambda = 4D_I = 61$ cm. At the beginning of each experiment the flume bed consisted of a 10 cm thick sediment layer whose grain size distribution (GSD) was downscaled by a factor of 4.3 from samples collected at Reynolds Creek (Figure 4.1 b), a 3% slope river located in Idaho, USA. The lower portion of the GSD curve was truncated at 2 mm to avoid the use of sand or finer particles. All grain sizes present in the bed and the upstream sediment supply were mobile under our flow conditions.

The Reynolds number, $Re = U_a h_a / \nu$, and particle Reynolds number , $Re^* = u^* k_s / \nu$, (U_a is the reach-averaged flow velocity, ν the fluid's kinematic viscosity, $u^* = \sqrt{\overline{\tau}_m / \rho_w}$ the shear velocity, $\overline{\tau}_m$ the reach-averaged shear stress acting on the mobile grains [*Yager et al.*, 2007], ρ_w the water density, and k_s the roughness length scale) for all of our experiments were within the typical range of mountain gravel-bedded rivers [*Buffington and Montgomery*, 1997; *Lenzi et al.*, 2006; *Yager et al.*, 2007] and represented fully developed turbulent and hydraulically rough flow (see Chapter 3 for more details). The Froude numbers $Fr = U_a / \left[g h_a \right]^{0.5}$ (g is the acceleration due to the gravity) were sub-critical ($Fr < 1$) on average.

We varied the relative submergence between experiments by simultaneously adjusting slope and water discharge to make transport capacity ($q_b = 0.06$ kg/s) constant between runs. Varying the relative submergence created different shear stress fields around the hemispheres and we expected variations in local adjustments in bed elevation and GSD between experiments. Our experiments called S2.15%, S2.40%, and S2.70% had slopes of 0.0215, 0.0240, and 0.0270, respectively, and were called I or F (for example S2.40%F) for initial or final bed conditions, respectively. All our experiments were in low relative submergence flow regime [*Shamloo et al.*, 2001] but the hemispheres were fully submerged. Instead of the reach-averaged water depth (h_a) [*Shamloo et al.*, 2001] we used the average water depth immediately upstream of the hemispheres (h_{au}) to define the relative submergence ($h_{au} / 0.5D_I$, 0.5 denotes the use of hemispheres) (Table 4.1). We imposed an upstream sediment supply rate equal to the transport capacity (q_s) and with GSD identical to the initial bed sediment. The ratio q_b / q_s may significantly impact coarse surface layer development and we held it constant and equal to one to minimize its influence on the bed and enable comparisons between experiments [*Dietrich et al.*, 1989, 2005; *Lisle et al.*, 1993; *Cui and Parker*, 2005; *Yager et al.*, 2007; *Madej et al.*, 2009; *Nelson et al.*, 2009; *Yu et al.*, 2009; *Recking*, 2012]. We let the bed to adjust to the imposed flow and upstream sediment supply until equilibrium conditions were reached. Equilibrium occurred when the bed and mean water surface slope no longer changed, reach-averaged velocity was constant, $q_s = q_b$, and the GSD of the sediment exiting the flume was identical to that of the upstream supply.

4.3.2 Experimental procedures

Our data collection plan had three components: i) verification of equilibrium conditions, ii) characterization of the changes in bed elevation and GSD between the initial and final bed conditions, and iii) application and validation of an unsteady 3D model. Because of the spatially variable water surface elevation and plunging flow with air entrainment around the hemispheres, our attempts to characterize the full flow variability exclusively with measurements were unsuccessful. Our flow model allowed us to include such complex flow features and obtain a detailed description of the spatial and temporal flow variability (more details in section 4.3.3).

To verify equilibrium conditions we measured bed and water surface elevations, reach-averaged velocity, bed load transport rates, and the GSD of sediment exiting the flume. Bed surface elevations (dry) were measured at the beginning and end of each experiment from X = 1 to 9 m (X, Y, and Z are the streamwise, cross-stream and vertical directions of the flume, respectively; test section starts at $X = 0$) with a high-speed (50 kHz sampling rate), high accuracy (~0.1 mm), charge-coupled device laser displacement sensor at a resolution of 5 mm × 5 mm. The water surface elevation (WSE) was monitored every 20 min along three longitudinal profiles ($Y = 0$ and ± 0.152 m, where $Y = 0$ is the channel center, and from X = 1 to 9 m at 5 cm intervals) using an ultrasonic water level sensor (Massa M-300, ~0.1 mm accuracy). Reach-averaged velocity was calculated at intervals of 20 min using the harmonic mean travel times [*Waldon*, 2004] obtained with the tracer dilution method [*MacMurray*, 1985; *Kilpatrick and Wilson*, 1989; *Leibundgut et al.*, 2009], in which we used sodium chloride as tracer and measured the water's conductivity (every 1 s and corrected by temperature using a Campbell Scientific® CS547A-L). We used an ADV (SonTek® 16-MHZ MicroADV, sampling rate: 50 Hz, during periods of 80 s) to measure the three dimensional velocity field at different locations around a hemisphere (see Chapter 3) when equilibrium conditions occurred. The despiking algorithm of *Islam and Zhu* [2013] was used to find spikes which were replaced with linearly interpolated values.

At the upstream end of the flume an overhead sediment conveyor system fed and spread the sediment mixture evenly across the flume (Figure 4.1). A 0.85 m^3 submerged bag held by an overhead crane received all the sediment leaving the flume, which was measured at intervals of 3 s using a calibrated load cell. Bags were replaced when they were 80% full. We used simple moving average (periods of one hour) to calculate q_b and once it was within 5% of q_s we collected sediment samples (during 120 s). Equilibrium occurred when the bed load sample contained all fed grain sizes and the differences in feed and outflux D_{50m} and D_{84m} were less than 10 % (D_{84m} is the 84th percentile grain size).

We collected sediment samples from the bed surface at the beginning and end of each experiment. We sampled the areas upstream and downstream of randomly selected hemispheres. These areas were relatively small compared to coarser grains in the mobile

sediment and the samples did not follow the minimum sample weight recommendations of *Church et al.* [1987] and *Bunte and Abt* [2001]. We visually identified sharp transitions in GSD (Figure 4.2), which defined a patch boundary, and sampled the entire surface delimited by these patches. The delineation process has a degree of subjectivity [*Nelson et al.*, 2014] and all samples were collected by the same operator to ensure that an identical patch criteria was applied. We also collected samples from patches that were not adjacent to the hemispheres using the same procedure. In addition to sediment patches, the reach-averaged surface GSD was sampled from a mixture of randomly selected locations, in this case the thickness of the samples was smaller than the largest particle in the original GSD and the minimum sample weight recommendations of *Church et al.* [1987] and *Bunte and Abt* [2001] were met. Changes in GSD between the initial and final beds in each of our samples were evaluated using the χ^2 test (0.05 significance level). An analysis of the complete test section is beyond the scope of this study; we largely focused our observations and analyses on the areas adjacent the hemispheres and within the limits of the numerical model (see section 4.3.3).

4.3.3 Fluid flow model, numerical implementation and boundary conditions

We used the volume of fluid method (VOF) of Hirt and Nichols [1981] to calculate the elevation of the free surface (i.e. WSE) and the unsteady Reynolds-averaged Navier-Stokes equations (URANS) to solve for the flow field. Here, we only highlight the model's characteristics that made it suitable for our flow conditions, for details on all the model's equations, assumptions, and limitations refer to Chapter 3 and the work of Hirt and Nichols [1981]; Weller et al. [1998]; Weller [2005]; Bohorquez [2008]; Rodriguez [2008]; Berberović et al. [2009]; Deshpande et al. [2012]; Shevchuk et al. [2012]; Zhainakov and Kurbanaliev [2013]; Morgan [2013]; and Karagiannis et al. [2015a, 2015b]. The VOF method tracks the interface between two immiscible fluids, in our case air-water, using an indicator function (, known as phase fraction) that defines the portion of a cell that is occupied by either phase (i.e. air or water). The transport of γ (Equation (4.1)) was solved using the Multidimensional Universal Limiter with Explicit Solution (MULES) [Zalesak, 1979] and the artificial compression term of Weller [2005], which accounts for the high density ratios between fluids. MULES guarantees a strictly bounded solution between $0 \le \gamma \le 1$, where $\gamma = 0$ or $\gamma = 1$ indicates that a cell contains exclusively air or water, respectively, and any other value denotes

the presence of an interface. We used the isosurface $\gamma = 0.5$ to define the WSE. The transport equation for γ is solved simultaneously with the URANS equations,

$$\frac{\partial \gamma}{\partial t} + \nabla \cdot \left(U\gamma \right) + \nabla \cdot \left(U_r \gamma \left(1 - \gamma \right) \right) = 0, \tag{4.1}$$

$$\nabla \cdot U = 0, \tag{4.2}$$

$$\frac{\partial \left(\rho U \right)}{\partial t} + \nabla \cdot \left(\rho UU \right) = -\nabla p + \nabla \cdot \tau + \rho f_b, \tag{4.3}$$

where equations (4.2) and (4.3) represent the conservation of mass and momentum, respectively, and U is the velocity field, ρ the fluid density, t the time, p the pressure, τ the deviatoric viscous stress tensor, and f_b the body forces per unit mass, which include gravity and surface tension effects at the interface. Only one fluid is specified in equations (4.2) and (4.3) because in the VOF method two immiscible fluids are treated as a single fluid, in which ρ and the dynamic viscosity (μ) are a weighted average of γ,

$$\rho = \rho_w \gamma + \rho_a \left(1 - \gamma \right), \tag{4.4}$$

$$\mu = \mu_w \gamma + \mu_a \left(1 - \gamma \right), \tag{4.5}$$

the subscripts a and w stands for air and water phases, respectively.

We used the two equation $k - \omega$ SST model of *Menter* [1994] and *Menter and Esch* [2001] to estimate the effects of turbulence. Compared to other commonly used turbulence models the $k - \omega$ SST provides more accurate predictions of wall shear stress [*Rodi and Scheuerer*, 1986] than the $k - \varepsilon$ model and also performs better in adverse pressure gradients [*Hellsten*, 1998], which are expected in our simulations because of the presence of immobile elements. Accurate shear stresses are key to link the flow and sedimentation patterns we observe in the flume. We used a portion of the test section that includes three sequences of hemispheres in our numerical simulations ($3.4 \le X \le 6.4$). A very fine mesh with an average cell volume of ~ 0.15 cm^3 was used to capture the bed topography in detail. Flow discharge was specified at the upstream boundary and inside the whole domain the WSE adjusted itself without an

imposed elevation. We used the modified pressure of *Rusche* [2002] to avoid needing different pressure boundary conditions at the side walls for each fluid phase. At the bed we used the near wall formulation of *Grotjans and Menter* [1998] (also described in *Menter and Esch* [2001] and *Menter et al.* [2003]), which allowed us to consider the highly complex bed geometry of our experiments without needing locally excessive cell aspect ratios or an extremely fine mesh to solve the viscous sub-layer. The OpenFOAM® flow solver interFoam (www.openfoam.org) was used to solve the system of equations. The flow model has been validated and tested in Chapter 3 using our WSE and velocity measurement for all of our flume experiments.

Flow variables such as WSE, velocity, and shear stress are time-averaged (over 60 s) from the model's results. The spatial distribution of near-bed shear stresses was calculated at 1 cm above the bed using the Boussinesq approximation. The spatial distribution of shear stress divergences was slightly smoothed by averaging the near-bed shear stresses over squared cells (5 mm sides). See Chapter 3 for more details and analyses.

4.4 Results

4.4.1 Bed surface response

On average the bed accumulated sediment and deposited sediment volumes increased with greater bed slopes (8.1, 9.2, and $12.5 \cdot 10^{-3}$ m^3/m for the S2.15%, S2.40% and S2.70% experiments, respectively (Figure 4.3). Most of the sediment accumulated near the walls and switched from the right to left walls moving downstream. Experiment S2.70% presented the most regular pattern of deposition; at the center of the channel ($Y = 0$) a dune-like bedform formed and sediment deposition occurred upstream of all hemispheres whereas little to no erosion was observed immediately downstream (Figure 4.3 d and g, Figure 4.4). Only the bed of S2.15% developed large approximately 7 cm deep elongated pool-like bedforms that had a planform size similar to the hemisphere diameter and were located between hemispheres (Figure 4.3 b and e). Upstream of the hemispheres in S2.15% there was mostly deposition; in the downstream area erosion and deposition occurred, but on average no change in elevation was observed (Figure 4.3 b and e, Figure 4.4). Experiment S2.40% had on average the largest deposition upstream of the hemispheres with some hemispheres almost completely covered. Deposition and scour occurred downstream of the hemispheres in S2.40 % (Figure 4.3 f) but

on average no significant change in elevation was observed (Figure 4.4). The center of channel in all experiments ($Y = 0$) had deposition overall (Figure 4.3 f). No systematic relation between mean elevation change and slope or relative submergence was observed for either region around the hemispheres (Figure 4.4).

In addition to elevation adjustments changes in GSD were observed in each experiment. A visual inspection of the bed revealed clustering of coarse grains as well as zones of fine sediment across the test section (Figure 4.2 and Figure 4.5 a and b). At the end of the experiments the median grain size (D_{50}) of the sampled upstream areas was on average 18.1, 17.7, and 17.9 mm in S2.15%, S2.40%, and S2.70%, respectively, which corresponds to an increase of about 75% (D_{50} at the beginning was 10.08 mm, Figure 4.6) that was statistically significant (χ^2 test; Figure 4.5 a). The coarsening of this region was mostly caused by deposition of 16 mm particles and the removal of grains finer than 11.2 mm (Figure 4.5 a and b).

In the region downstream of the hemispheres S2.15% and S2.70% had no changes in D_{50} and GSD whereas S2.40% had a statistically significant change in GSD and the D_{50} increased by about 50% (Figure 4.5 c and d, Figure 4.6). Similar to the upstream patch, the coarsening observed in the downstream region of S2.40% was caused by the removal of the finer grain fractions and deposition of 16 mm particles (Figure 4.5 c).

Samples collected between hemispheres in S2.70% showed areas of finer texture whereas samples of a mixture of the whole bed surface were not statistically different than the initial GSD. All samples between hemispheres in S2.15% showed a degree of coarsening (Figure 4.5 f), whereas S2.40% presented local coarsening but no statistically significant changes at reach-averaged scale, just like S2.70%.

Compared to the initial GSD the samples collected between hemispheres in S2.15% and S2.40% were coarser, whereas in S2.70% were finer. We also observed that in both, S2.40% and S2.70%, one sample had no statistically significant change with respect to the initial GSD. At a reach-averaged scale the GSD in experiments S2.40% and S2.70% was not statistically different than the initial GSD.

4.4.2 Near-bed shear stress, free surface profiles and recirculation zone

The different relative submergence conditions between experiments affected the spatial distribution of near-bed shear stresses and shear stress divergences (Figure 4.7 a). In the initial bed conditions there was a negative shear stress divergence upstream the hemispheres, which suggests that this area is likely to have an increase in bed elevation. This was confirmed by our measurements. The spatial distribution of near-bed shear stresses (Figure 4.7 b) as well as reach-averaged near-bed shear stress ($\overline{\tau}$) varied between initial and final bed conditions; in S2.40% and S2.70% significant changes in $\overline{\tau}$ occurred, whereas S2.15% had practically no change in $\overline{\tau}$ (Table 4.1, for more details see Chapter 3). A detailed analysis of the variability in shear stress was completed in Chapter 3, and in this study we focused only on the local changes around the hemispheres (see section 4.3.3).

The WSE was highly spatially variable and the most remarkable characteristics were the plunging flow over the hemispheres and the formation of undular hydraulic jumps (Figure 4.8). Upstream of the hemispheres the WSE started to increase as a response to the obstacle and reached a maximum on top of the hemispheres. Immediately after this peak a drastic decrease in WSE occurred and the flow depth was lower than the hemisphere height in the hemisphere wake because of plunging flow. Although we did not measured air content in the water column we observed significant air entrainment immediately downstream of the hemispheres. The WSE then increased again until it practically reached or surpassed that observed over the hemispheres and then gradually declined. A recirculation zone was attached to the bed downstream of the hemispheres and by the end of the experiments had extended farther into the water column. The recirculation zone was also present upstream of the hemispheres but it was considerably thinner than the one located downstream (Figure 4.8). Some of largest grains (of the mobile fraction) also produced small scale recirculation zones at the bed.

4.4.3 Changes in near bed shear stress and bed stability

We observed that once equilibrium conditions were reached most of the sediment patches around the hemispheres were relatively stable with only a minor exchange of particles of similar sizes. We did not measure local sediment transport around the hemispheres, and used an indirect method to explore the role of bed surface adjustments on the stability of sediment

patches. We calculated the spatial distribution of dimensionless near-bed shear stress (τ') and the critical shear stress (τ'_c), at the beginning and end of each experiment. Areas where $\tau' < \tau'_c$ were considered to be relatively stable zones where little sediment transport occurred, and when $\tau' > \tau'_c$ the likelihood of sediment motion increases with higher $(\tau' - \tau'_c)$. Our method was very sensitive to the specification of τ'_c and there is evidence that the critical shear stress can vary significantly between reaches with similar conditions (see discussion by *Buffington and Montgomery* [1997]). For our experimental conditions the typical range of τ'_c is between 0.03 and 0.06 [*Lamb et al.*, 2008]. When we used $\tau'_c = 0.030$, almost the entire bed at the beginning of S2.70% was mobile, which did not correspond to what we observed. At the other extreme, using $\tau'_c = 0.060$ resulted in almost no sediment motion at the end of S2.15% and S2.40%, which was also incorrect. Using $\tau'_c = 0.035$ indicated the areas where most of bedload transport was occurring in all experiments for both initial and final bed conditions (Figure 4.9 a).

For the initial bed conditions all experiments had the same bed GSD and we used $D_{50m} = 1\,\text{cm}$ to normalize the local shear stress. For the final bed conditions we conducted our analyses around the hemispheres where we collected GSD data and we normalized the shear stress using the corresponding D_{50m} for each patch in each experiment (Figure 4.6 and Figure 4.9 b, c, and d). The areas where $\tau' > \tau'_c$ were non-uniformly distributed across the bed at the beginning of the experiments (Figure 4.9 a); the highest τ' were typically located downstream of the hemispheres but were observed in some upstream regions. A clear difference in the spatial distribution of τ' around the hemispheres between the initial and final beds was observed in all experiments. For example, at the beginning of experiment S2.40% (Figure 4.9 c) most of the upstream and downstream areas were expected to be relatively mobile. In S2.40%F the upstream region had a slight reduction in τ, which combined with the coarse sediment patch (see photo in Figure 4.9 c) caused τ' to decrease (compared to the initial bed) and be lower than τ'_c, indicating a relatively stable area. The downstream region in S2.40%F had relatively no change in elevation and a slight increase in τ. However, the increase in D_{50m} resulted in a $\tau' < \tau'_c$ and consequently a reduction in the potentially mobile area. In experiments S2.15% and S2.70% we generally observed the same results as in S2.40% for the upstream region; the

formation of a coarse patch made this area relatively stable. The downstream regions of S2.15% and S2.70% had practically no change in elevation and GSD (see section 4.4.1) but τ slightly decreased, which resulted in a lower τ' and a smaller area of bed mobility.

4.5 Discussion

The topography and GSD at the end of each experiment were likely a result of the different hydraulic conditions between experiments, particularly in how the relative submergence controlled the flow routing in each run. The evolution of sediment patches and bed elevation depend on flow patterns in a channel as well as the initial bed configuration [*Nelson et al.*, 2015b]. In our case the spatial distribution of near-bed shear stresses for the initial bed conditions varied between experiments (Figure 4.7, more details in Chapter 3) but the bed configuration and sediment supply were identical suggesting that the local flow conditions controlled bed evolution. For example, although the initial flow reach-averaged flow depth, velocity and shear stress of experiments S2.15% and S2.40% were not dramatically different (Table 4.1) their final bed topographies had significant differences. The formation of pools in S2.15% (Figure 4.3) indicated that even slight changes in the initial local flow and relative submergence conditions affect bed evolution

In the regions upstream and downstream of the hemispheres we also observed different elevation changes between experiments. Experiments S2.15% and S2.40% had a difference in final upstream elevation of about 16 mm, which is equivalent to 1.5 D_{50} of the initial bed (Figure 4.4). However, the differences in GSD (Figure 4.5 a and b), in particular the local D_{50} (Figure 4.6), in this same region (upstream area) were not very pronounced. In the downstream region, the changes in elevation were very close to zero in all experiments (Figure 4.6) and, although there was an increase in local D_{50} and some coarsening in S2.40%, the GSD of all experiments were relatively similar. The variation of relative submergence between experiments therefore did not exert a strong control on the GSD changes but had an important effect on the topography.

The bed surface adjustment could have also been influenced by the imposed sediment supply. All of our experiments had bed aggradation on average, which could suggest that the sediment supply exceeded the transport capacity [*Lisle and Madej*, 1992]. There is evidence in

the literature that channels with high sediment supplies develop a finer bed surface (see for example [*Dietrich et al.*, 1989; *Buffington and Montgomery*, 1999b; *Madej et al.*, 2009; *Nelson et al.*, 2009]) but our overall bed GSD did not statistically change between experiments, suggesting that the initial supply imbalance was not large, if it existed. The accumulated volumes were also relatively small (see section 4.5.1) and any slight initial imbalance in sediment supply to transport capacity did not likely dominate bed evolution.

Our observations of sediment deposition upstream of an obstacle were consistent with previous studies of depositional patterns in LRS [*Papanicolaou and Kramer*, 2005; *Papanicolaou et al.*, 2010, 2011]. However, our experiments showed that the bed surface adjusts to the spatial variability in the flow field by varying both its elevation and GSD. Bed scouring was one of the responses and is a key process for bed evolution in real mountainous rivers and must be included in future experiments and models for more realistic predictions. Similar bed elevation adjustments were observed around bridge piers [e.g. *Ettema et al.*, 2006; *Link et al.*, 2012] and emergent vegetation [*Rominger et al.*, 2010; *Ortiz et al.*, 2013; *Yager and Schmeeckle*, 2013; *de Lima et al.*, 2015] where scour holes developed immediately adjacent to the obstacles and deposition occurred farther downstream between the elements. This indicates that the patterns of sediment deposition and near constant elevation that we observed upstream and downstream of the hemispheres, respectively, are only valid in LRS. Therefore, the design of submerged structures must consider a range of water depths to ensure their stability for cases when they are fully or partially submerged because flow and sedimentation patterns are a function of relative submergence. More research is also needed to investigate when the transition from deposition in the region upstream or downstream of an obstacle occurs in fully submerged conditions [*Papanicolaou and Kramer*, 2005].

4.5.1 Links between flow hydraulics and local grain size distribution

The upstream region of our hemispheres had selective deposition of coarse sediment and developed a coarse sediment patch whereas the downstream region had little change in GSD, except for S2.40% that had some minor coarsening that was not as pronounced as the upstream zones. To help explain this pattern of sediment deposition we analyzed the combined effects of size-selective transport, local flow structure and local sediment supply. The local flow structure upstream and downstream of a hemisphere helps explain the observed sediment

deposition patterns. We assumed that local sediment supply sources followed flow streamlines, which were based on the velocity field averaged over 60 s. The streamlines were calculated through a line parallel to the Y direction, located 1 cm over the bed and whose length was equal to the measured sediment patch width; streamlines entering the upstream and downstream hemisphere regions were calculated separately. For simplicity only one hemisphere was analyzed (S2.40%, same as Figure 4.9 c) but the flows structures were similar in all experiments.

The upstream region was dominated by the formation of a horseshoe vortex (Figure 4.11 a) and incoming coarse sediment particles entering this region were deposited and trapped near this flow structure (Figure 4.9 c). The development of the coarse sediment patch changed the local bed surface elevation, which affected the flow streamlines (Figure 4.10 c). At the beginning of the experiment most of the flow entering the upstream region came from a straight line aligned with the hemisphere center (X direction), whereas at the end most flow was routed around the coarse patch (Figure 4.11 c). This new routing likely further enhanced the stability of the coarse patch. In contrast, the downstream region (Figure 4.11 b) was dominated by low velocities at the beginning of the experiment and the sources of sediment were mostly from the areas immediately adjacent to the hemisphere. Streamlines on top of the hemisphere did not correspond to a sediment source, we did not observe transport here. By the end of the experiment a recirculation zone developed and the sediment downstream of the hemisphere was likely trapped. The recirculation zone was already well developed at the beginning of the other experiments (S2.15% and S2.70%).

We also used the local (each location was an average over 3 by 3 cm squares) shear stress and the *Parker* [1990] equations to calculate the volumetric transport rate per unit width for each grain size in several locations within the patch upstream of a hemisphere (Figure 4.11). Although we did not performed a mass balance here, this method allowed us to understand how different grain sizes move in or out the region where the patch will form. In this particular example we used a hemisphere of experiment S2.40% (Figure 4.9) but similar results were obtained for other runs.

At the beginning of the experiment the local shear stress upstream of the hemisphere (Figure 4.11 c, location 2) was able to transport all of the available grain sizes in a similar

proportion to their frequency on the bed. Location 3 downstream received all available grain sizes but could only mobilize the fine fraction (Figure 4.11 b), which means that size-selective transport starts to occur here. Other locations relatively close to the hemisphere's upstream face (locations 8 and 9) also experienced size-selective transport; coarse grain sizes were not mobile whereas fine sediment fractions were transported out of each location (Figure 4.11 b, c, and d). This suggest that patch formation requires a shear stress divergence such that size-selective bedload transport occurs, in this case the divergence in shear stress is caused by the hemispheres. Over the experiment duration selective deposition of coarse particles will continue occurring and the increase in bed elevation will alter the spatial distribution of shear stresses around the hemisphere (Figure 4.7 b, Figure 4.11 a). In this particular case, shear stresses magnitude declined at the end of the experiment, which combined with an increase in D_{50} created a relatively stable local sediment patch (Figure 4.9, Figure 4.11 e) that did not transport large amounts of sediment (Figure 4.11 b).

Based on the analyses of local flow streamlines (Figure 4.10) and volumetric transport rates (Figure 4.11) we propose that the mechanism for patch formation was a result of the spatial variability of shear stress, in particular to the combination of shear stress divergence and magnitude and direction of the shear stress vectors. A divergence in shear stress is required to promote size-selective bedload transport. However, the divergence must be generated within a certain magnitude of shear stress. For a given shear stress divergence, if the divergence is the result of the spatial gradient of high or low magnitude shear stresses (relative to the transport capacity for available grain sizes) size-selective sediment transport will not occur and all grain fractions will be mobilized (high shear stresses) or no sediment transport will occur at all (low shear stresses). The direction of the shear stress vector is also important because it controls the path of grain to enter or leave a certain region.

In the region upstream of the hemisphere, the streamwise shear stress was larger than the cross-stream component and had a more important role in size-selective transport and patch formation (Figure 4.11 f). This differs from bar formation in gravel bed rivers, where the cross-stream sediment flux is an important mechanism for coarse bar tops and fine pool development [*Nelson et al.*, 2010, 2015a]. Our results suggest that the importance of the streamwise or cross-stream sediment fluxes in patch formation depends on the shear stress divergence generated by

the bed topography or channel obstructions. Additional research is required on the effects of flow obstructions densities and distributions on local depositional patterns and the relative role of streamwise and cross-stream sediment fluxes in patch formation.

Coarsening in the downstream region of the hemisphere in experiment S2.40% could also be caused by size-selective bedload transport (Figure 4.11 b and d). Locations 13 and 15 at the beginning of the experiment were able to transport the finer fractions but not coarse ones. However, our indirect methods do not provided evidence whether the coarse particles in our samples were deposited there or stayed from the beginning of the experiment. At the end of the experiment, and similar to the upstream region, the downstream zone was relatively stable. Our approximations of sediment supply sources are based on velocity-averaged streamlines (Figure 4.10) and local shear stresses (Figure 4.9, Figure 4.11) and do not considered the unsteady nature of the flow in our simplifications and in particular the wake dynamics. At certain moments throughout the experiment the downstream area must have received some coarse grains. The counter-rotating limbs observed at the sides of hemispheres (Figure 4.11 b) may have introduced some sediment inside the recirculation zone. Our calculations have several limitations and do not explain how patches evolve through time or incorporate the effects of particle-particle interactions [*Mikael Malmaeus and Hassan*, 2002; *Xu and Michaelides*, 2003; *Czernuszenko*, 2009]. Other numerical models could be used in future research to account for the effects of bed surface and GSD evolution under flow conditions that are difficult to control in the field or laboratory studies. One example is the 2D model flow model of *Nelson et al.* [2015a, 2015b], which nicely reproduced bar formation from a sediment mixture and predicted bed elevations and GSDs accurately. However, care must be taken when using this model in cases of significant vertical velocities and accelerations (see chapter 3). Also, an extension of the model of *Schmeeckle* [2014] to sediment mixtures could completely include the dynamic of individual particles (discrete element method model, DEM) and their interactions with the flow (large eddy simulation, LES). Very specific analyses on the formation and disintegration of sediment patches, and sediment deposition and scour in general, could be completed using this type of model (LES-DEM). Potential applications of detailed modeling of patches are studies on the stability of salmon redds, deposition around vegetation and bridge pier scour protection.

4.6 Conclusion

Our experiments adjusted to the imposed flow through changes in bed surface elevations and local grain size distributions. Upstream of a hemisphere preferential deposition of coarse grains occurred whereas downstream little to no changes were observed. The flow structure created by the immobile hemispheres (i.e. divergence in shear stress and horseshoe vortex) controlled sediment deposition patterns. The mechanism for patch formation in LRS was a result of the spatial variability of shear stress, in particular to the combination of shear stress divergence and magnitude and direction of the shear stress vectors. However, the shear stress variability must be within an appropriate range such that size-selective bedload transport occurs. The recirculation zone located downstream of the hemispheres acted to shelter this region and little to no change in elevation or GSD were observed in that area. Our results are applicable only in LRS, other flow conditions such as partially submerged or fully emergent elements will have different patterns of sediment deposition and flow structures.

4.7 Acknowledgements

Funding for this research was provided by an NSF Career award to E.M. Yager (0847799) and the Chilean Government - CONICYT “Becas de Doctorado en el Extranjero – Becas Chile”. Invaluable laboratory assistance was provided by Bob Basham and Christina Beeson. Thoughtful discussions with Megan Kenworthy helped in the planning and execution of the laboratory experiments.

4.8 References

Afzalimehr, H., and C. D. Rennie (2009), Determination of bed shear stress in gravel-bed rivers using boundary-layer parameters, *Hydrol. Sci. J.*, *54*(1), 147–159, doi:10.1623/hysj.54.1.147.

Assani, A. A., and F. Petit (1995), Log-jam effects on bed-load mobility from experiments conducted in a small gravel-bed forest ditch, *Catena*, *25*, 117–126, doi:10.1016/0341-8162(95)00004-C.

Bathurst, J. C. (1978), Flow resistance of large-scale roughness, *J. Hydraul. Div.*, *104*(12), 1587–1603.

Bathurst, J. C. (1985), Flow resistance estimation in mountain rivers, *J. Hydraul. Eng.*, *111*(4), 625–643.

Bathurst, J. C. (2002), At-a-site variation and minimum flow resistance for mountain rivers, *J. Hydrol.*, *269*(1-2), 11–26, doi:10.1016/S0022-1694(02)00191-9.

Blanckaert, K. (2010), Topographic steering, flow recirculation, velocity redistribution, and bed topography in sharp meander bends, *Water Resour. Res.*, *46*(9), 1–23, doi:10.1029/2009WR008303.

Budwig, R. S., and P. Goodwin (2012), The Center for Ecohydraulics Research Mountain Stream Lab – a facility for collaborative research and education, in *Innovations 2012: world innovations in engineering education and research*, edited by W. Aung, V. Ilic, O. Mertanen, J. Moscinski, and J. Uhomoibhi, pp. 17–28, iNEER, Potomac, Maryland, USA.

Buffington, J. M., and D. R. Montgomery (1997), A systematic analysis of eight decades of incipient motion studies, with special reference to gravel-bedded rivers, *Water Resour. Res.*, *33*(8), 1993–2029, doi:10.1029/97WR03138.

Buffington, J. M., and D. R. Montgomery (1999a), Effects of hydraulic roughness on surface textures of gravel-bedded rivers, *Water Resour. Res.*, *35*(11), 3507–3521.

Buffington, J. M., and D. R. Montgomery (1999b), Effects of sediment supply on surface textures of gravel-bed rivers, *Water Resour. Res.*, *35*(11), 3523–3530, doi:10.1029/1999WR900232.

Buffington, J. M., T. E. Lisle, R. D. Woodsmith, and S. Hilton (2002), Controls on the size and occurrence of pools in coarse-grained forest rivers, *River Res. Appl.*, *18*, 507–531, doi:10.1002/rra.693.

Bunte, K. (2004), *State of the science review - Gravel mitigation and augmentation below hydroelectric dams : A geomorphological perspective*, Stream Systems Technology Center, USDA Forest Service Rocky Mountain Research Station, Fort Collins, CO.

Bunte, K., and S. R. Abt (2001), *Sampling Surface and Subsurface Particle-Size Distributions in Wadable Gravel- and Cobble-Bed Streams for Analyses in Sediment Transport, Hydraulics, and Streambed Monitoring*, General Technical Report RMRS-GTR-74, U.S. Dept. of Agriculture, Forest Service, Rocky Mountain Research Station, Fort Collins, CO.

Buxton, T. H., J. M. Buffington, D. Tonina, A. K. Fremier, and E. M. Yager (2015a), Modeling the Influence of Salmon Spawning on Hyporheic Exchange of Marine-Derived Nutrients in Gravel Stream beds, *Can. J. Fish. Aquat. Sci., 72,* 1146–1158, doi:10.1139/cjfas-2014-0413.

Buxton, T. H., J. M. Buffington, E. M. Yager, M. A. Hassan, and A. K. Fremier (2015b), The relative stability of salmon redds and unspawned streambeds, *Water Resour. Res., 51,* 6074–6092, doi:10.1002/ 2015WR016908.

Church, M., D. G. McLean, and J. F. Wolcott (1987), River bed gravels: Sampling and analysis, in *Sediment transport in gravel bed rivers,* edited by C. R. Thorne, J. C. Bathurst, and R. D. Hey, pp. 43–88, John Wiley & Sons.

Clayton, J. A. (2012), Spatial Variations in Excess Shear Stress in a Gravel-Bed River Bend, *Phys. Geogr.*, *33*(1), 68–85, doi:10.2747/0272-3646.33.1.68.

Clayton, J. A., and J. Pitlick (2007), Spatial and temporal variations in bed load transport intensity in a gravel bed river bend, *Water Resour. Res., 43,* W02426, doi:10.1029/2006WR005253.

Constantinescu, G., M. Koken, and J. Zeng (2011), The structure of turbulent flow in an open channel bend of strong curvature with deformed bed: Insight provided by detached eddy simulation, *Water Resour. Res.*, *47*(5), 1–17, doi:10.1029/2010WR010114.

Cooper, J. R., J. Aberle, K. Koll, and S. J. Tait (2013), Influence of relative submergence on spatial variance and form-induced stress of gravel-bed flows, *Water Resour. Res.*, *49*(9), 5765–5777, doi:10.1002/wrcr.20464.

Cui, Y., and G. Parker (2005), Numerical Model of Sediment Pulses and Sediment-Supply Disturbances in Mountain Rivers, *J. Hydraul. Eng.*, *131*(8), 646–656, doi:10.1061/(ASCE)0733-9429(2005)131:8(646).

Curran, J., and E. Wohl (2003), Large woody debris and flow resistance in step-pool channels, Cascade Range, Washington, *Geomorphology, 51,* 141–157.

Czernuszenko, W. (2009), Model of particle-particle interaction for saltating grains in water, *Arch. Hydroengineering Environ. Mech.*, *56*(3-4), 101–120.

Dey, S., and R. V Raikar (2007), Characteristics of loose rough boundary streams at near-threshold, *J. Hydraul. Eng.*, *133*(3), 288–304, doi:10.1061/(asce)0733-9429(2007)133:3(288).

Dietrich, W. E., and P. Whiting (1989), Boundary Shear Stress and Sediment Transport In River Meanders of Sand and Gravel, in *River Meandering, American Geophysical Union - Water Resources. Monographs*, vol. 12, edited by S. Ikeda and G. Parker, pp. 1–50, American Geophysical Union, Washington, D.C., USA.

Dietrich, W. E., J. W. Kirchner, H. Ikeda, and F. Iseya (1989), Sediment supply and the development of the coarse surface layer in gravel-bedded rivers, *Nature, 340,* 215–217, doi:10.1038/340215a0.

Dietrich, W. E., P. a. Nelson, E. Yager, J. G. Venditti, M. P. Lamb, and L. Collins (2005), Sediment patches, sediment supply, and channel morphology, in *4th IAHR Symposium on River, Coastal and Estuarine.*, edited by G. Parker and M. H. Garcia, pp. 79–90, Taylor & Francis Group, Urbana, Illinois, USA.

Downs, P. W., M. S. Singer, B. K. Orr, Z. E. Diggory, and T. C. Church (2011), Restoring ecological integrity in highly regulated rivers: The role of baseline data and analytical references, *Environ. Manage.*, *48*, 847–864, doi:10.1007/s00267-011-9736-y.

Ettema, R., G. Kirkil, and M. Muste (2006), Similitude of Large-Scale Turbulence in Experiments on Local Scour at Cylinders, *J. Hydraul. Eng.*, *132*(1), 33–40, doi:10.1061/(ASCE)0733-9429(2006)132:1(33).

Faustini, J. M., and J. A. Jones (2003), Influence of large woody debris on channel morphology and dynamics in steep, boulder-rich mountain streams, western Cascades, Oregon, *Geomorphology*, *51*(1-3), 187–205, doi:10.1016/S0169-555X(02)00336-7.

Ferguson, R., and M. Church (2009), A critical perspective on 1-D modeling of river processes: Gravel load and aggradation in lower Fraser River, *Water Resour. Res.*, *45*(11), 1–15, doi:10.1029/2009WR007740.

Ferguson, R. I. (2003), The missing dimension: Effects of lateral variation on 1-D calculations of fluvial bedload transport, *Geomorphology*, *56*, 1–14, doi:10.1016/S0169-555X(03)00042-4.

Francalanci, S., G. Parker, and E. Paris (2005), Effects of non-hydrostatic pressure distribution on bedload transport, in *4th IAHR Symposium on River, Estuarine, and Coastal Morphodynamics*, edited by G. Parker and M. H. Garcia, pp. 13–21, Taylor & Francis.

Grotjans, H., and F. R. Menter (1998), Wall functions for industrial applications, in *Computational Fluid Dynamics' 98*, edited by K. D. Papailiou, D. Tsahalis, J. Périaux, C. Hirsch, and M. Pandolfi, pp. 1112–1117, John Wiley Sons, Chichester, UK.

Hajimirzaie, S. M., A. G. Tsakiris, J. H. J. Buchholz, and A. N. Papanicolaou (2014), Flow characteristics around a wall-mounted spherical obstacle in a thin boundary layer, *Exp. Fluids*, *55*(6), 1–14, doi:10.1007/s00348-014-1762-0.

Harrison, L. R., and E. A. Keller (2007), Modeling forced pool–riffle hydraulics in a boulder-bed stream, southern California, *Geomorphology*, *83*(3-4), 232–248, doi:10.1016/j.geomorph.2006.02.024.

Hassan, M. A., M. Church, T. E. Lisle, F. Brardinoni, L. Benda, and G. E. Grant (2005), Sediment Transport and Channel Morphology of Small , Forested Streams, *J. Am. Water Resour. Assoc.*, *41*(4), 853–876, doi:10.1111/j.1752-1688.2005.tb03774.x.

Hassan, M. A., D. Tonina, and T. H. Buxton (2015), Does small-bodied salmon spawning activity enhance streambed mobility?, *Water Resour. Res.*, *51*, 1–18, doi:10.1002/2015WR017079.

Hellsten, A. (1998), Some improvements in Menter's k-omega SST turbulence model, *29th AIAA, Fluid Dyn. Conf.*, 1–11, doi:10.2514/6.1998-2554.

Hiraoka, M., T. Gomi, T. Oda, T. Egusa, and Y. Uchiyama (2015), Responses of bed load yields from a forested headwater catchment in the eastern Tanzawa Mountains , Japan, *Hydrol. Res. Lett.*, *9*(3), 41–46, doi:10.3178/hrl.9.41.

Hooke, R. (1975), Distribution of Sediment Transport and Shear Stress in a Meander Bend, *J. Geol.*, *83*(5), 543–565.

Imaizumi, F., and R. C. Sidle (2012), Effect of forest harvesting on hydrogeomorphic processes in steep terrain of central Japan, *Geomorphology*, *169-170*, 109–122, doi:10.1016/j.geomorph.2012.04.017.

Islam, M. R., and D. Z. Zhu (2013), Kernel Density–Based Algorithm for Despiking ADV Data, *J. Hydraul. Eng.*, *139*(7), 785–739, doi:10.1061/(ASCE)HY .1943-7900.0000734.

Jarrett, R. D. (1985), Analyses of Vertical-Velocity Profiles in Higher-Gradient Streams in Colorado, *EOS, Am. Geophys. Union*, *66*(46), 913.

Jarrett, R. D. (1990), Hydrologic and hydraulic research in mountain rivers, *J. Am. Water Resour. Assoc.*, *26*(3), 419–429, doi:10.1111/j.1752-1688.1990.tb01381.x.

Johnson, R. C. (1993), Effects of forestry on suspended solids and bedload yields in the Balquhidder catchments, *J. Hydrol.*, *145*(3-4), 403–417, doi:doi:10.1016/0022-1694(93)90066-I.

Jones, J. A., F. J. Swanson, B. C. Wemple, and K. U. Snyder (2000), Effects of Roads on Hydrology, Geomorphology, and Disturbance Patches in Stream Networks, *Conserv. Biol.*, *14*(1), 76–85, doi:10.1046/j.1523-1739.2000.99083.x.

Katul, G. (2002), A mixing layer theory for flow resistance in shallow streams, *Water Resour. Res.*, *38*(11), 1–8, doi:10.1029/2001WR000817.

Kilpatrick, F. A., and J. F. Wilson (1989), Measurement of time of travel in streams by dye tracing, in *Techniques of water-resources investigations of the United States Geological Survey - Applications of Hydraulic*, pp. 1–27, U.S. Geological Survey, Water Resources Division, Reston, VA.

Kinerson, D. (1990), Surface response to sediment supply, M.S., Thesis. University of California, Berkeley, CA. 108 pp.

Kondolf, G. M., and M. G. Wolman (1993), The sizes of salmonid spawning gravels, *Water Resour. Res.*, *29*(7), 2275–2285, doi:10.1029/93WR00402.

Lacey, R. W. J. W. J., and A. G. Roy (2008), The spatial characterization of turbulence around large roughness elements in a gravel-bed river, *Geomorphology*, *102*(3-4), 542–553, doi:10.1016/j.geomorph.2008.05.045.

Lamb, M. P., W. E. Dietrich, and J. G. Venditti (2008), Is the critical shields stress for incipient sediment motion dependent on channel-bed slope?, *J. Geophys. Res. Earth Surf.*, *113*(2), 1–20, doi:10.1029/2007JF000831.

Laronne, J. B., C. García, and I. Reid (2000), Mobility of patch sediment in gravel bed streams: patch character and its implications for bedload, in *Gravel-Bed Rivers V*, edited by M. P. Mosley, pp. 249–289, New Zealand Hydrological Society Inc., Wellington, New Zealand.

Legleiter, C. J., L. R. Harrison, and T. Dunne (2011), Effect of point bar development on the local force balance governing flow in a simple, meandering gravel bed river, *J. Geophys. Res. Earth Surf.*, *116*(1), 1–29, doi:10.1029/2010JF001838.

Leibundgut, C., P. Maloszewski, and C. Külls (2009), *Tracers in Hydrology*, John Wiley & Sons, Ltd.

Lenzi, M. A. (2004), Displacement and transport of marked pebbles, cobbles and boulders during floods in a steep mountain stream, *Hydrol. Process.*, *18*(10), 1899–1914, doi:10.1002/hyp.1456.

Lenzi, M. A., L. Mao, and F. Comiti (2006), When does bedload transport begin in steep boulder-bed streams?, *Hydrol. Process.*, *20*(16), 3517–3533, doi:10.1002/hyp.6168.

de Lima, P. H. S., J. G. Janzen, and H. M. Nepf (2015), Flow patterns around two neighboring patches of emergent vegetation and possible implications for deposition and vegetation growth, *Environ. Fluid Mech.*, 881–898, doi:10.1007/s10652-015-9395-2.

Lin, J.-C., Y. Yang, and D. Rockwell (2002), Flow Past Two Cylinders in Tandem: Instantaneous and Averaged Flow Structure, *J. Fluids Struct.*, *16*(8), 1059–1071, doi:10.1006/jfls.2002.0469.

Link, O., C. Gonzalez, M. Maldonado, and C. Escauriaza (2012), Coherent structure dynamics and sediment particle motion around a cylindrical pier in developing scour holes, *Acta Geophys.*, *60*(6), 1689–1719, doi:DOI 10.2478/s11600-012-0068-y.

Lisle, T. E., and M. A. Madej (1992), Spatial Variation in Armouring in a Channel with High Sediment Supply, in *Dynamics of Gravel-bed Rivers*, edited by P. Billi, R. D. Hey, C. R. Thorne, and P. Tacconi, pp. 277–293, John Wiley & Sons, Inc., Chichester, UK.

Lisle, T. E., H. Ikeda, and F. Iseya (1991), Formation of stationary alternate bars in a steep channel with mixed-size sediment: A flume experiment, *Earth Surf. Process. Landforms*, *16*(5), 463–469, doi:10.1002/esp.3290160507.

Lisle, T. E., F. Iseya, and H. Ikeda (1993), Response of a channel with alternate bars to a decrease in supply of mixed-size bed load: A flume experiment, *Water Resour. Res.*, *29*(11), 3623–3629, doi:10.1029/93WR01673.

Lisle, T. E., J. M. Nelson, J. Pitlick, M. A. Madej, and B. L. Barkett (2000), Variability of bed mobility in natural, gravel-bed channels and adjustments to sediment load at local and reach scales, *Water Resour. Res.*, *36*(12), 3743–3755, doi:10.1029/2000WR900238.

MacMurray, H. L. (1985), The use of the salt-velocity method for the precise measurement of resistance to flow in rough-boundary open channels, PhD Thesis, Department of Environmental Management, University of Canterbury.

Maddux, T. B., J. M. Nelson, and S. R. McLean (2003), Turbulent flow over three-dimensional dunes: 1. Free surface and flow response, *J. Geophys. Res. Surf.*, *108*(F1), F16009, doi:F16009\r10.1029/2003jf000017.

Madej, M. A., D. G. Sutherland, T. E. Lisle, and B. Pryor (2009), Channel responses to varying sediment input: A flume experiment modeled after Redwood Creek, California, *Geomorphology*, *103*(4), 507–519, doi:10.1016/j.geomorph.2008.07.017.

Manga, M., and J. W. Kirchner (2000), Stress partitioning in streams by large woody debris, *Water Resour. Res.*, *36*(8), 2373–2379, doi:10.1089/jmf.2009.0090.

Marcus, W. A., K. Roberts, L. Harvey, and G. Tackman (1992), An Evaluation of Methods for Estimating Manning's n in Small Mountain Streams, *Mt. Res. Dev.*, *12*(3), 227–239, doi:10.2307/3673667.

Mclean, S. R., and J. D. Smith (1986), A model for flow over two-dimensional bed forms, *J. Hydraul. Eng.*, *112*(4), 300–317.

Menter, F. R. (1994), Two-equation eddy-viscosity turbulence models for engineering applications, *AIAA J.*, *32*(8), 1598–1605.

Menter, F. R., and T. Esch (2001), Elements of Industrial Heat Transfer Predictions, in *16th Brazilian Congress of Mechanical Engineering*, pp. 117–127, COBEM.

Menter, F. R., J. C. Ferreira, and T. Esch (2003), The SST Turbulence Model with Improved Wall Treatment for Heat Transfer Predictions in Gas Turbines, *Int. Gas Turbine Congr. 2003*, (1992), 1–7.

Mikael Malmaeus, J., and M. A. Hassan (2002), Simulation of individual particle movement in a gravel streambed, *Earth Surf. Process. Landforms*, *27*(1), 81–97, doi:10.1002/esp.305.

Montgomery, D. R., J. M. Buffington, N. P. Peterson, D. Schuett-Hames, and T. P. Quinn (1996), Stream-bed scour, egg burial depths, and the influence of salmonid spawning on bed surface mobility and embryo survival, *Can. J. Fish. Aquat. Sci.*, *53*(5), 1061–1070, doi:10.1139/f96-028.

Montgomery, D. R., T. M. Massong, and S. C. S. Hawley (2003), Influence of debris flows and log jams on the location of pools and alluvial channel reaches, Oregon Coast Range, *Bull. Geol. Soc. Am.*, *115*(1), 78–88, doi:10.1130/0016-7606(2003)115<0078:IODFAL>2.0.CO;2.

Mueller, E. R., and J. Pitlick (2014), Sediment supply and channel morphology in mountain river systems: 2. Single thread to braided transitions, *J. Geophys. Res. Earth Surf.*, *119*, 1516–1541, doi:10.1002/2013JF002843.Sediment.

Nelson, J. M., and J. D. Smith (1989), Flow in meandering channels with natural topography, in *River Meandering, Water Resources Monographs*, vol. 12, edited by S. Ikeda and G. Parker, pp. 69–102, American Geophysical Union, Washington, D.C., USA.

Nelson, P. A. (2010), Bed Surface Patchiness in Gravel-Bed Rivers, PhD Thesis. University of California, Berkeley, CA. 154 pp.

Nelson, P. A., J. G. Venditti, W. E. Dietrich, J. W. Kirchner, H. Ikeda, F. Iseya, and L. S. Sklar (2009), Response of bed surface patchiness to reductions in sediment supply, *J. Geophys. Res. Earth Surf.*, *114*(2), 1–18, doi:10.1029/2008JF001144.

Nelson, P. A., W. E. Dietrich, and J. G. Venditti (2010), Bed topography and the development of forced bed surface patches, *J. Geophys. Res. Earth Surf.*, *115*, F04024, doi:10.1029/2010JF001747.

Nelson, P. a., D. Bellugi, and W. E. Dietrich (2014), Delineation of river bed-surface patches by clustering high-resolution spatial grain size data, *Geomorphology*, *205*, 102–119, doi:10.1016/j.geomorph.2012.06.008.

Nelson, P. A., R. R. Mcdonald, J. M. Nelson, W. E. Dietrich, and N. E. T. Al (2015a), Coevolution of bed surface patchiness and channel morphology : 1 . Mechanisms of forced patch formation, *J. Geophys. Res. Earth Surf.*, *120*, 1687–1707, doi:10.1002/2014JF003428.

Nelson, P. A., R. R. Mcdonald, J. M. Nelson, and W. E. Dietrich (2015b), Coevolution of bed surface patchiness and channel morphology : 2 . Numerical experiments, *J. Geophys. Res. Earth Surf.*, 1–16, doi:10.1002/2014JF003428.Key.

Nicholas, A. P. (2000), Modelling bedload yield braided gravel bed rivers, *Geomorphology*, *36*, 89–106, doi:10.1016/S0169-555X(00)00050-7.

Nikora, V., D. Goring, I. McEwan, and G. Griffiths (2001), Spatially averaged open-channel flow over rough bed, *J. Hydraul. Eng.*, *127*(2), 123–133.

Nitsche, M., D. Rickenmann, J. M. Turowski, A. Badoux, and J. W. Kirchner (2011), Evaluation of bedload transport predictions using flow resistance equations to account for macro-roughness in steep mountain streams, *Water Resour. Res.*, *47*, W08513, doi:10.1029/2011WR010645.

Nitsche, M., D. Rickenmann, J. W. Kirchner, J. M. Turowski, and a. Badoux (2012), Macroroughness and variations in reach-averaged flow resistance in steep mountain streams, *Water Resour. Res.*, *48*(12), 1–16, doi:10.1029/2012WR012091.

Nowell, A. R. M., and P. A. Jumars (1984), Flow Environments of Aquatic Benthos, *Annu. Rev. Ecol. Syst.*, *15*, 303–328.

Olsen, N. R. B. (2003), Three-Dimensional CFD Modeling of Self-Forming Meandering Channel, *J. Hydraul. Eng.*, *129*(5), 366–372.

Ortiz, A. C., A. Ashton, and H. Nepf (2013), Mean and turbulent velocity fields near rigid and flexible plants and the implications for deposition, *J. Geophys. Res. Earth Surf.*, *118*(4), 2585–2599, doi:10.1002/2013JF002858.

Palau-Salvador, G., T. Stoesser, and W. Rodi (2008), LES of the flow around two cylinders in tandem, *J. Fluids Struct.*, *24*(8), 1304–1312, doi:10.1016/j.jfluidstructs.2008.07.002.

Papanicolaou, A., A. Tsakiris, and C. Kramer (2010), Effects of relative submergence on flow and sediment patterns around clasts, in *River flow 2010 : Proceedings of the International Conference on Fluvial Hydraulics*, edited by A. Dittrich, K. Koll, J. Aberle, and P. Geisenhainer, Braunschweig, Germany.

Papanicolaou, A. N., and C. Kramer (2005), The role of relative submergence on cluster microtopography and bedload predictions in mountain streams, in *River, Coastal and Estuarine Morphodynamics. Proceeding of the 4th IAHR conference*, edited by G. Parker and M. H. Garcia, pp. 1083–1086, Urbana, Illinois, USA.

Papanicolaou, A. N., C. M. Kramer, A. G. Tsakiris, I. Moustakidis, and T. L. Huff (2011), Depositional patterns in steep mountainous streams under low relative submergence (LRS) regime, in *World Environmental and Water Resources Congress*, edited by R. E. Beighley and M. W. Kilgore, pp. 2379–2388, American Society of Civil Engineers, Palm Springs, CA, USA.

Papanicolaou, A. N., C. M. Kramer, A. G. Tsakiris, T. Stoesser, S. Bomminayuni, and Z. Chen (2012), Effects of a fully submerged boulder within a boulder array on the mean and turbulent flow fields: Implications to bedload transport, *Acta Geophys.*, *60*(6), 1502–1546, doi:10.2478/s11600-012-0044-6.

Parker, G. (1990), Surface-based bedload transport relation for gravel rivers, *J. Hydraul. Res.*, *28*(4), 417–436, doi:10.1080/00221689009499058.

Pitlick, J., and P. Wilcock (2001), Relations between streamflow, sediment transport, and aquatic habitat in regulated rivers, in *Geomorphic processes and riverine habitat. Water Science and applications. Vol. 4.*, edited by J. M. Dorava, D. R. Montgomery, B. B. Palcsak, and F. A. Fitzpatrick, pp. 185–198, American Geophysical Union, Washington, D.C., USA.

Pitlick, J., E. R. Mueller, and C. Segura (2012), Differences in Sediment Supply to Braided and Single-Thread River Channels: What Do the Data Tell Us?, in *Gravel-Bed Rivers: Processes, Tools, Environments*, edited by M. Church, P. M. Biron, and A. G. Roy, pp. 502–511, John Wiley & Sons, Ltd., Chichester, UK.

Pournazeri, S., S. S. Li, and F. Haghighat (2014), Efficient non-hydrostatic modelling of flow and bed shear stress in a pier scour hole, *Can. J. Civ. Eng.*, *41*(5), 450–460, doi:10.1139/cjce-2013-0160.

Power, M., W. Dietrich, and J. Finlay (1996), Dams and Downstream Aquatic Biodiversity: Potential Food Web Consequences of Hydrologic and Geomorphic Change, *Environ. Manage.*, *20*(6), 887–95, doi:10.1007/BF01205969.

Recking, A. (2012), Influence of sediment supply on mountain streams bedload transport, *Geomorphology*, *175-176*, 139–150, doi:10.1016/j.geomorph.2012.07.005.

Recking, A., P. Frey, A. Paquier, P. Belleudy, and J. Y. Champagne (2008), Feedback between bed load transport and flow resistance in gravel and cobble bed rivers, *Water Resour. Res.*, *44*(5), 1–21, doi:10.1029/2007WR006219.

Recking, A., P. Leduc, F. Liébault, and M. Church (2012), A field investigation of the influence of sediment supply on step-pool morphology and stability, *Geomorphology*, *139-140*, 53–66, doi:10.1016/j.geomorph.2011.09.024.

Rodi, W., and G. Scheuerer (1986), Scrutinizing the k-ε Turbulence Model Under Adverse Pressure Gradient Conditions, *J. Fluids Eng.*, *108*(2), 174–179.

Rominger, J. T., A. F. Lightbody, and H. M. Nepf (2010), Effects of Added Vegetation on Sand Bar Stability and Stream Hydrodynamics, *J. Hydraul. Eng.*, *136*(December), 994–1002, doi:10.1061/(ASCE)HY.1943-7900.0000215.

Rusche, H. (2002), Computational Fluid Dynamics of Dispersed Two-Phase Flows at High Phase Fractions, Imperial College Imperial College of Science, Technology and Medicine, London.

Schmeeckle, M. W. (2014), Numerical simulation of turbulence and sediment transport of medium sand, *J. Geophys. Res. Earth Surf.*, *119*(6), 1240–1262, doi:10.1002/2013JF002911.

Schuerch, P., A. L. Densmore, B. W. McArdell, and P. Molnar (2006), The influence of landsliding on sediment supply and channel change in a steep mountain catchment, *Geomorphology*, *78*(3-4), 222–235, doi:10.1016/j.geomorph.2006.01.025.

Shamloo, H., N. Rajaratnam, and C. Katopodis (2001), Hydraulics of simple habitat structures, *J. Hydraul. Res.*, *39*(4), 351–366.

Smith, R. D., R. C. Sidle, P. E. Porter, and J. R. Noel (1993), Effects of experimental removal of woody debris o n the channel morphology of a forest, gravel-bed stream, *J. Hydrol.*, *152*, 153–179.

Strom, K., A. Papanicolaou, N. Evangelopoulos, and M. Odeh (2004), Microforms in gravel bed rivers: Formation, disintegration, and effects on bedload transport, *J. Hydraul. Eng.*, *130*(6), 554–567, doi:10.1061/(ASCE)0733-9429(2004)130:6(544).

Strom, K. B., and A. N. Papanicolaou (2007), ADV Measurements around a Cluster Microform in a Shallow Mountain Stream, *J. Hydraul. Eng.*, *133*(12), 1379–1389, doi:10.1061/(ASCE)0733-9429(2007)133:12(1379).

Sukhodolov, A. N., J. J. Fedele, and B. L. Rhoads (2006), Structure of flow over alluvial bedforms: an experiment on linking field and laboratory methods, *Earth Surf. Process. Landforms*, *31*(10), 1292–1310, doi:10.1002/esp.1330.

Swanson, F. J., and G. W. Lienkaemper (1978), *Physical consequences of large organic debris in pacific northwest streams*, Pacific Northwest Forest and Range Experiment Station. USDA Forest Service PNW-69, Portland, Or.

Thompson, D. M. (2007), The characteristics of turbulence in a shear zone downstream of a channel constriction in a coarse-grained forced pool, *Geomorphology*, *83*(3-4), 199–214, doi:10.1016/j.geomorph.2006.05.001.

Thompson, D. M., J. M. Nelson, and E. E. Wohl (1998), Interactions between pool geometry and hydraulics, *Water Resour. Res.*, *34*(12), 3673–3681.

Tritico, H. M., and R. H. Hotchkiss (2005), Unobstructed and Obstructed Turbulent Flow in Gravel Bed Rivers, *J. Hydraul. Eng.*, *131*(8), 635–645, doi:10.1061/(ASCE)0733-9429(2005)131:8(635).

Tsakiris, A. G., a. N. T. Papanicolaou, S. M. Hajimirzaie, and J. H. J. Buchholz (2014), Influence of collective boulder array on the surrounding time-averaged and turbulent flow fields, *J. Mt. Sci.*, *11*(6), 1420–1428, doi:10.1007/s11629-014-3055-8.

Vallé, B. L., and G. B. Pasternack (2006), Submerged and unsubmerged natural hydraulic jumps in a bedrock step-pool mountain channel, *Geomorphology*, *82*(1-2), 146–159, doi:10.1016/j.geomorph.2005.09.024.

Waldon, M. G. (2004), Estimation of Average Stream Velocity, *J. Hydraul. Eng.*, *130*(11), 1119–1122, doi:10.1061/(ASCE)0733-9429(2004)130:11(1119).

Whiting, P. J., and W. E. Dietrich (1991), Convective accelerations and boundary shear stress over a channel bar, *Water Resour. Res.*, *27*(5), 783–796, doi:10.1029/91WR00083.

Wilcox, A. C., and E. E. Wohl (2006), Flow resistance dynamics in step-pool stream channels: 1. Large woody debris and controls on total resistance, *Water Resour. Res.*, *42*(5), 1–16, doi:10.1029/2005WR004277.

Wilcox, A. C., E. E. Wohl, F. Comiti, and L. Mao (2011), Hydraulics, morphology, and energy dissipation in an alpine step-pool channel, *Water Resour. Res.*, *47*(7), 1–17, doi:10.1029/2010WR010192.

Wohl, E. E., and D. M. Thompson (2000), Velocity Characteristics Along a Small Step-Pool Channel, *Earth Surf. Process. Landforms*, *25*, 353–367.

Xu, Z. J., and E. E. Michaelides (2003), The effect of particle interactions on the sedimentation process of non-cohesive particles, *Int. J. Multiph. Flow*, *29*(6), 959–982, doi:10.1016/S0301-9322(03)00060-0.

Yager, E. M., and M. W. Schmeeckle (2013), The influence of vegetation on turbulence and bed load transport, *J. Geophys. Res. Earth Surf.*, *118*(3), 1585–1601, doi:10.1002/jgrf.20085.

Yager, E. M., J. W. Kirchner, and W. E. Dietrich (2007), Calculating bed load transport in steep boulder bed channels, *Water Resour. Res.*, *43*(7), 1–24, doi:10.1029/2006WR005432.

Yager, E. M., W. E. Dietrich, J. W. Kirchner, and B. W. McArdell (2012a), Patch dynamics and stability in steep, rough streams, *J. Geophys. Res. Earth Surf.*, *117*(2), 1–16, doi:10.1029/2011JF002253.

Yager, E. M., W. E. Dietrich, J. W. Kirchner, and B. W. McArdell (2012b), Prediction of sediment transport in step-pool channels, *Water Resour. Res.*, *48*(1), 1–20, doi:10.1029/2011WR010829.

Yager, E. M., J. M. Turowski, D. Rickenman, and B. W. McArdell (2012c), Sediment supply, grain protrusion, and bedload transport in mountain streams, *Geophys. Res. Lett.*, *39*, L10402, doi:10.1029/2012GL051654.

Yarnell, S. M., J. F. Mount, and E. W. Larsen (2006), The influence of relative sediment supply on riverine habitat heterogeneity, *Geomorphology*, *80*(3-4), 310–324, doi:10.1016/j.geomorph.2006.03.005.

Ye, J., and J. A. Mccorquodale (1998), Simulation of curved open channel flows by 3D hydrodynamic model, *J. oh Hydraul. Eng.*, *124*(7), 687–698.

Yu, G., Z. Wang, K. Zhang, T. Chang, and H. Liu (2009), Effect of incoming sediment on the transport rate of bed load in mountain streams, *Int. J. Sediment Res.*, *24*(3), 260–273, doi:10.1016/S1001-6279(10)60002-9.

Zeng, J., G. Constantinescu, and L. Weber (2005), A fully 3D non-hydrostatic model for prediction of flow, sediment transport and bed morphology in open channels, in *31st International Association Hydraulic Research Congress*, pp. 554–560, Seoul, Korea.

Zeng, J., G. Constantinescu, and L. Weber (2008), A 3D non-hydrostatic model to predict flow and sediment transport in loose-bed channel bends, *J. Hydraul. Res.*, *46*(3), 356–372, doi:10.3826/jhr.2008.3328.

Table 4.1: Summary of the primary details of the experiments

Experiment	Channel slope	Flow discharge	Flow depth[a]	Flow depth upstream hemisphere[b]	Relative submergence[c]	Flow velocity[b]	Shear stress magnitude[b]
	S_{bed}	Q	h_a	h_{au}	$\frac{h_{au}}{D_I/2}$	U_a	$\overline{\tau}$
	[m/m]	[m^3/s]	[m]	[ ]	[ ]	[m/s]	
S2.15%I	0.0215	0.0596	0.082	0.113	1.48	0.620	4.57
S2.15%F	0.0215	0.0596	0.077	0.114	1.50	0.590	4.68
S2.40%I	0.0240	0.0530	0.074	0.100	1.31	0.620	4.85
S2.40%F	0.0240	0.0530	0.066	0.123	1.61	0.640	4.29
S2.70%I	0.0270	0.0466	0.062	0.093	1.22	0.520	8.20
S2.70%F	0.0270	0.0466	0.061	0.105	1.37	0.590	6.90

a) Reach-averaged flow depth, velocity or shear stress.
b) Flow depth measured at the upstream face of the hemisphere.
c) Half of the diameter is used to account for the hemisphere's height.

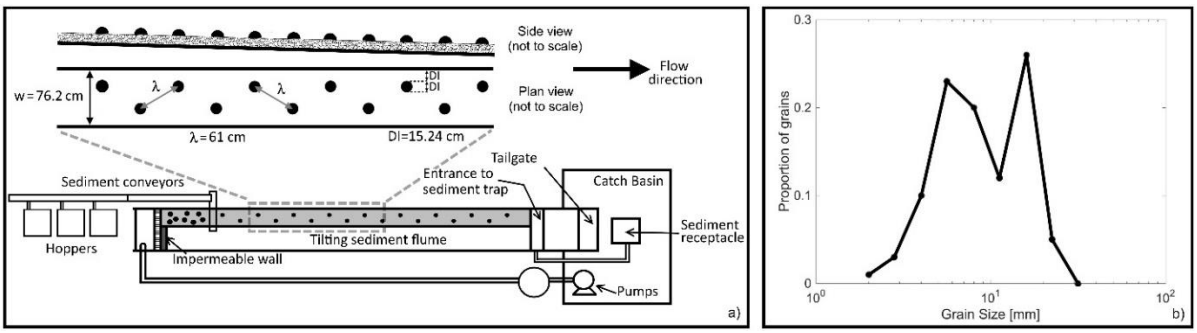

Figure 4.1: a) Sketch of the experiment setup (not to scale). An impermeable wall was placed near the middle of the flume to reduce the width (b) Grain size distribution used for the sediment and the upstream sediment supply.

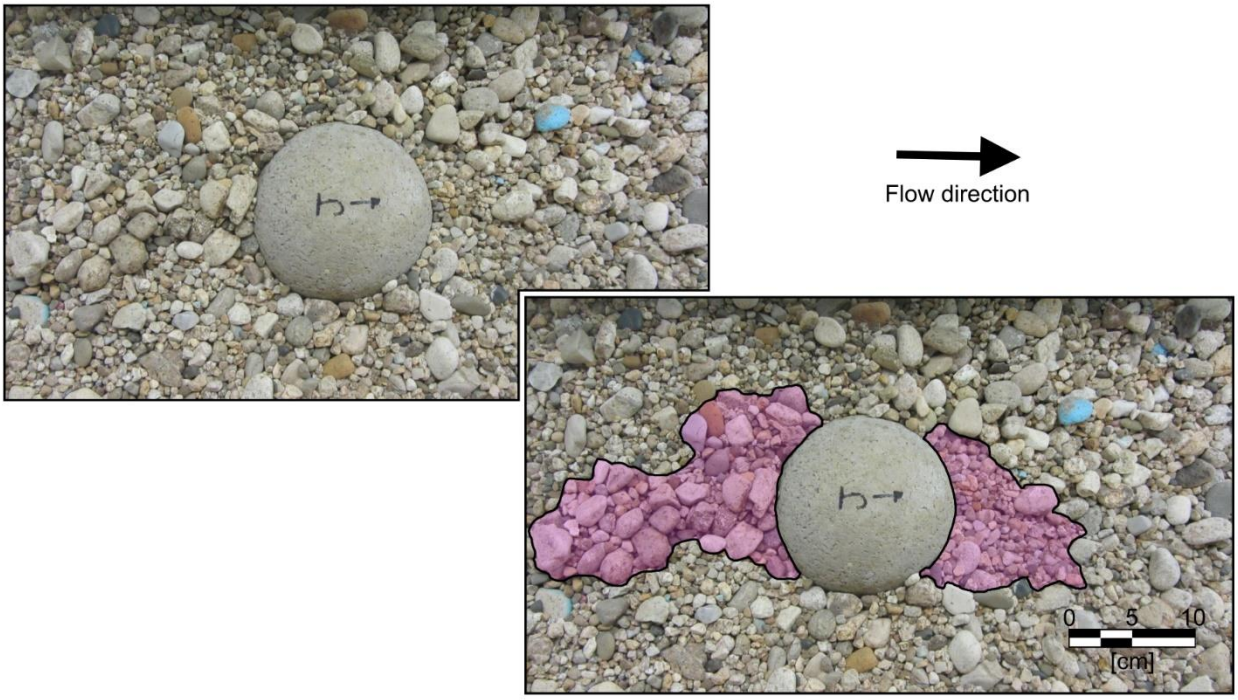

Figure 4.2: Patch delineation process. Patches were visually identified as sharp transitions in GSD. Upstream and downstream patches are highlighted in the lower figure

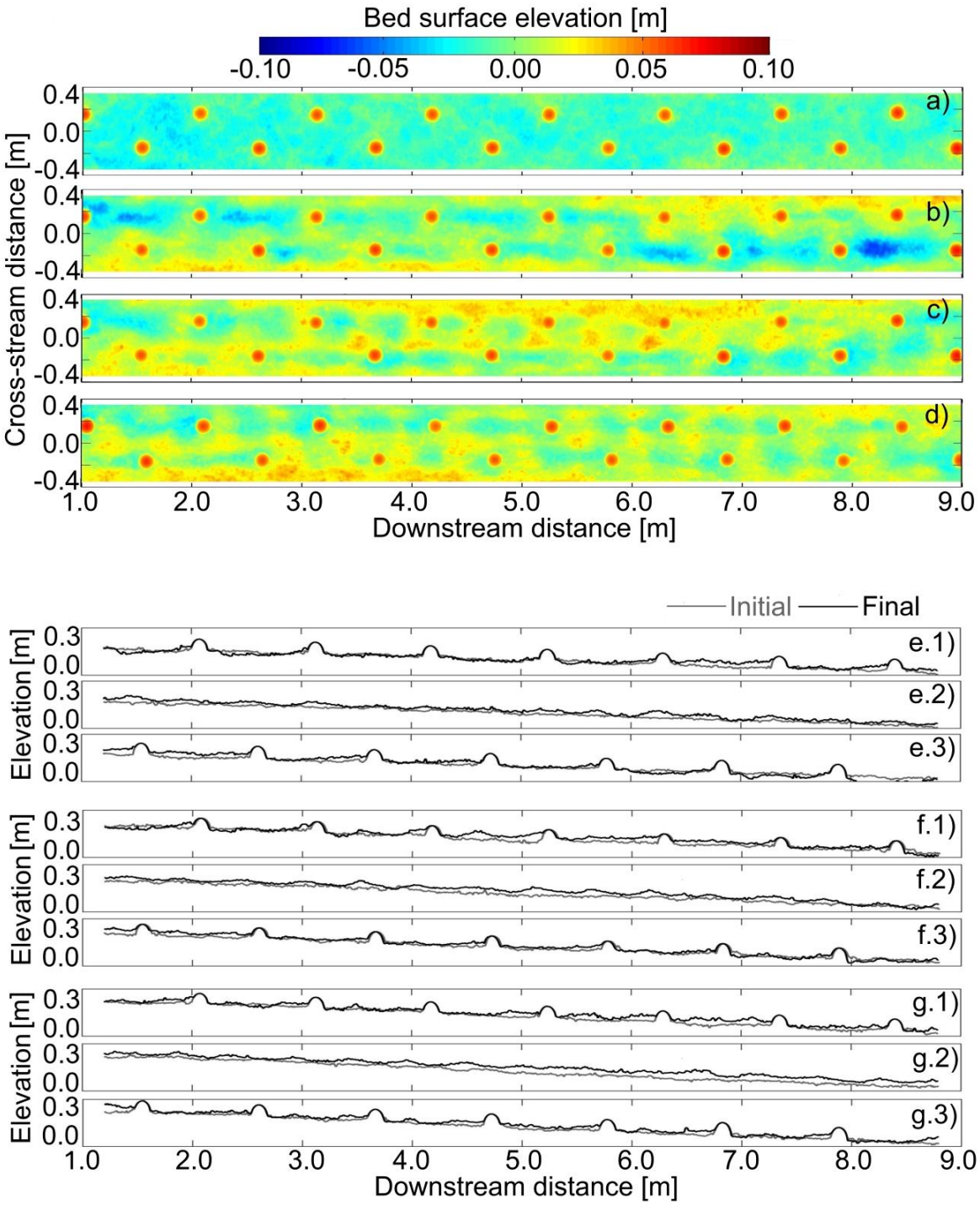

Figure 4.3: Topography (net bed slope removed) for the a) initial and final bed conditions for experiments b) S2.15%, c) 2.40%, and d) 2.70%. Change in bed surface elevation profile (number 1 and 3 after figure's label correspond to left and right side hemispheres profile, respectively, number 2 is the channel's center) for experiments e) S2.15%, f) 2.40%, and g) 2.70%.

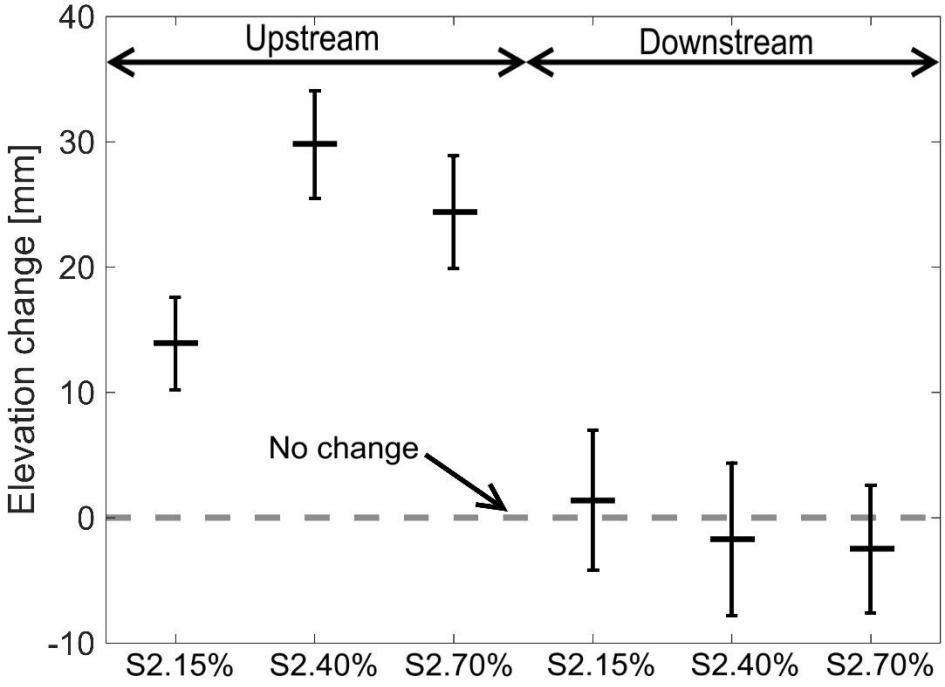

Figure 4.4: Elevation changes between the initial and final beds in the upstream and downstream regions in all experiments. The grey line denotes no change in elevation. The thicker horizontal black line for each experiment is the mean change in elevation and the vertical lines correspond to the standard error.

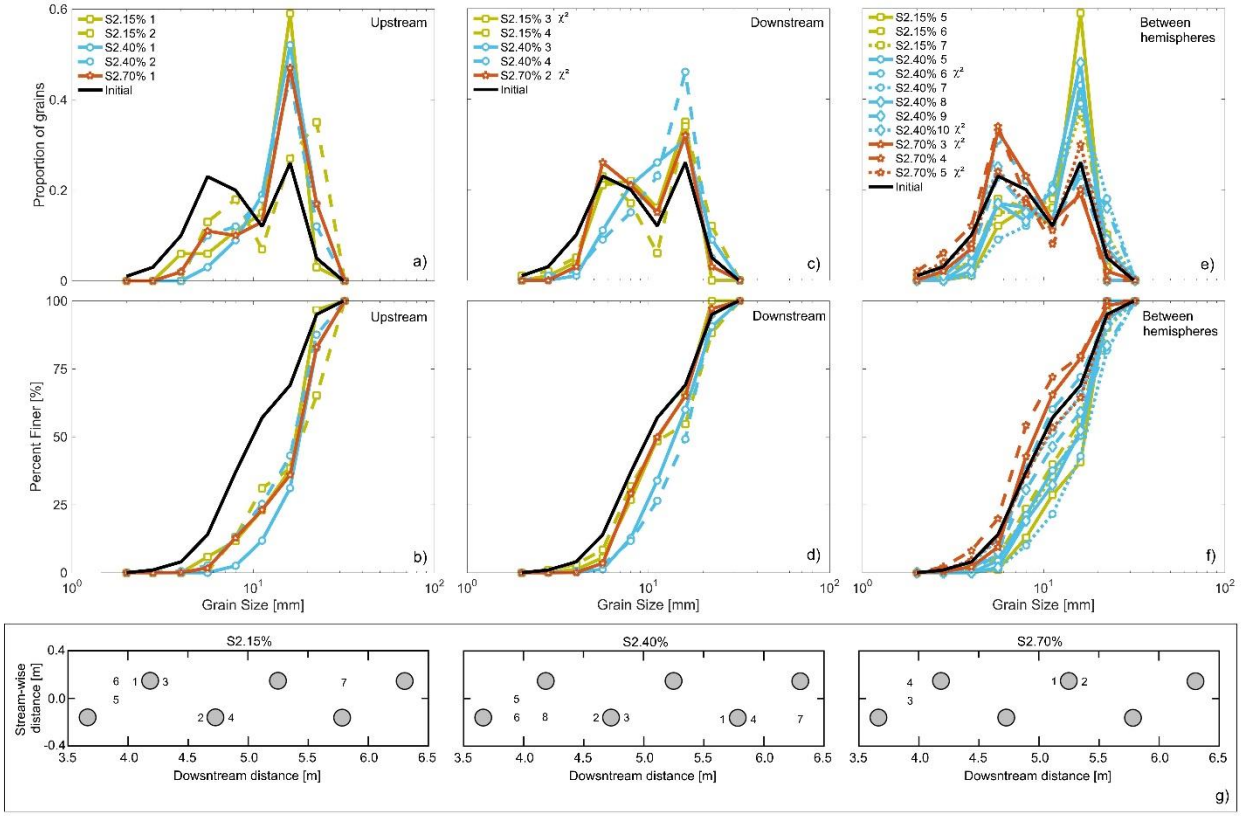

Figure 4.5: Proportion of grains and cumulative frequency of bed surface GSD measured in the a), b) upstream, c), d) downstream, and e), f) between hemispheres, respectively. The number next to experiment name corresponds to the sample number. If the number is followed by the symbol χ^2 it indicates that the sample is not statistically different than the initial GSD (black solid line). g) Locations where each sample was collected. If the sample number does not appear it indicates that it is a surface mixture sample (see text for details).

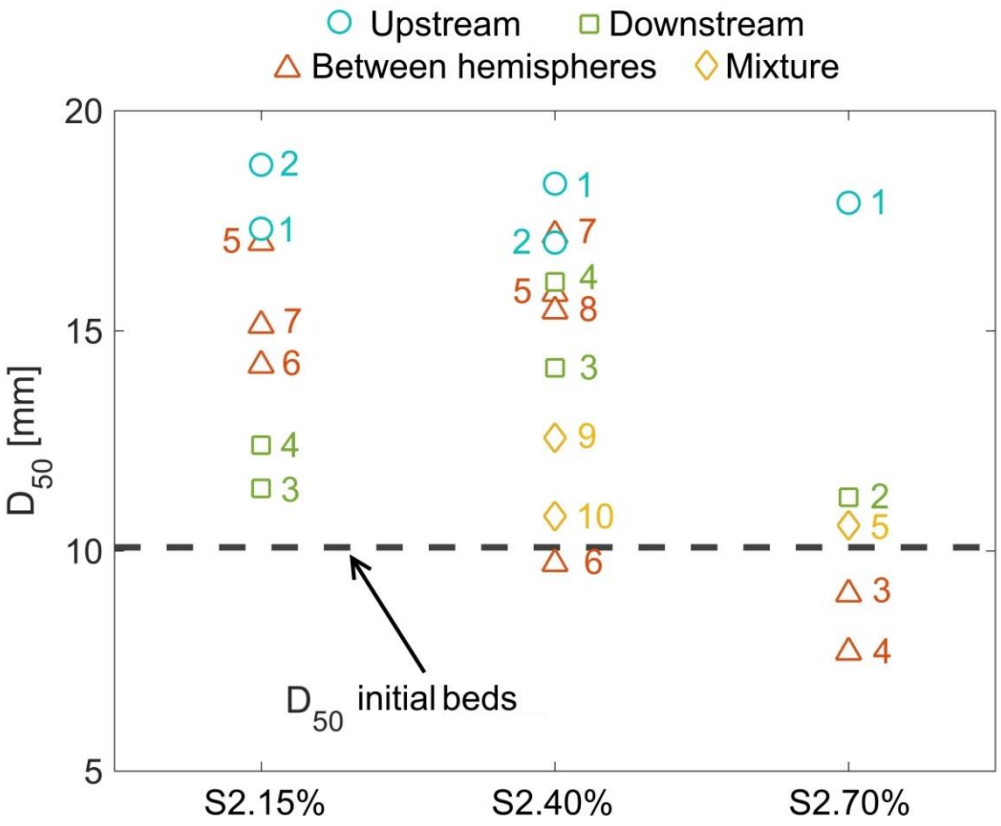

Figure 4.6: Median grain size at different locations at the end of the experiments. Numbers next to the symbols correspond to the sample number defined in Figure 4.5 g.

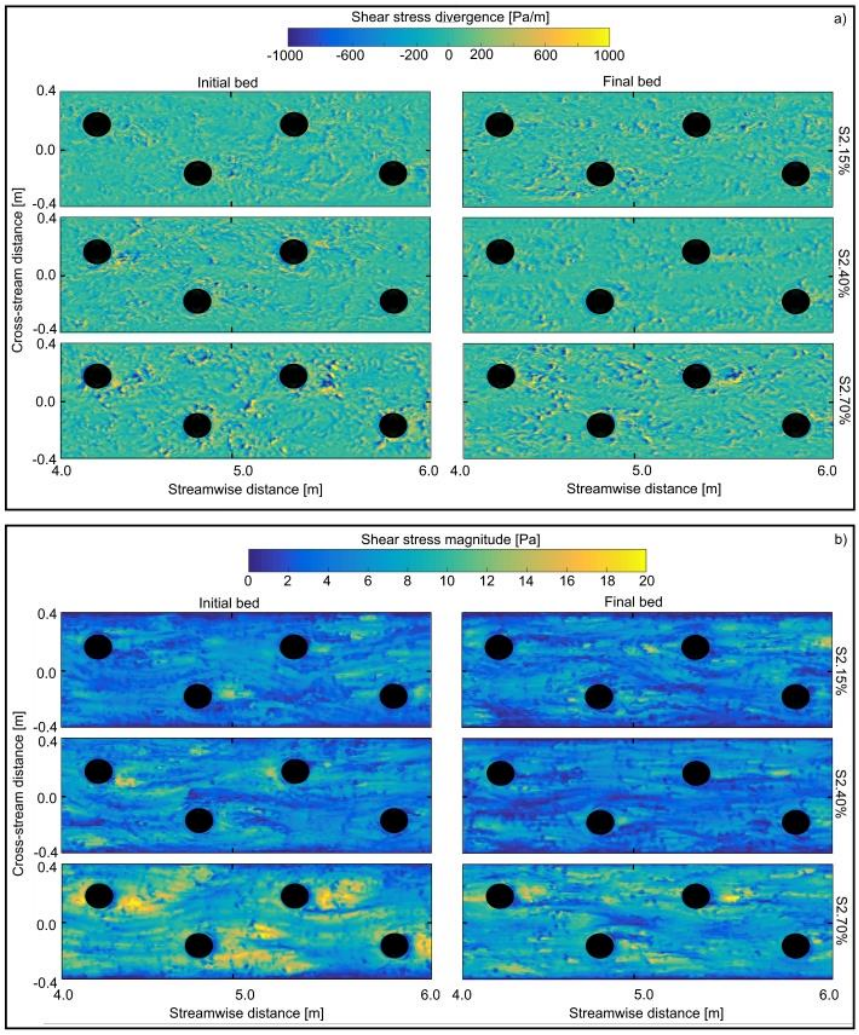

Figure 4.7: Spatial distribution of the near-bed shear stress a) divergence and b) magnitude. For clarity only a portion of the test section is shown here

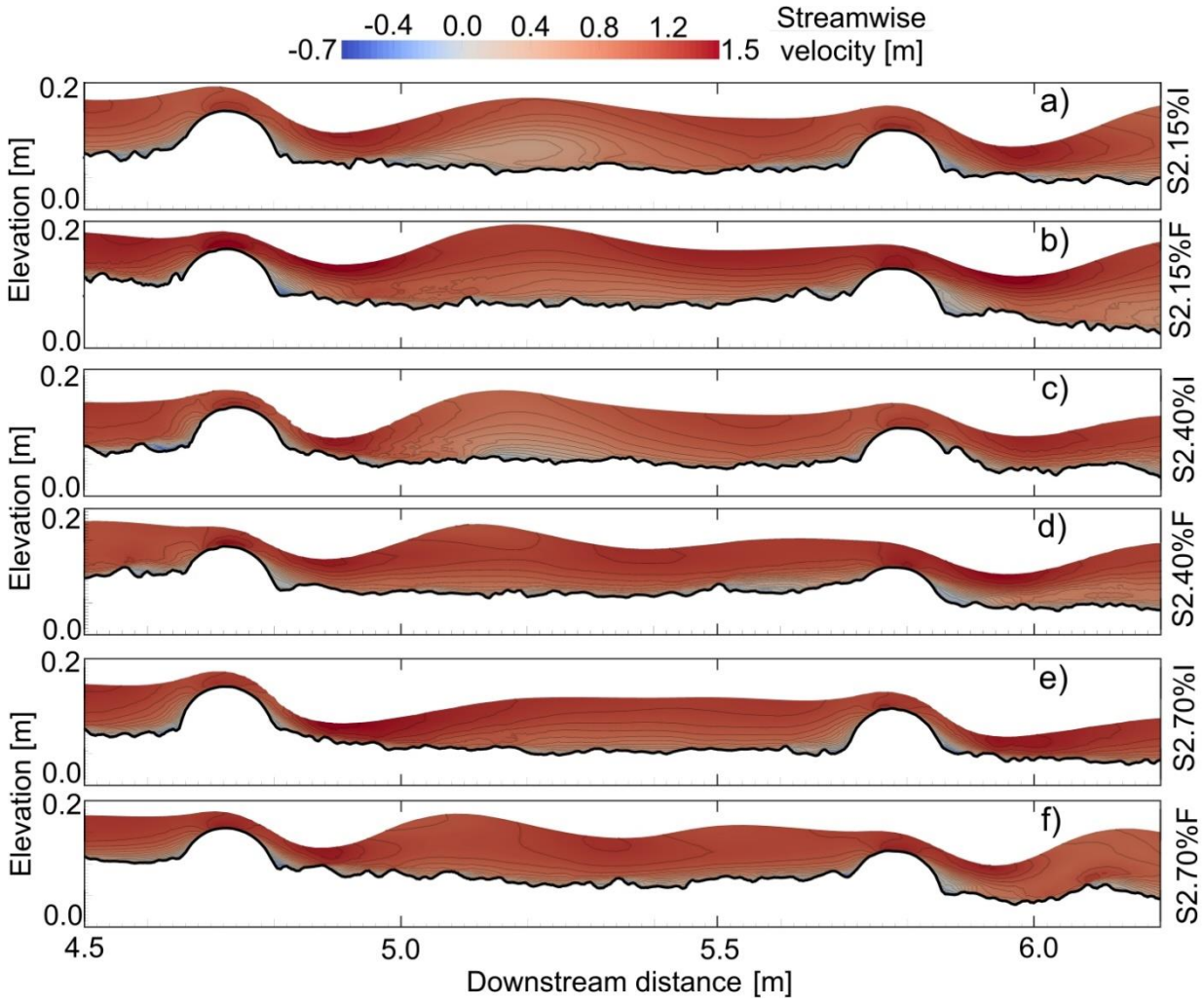

Figure 4.8: Water surface elevation and streamwise velocity contours for experiments a) S2.15I%, b) S2.15%F, c) S2.40I%, d) S2.40%F e) S2.70I% and f) S2.70%F. Flow is from left to right.

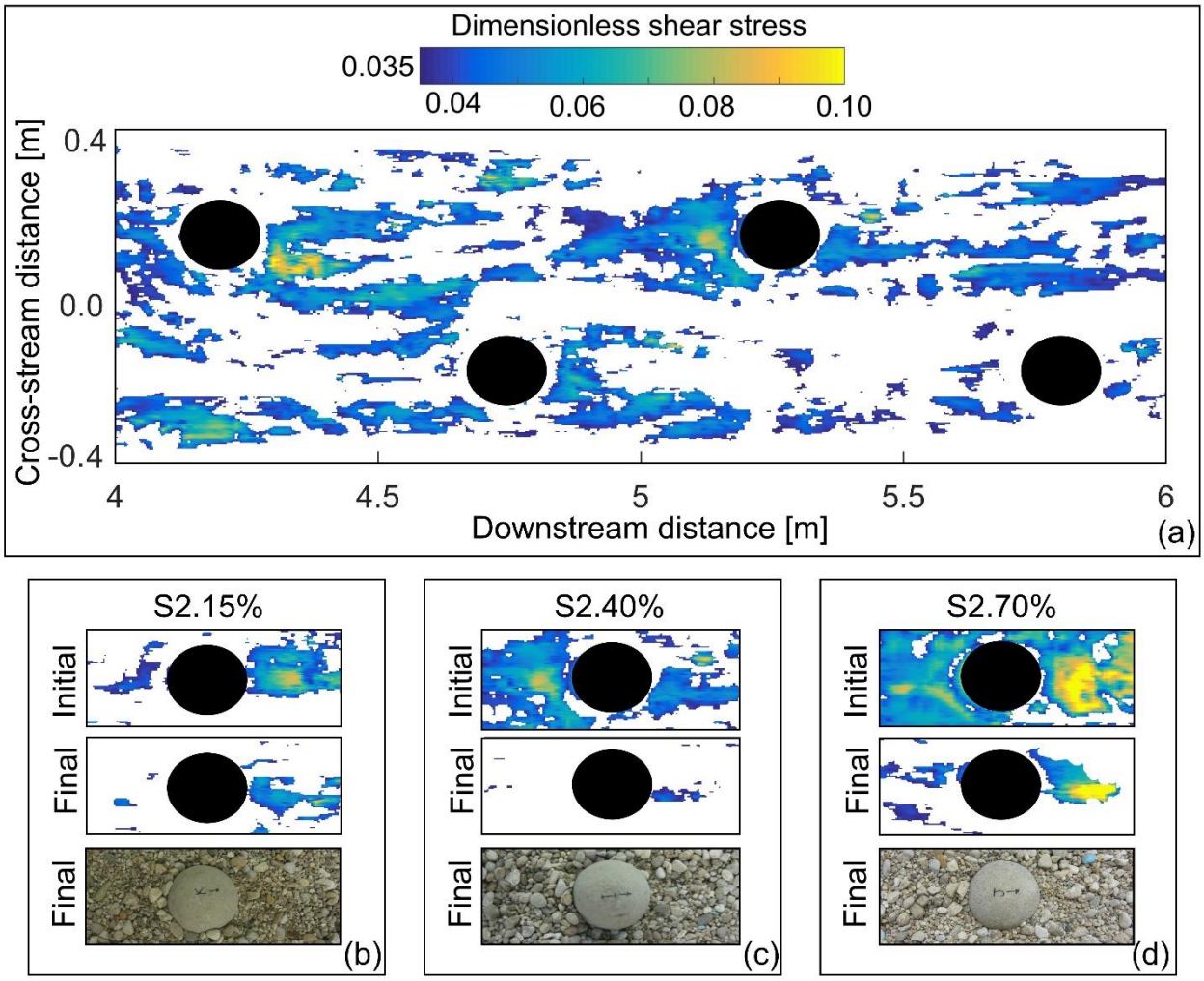

Figure 4.9: a) Spatial distribution of the dimensionless shear stress (τ') for the initial bed conditions in experiment S2.40%. Black filled circles correspond to the hemispheres and for clarity only a portion of the test section is shown here. Background white areas indicate that $\tau' < \tau'_c$. Spatial distribution of τ' around a hemisphere during the initial and final bed conditions for experiments b) S2.15%, c) S2.40%, and d) S2.70%. Photos at the bottom of figures b), c), and d) correspond to the same location shown in the initial and final τ' distributions. See text for detail on the normalization process.

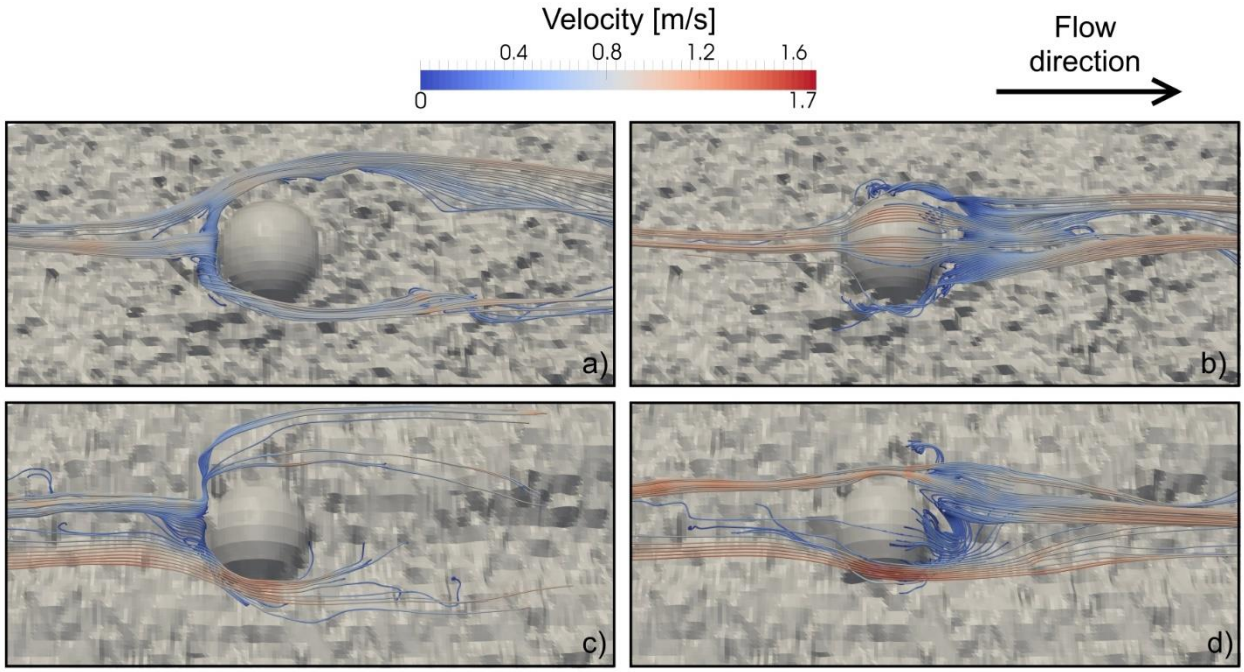

Figure 4.10: Velocity streamlines around a hemisphere (same as Figure 4.9 c) for experiment S2.40% for the initial bed conditions in the a) upstream and b) downstream regions, and for the final bed conditions in the c) upstream and d) downstream regions.

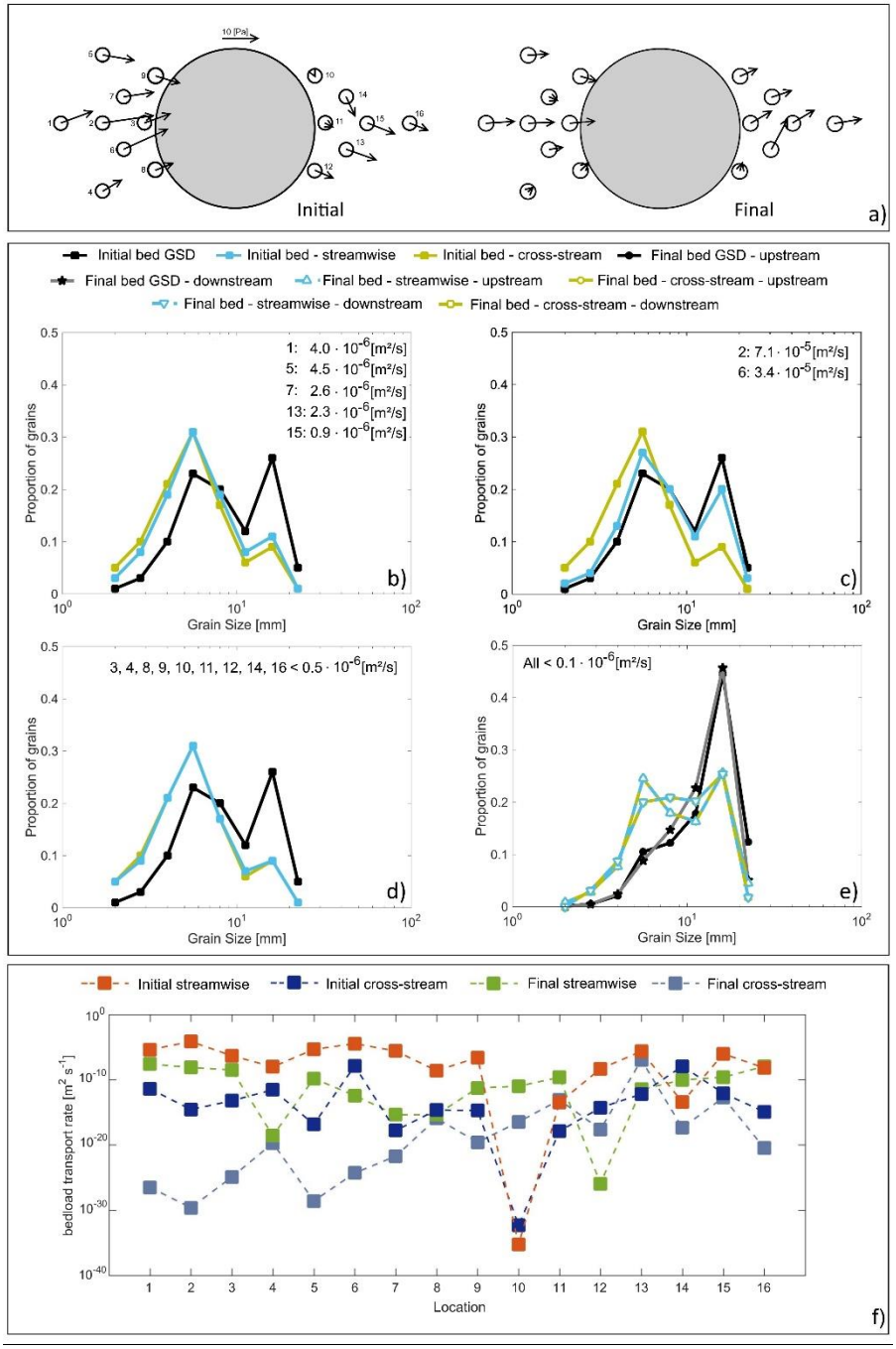

Figure 4.11: Volumetric transport rate per unit width for each grain size. a) Samples location around a hemisphere in experiment S2.40% (same than that used in Figure 4.8 c for the initial and final beds. Arrows in each location are shear stress vectors. A reference for shear stress magnitude is given for 10 Pa. Numbers next to the location is the sample number. b) Volumetric transport rate per unit width for each grain size in each location for the streamwise and cross-stream shear stress components and shear stress vector. Numbers at the bottom-left of each sub-figure indicate the sample location, I and F correspond to initial and final bed conditions, respectively.

Appendix A: Flow modelling

We obtained our spatially variable flow field using a quasi-3D model, FaSTMECH, which solves the full vertically averaged and Reynolds-averaged momentum equations. Vertical velocity profiles are calculated along the streamlines of the vertically averaged flow, and secondary flow is calculated across those streamlines [*Nelson and Smith*, 1989]. Vertical accelerations, as well as aeration, can be very important in a step-pool river and the model probably does not fully capture the vertical flow complexity. We attempted to simultaneously measure water surface elevation and local velocity to use a fully 3D model, but high velocities, even for moderate discharges, made the measuring process extremely dangerous. The use of a full 3D model could produce more accurate estimates of boundary shear stress, but given the good agreement between the measured and predicted surface water elevations and average velocities, and the quality of the topography and bathymetry we used, we believe that the use of a quasi-3D model is be appropriate for our analysis.

A.1 References

Nelson, J. M., and J. D. Smith (1989), Flow in meandering channels with natural topography, in *River Meandering, Water Resources Monographs*, vol. 12, edited by S. Ikeda and G. Parker, pp. 69–102, American Geophysical Union, Washington, D.C., USA.

Appendix B: Reach averaged velocity

The reach averaged velocity (U) was calculated with:

$$U = \sqrt{\frac{2gS\lambda_x h}{\frac{A_{IF}C_I}{w} + C_m\left(\lambda_x - \lambda_w\right)}}, \tag{B.1}$$

where g is the acceleration due to gravity, S the average bed slope, λ_x the downstream spacing between steps, h the average flow depth, A_{IF} the bed-perpendicular area of immobile grains, w the channel width, C_I $(=157\left(h/p_u\right)^{-1.6})$ the drag coefficient for immobile grains with p_u the protrusion of the immobile steps, C_m $(=0.4)$ the drag coefficient for mobile sediment, and λ_w the downstream step length. Equation (B.1) must be solved iteratively until the predicted unit discharge ($q = Uh$) equals the measured one.

Appendix C: Calibration of drag coefficients

We used a spatially constant drag coefficient, C_d, that inversely varied with discharge. This condition has been described by *Lisle et al.* [2000] as "equivalent to assuming that the flow responds extremely slowly to changes in roughness", meaning that roughness effects are averaged by the flow over spatial scales larger than that of the actual source of roughness. Although not for channels as steep as the Erlenbach, the studies of *Lisle et al.* [2000], *Nelson et al*. [2010] and *Segura and Pitlick* [2015] have shown that the use of constant drag coefficient results in similar local shear stress values compared to those determined using a variable drag coefficient. This is mainly because there is a trade-off between the local drag coefficient and velocity values. For example, if the grain size is included in the drag distribution patches of coarse grains will have a rougher surface than fine patches, consequently they will have a higher drag coefficient and the velocity will decrease. The opposite will occur in fine patches, a lower drag coefficient associated with their finer grain size will result is higher velocities. This feedback ultimately results in similar local shear stress values (see discussion by [*Lisle et al.*, 2000]). As a first guess for C_d we used the relation of *Pasternack et al.* [2006] and assumed a Manning's roughness factor (n) of 0.1. We then calibrated C_d by matching the water surface elevations predicted by the model to those obtained using the $h-Q$ rating curves and by matching the model-predicted reach-averaged velocity with the flow velocity obtained from the *Yager et al.* [2012] method. The selection of an initial n did not affect the final result, but did speed up the iteration process.

We tested if the distribution of dimensionless shear stresses in each patch class varied significantly when a spatially variable drag coefficient was considered instead of a spatially constant one. Our analysis considered only a set of representative discharges (Figure C.1) from where we compared the dimensionless mean shear stress for each patch class (τ_j^*) and its standard deviation. For the spatially variable case the drag coefficient was calculated as a function of roughness height (z_0) using *Whiting and Dietrich*'s [1991] equation, where $z_0 = 0.1D_{84j}$ (with j the patch class and D_{84j} the 84$^{\text{th}}$ percentile of bed material grain size dsitribution). However, given our fine topography the geometry of the relatively coarse patches

classes (bgC, gbC, cgB, and B) was captured and explicitly included in the numerical model, so using their respective D_{84j} would results in very large roughness heights relatively to the flow depth. Given that the spatial variation in topography of these relatively coarse patch classes was included in the mesh, we assumed that the D_{84j} of G patch class was a better representation to calculate z_0. Our results showed practically no variation in τ_j^* and its standard deviation due to the use of a variable drag coefficient compared to a constant one. These results are consistent with those of *Lisle et al.* [2000] , *Nelson et al.* [2010] and *Segura and Pitlick* [2015] and supported our choice of using a constant drag coefficient for all our discharges.

Our simulations used a grid with a 10 cm node spacing, which is a fairly fine considering that the median grain size for the mobile fraction (D_{50m}) was between 5.8 - 7.4 cm for the 2010 and 2011 data sets, respectively. Given this spatial resolution, a major portion of the form drag was captured by the topography, while skin drag was accounted in the drag coefficient (C_d).The drag coefficient was a function of the grid size, and we analyzed the model sensitivity to this. We found that a 10 cm spacing gave the best balance between the RMSE of the water surface elevations (WSE) and modelling efforts. A 20 cm grid size required larger C_d values and the WSE RMSE was higher despite the model converging faster than when a 10 cm grid was used. A 5 cm grid size required slightly lower C_d values than a 10 cm grid size, but we had several problems reaching convergence, and in some cases we did not achieve it. For those simulations in which we successfully reached convergence, the WSE RMSE was not lower than that of a 10 cm grid size model but was more comparable to that of the 20 cm grid size.

C.1 References

Lisle, T. E., J. M. Nelson, J. Pitlick, M. A. Madej, and B. L. Barkett (2000), Variability of bed mobility in natural, gravel-bed channels and adjustments to sediment load at local and reach scales, *Water Resour. Res.*, *36*(12), 3743–3755, doi:10.1029/2000WR900238.

Nelson, P. A., W. E. Dietrich, and J. G. Venditti (2010), Bed topography and the development of forced bed surface patches, *J. Geophys. Res. Earth Surf.*, *115*, F04024, doi:10.1029/2010JF001747.

Pasternack, G. B., A. T. Gilbert, J. M. Wheaton, and E. M. Buckland (2006), Error propagation for velocity and shear stress prediction using 2D models for environmental management, *J. Hydrol.*, *328*(1-2), 227–241, doi:10.1016/j.jhydrol.2005.12.003.

Segura, C., and J. Pitlick (2015), Coupling fluvial-hydraulic models to predict gravel transport in spatially variable flows, *J. Geophys. Res. Earth Surf.*, *120*, 834–855, doi:10.1002/2014JF003302.

Whiting, P. J., and W. E. Dietrich (1991), Convective accelerations and boundary shear stress over a channel bar, *Water Resour. Res.*, *27*(5), 783–796, doi:10.1029/91WR00083.

Yager, E. M., W. E. Dietrich, J. W. Kirchner, and B. W. McArdell (2012), Prediction of sediment transport in step-pool channels, *Water Resour. Res.*, *48*(1), 1–20, doi:10.1029/2011WR010829.

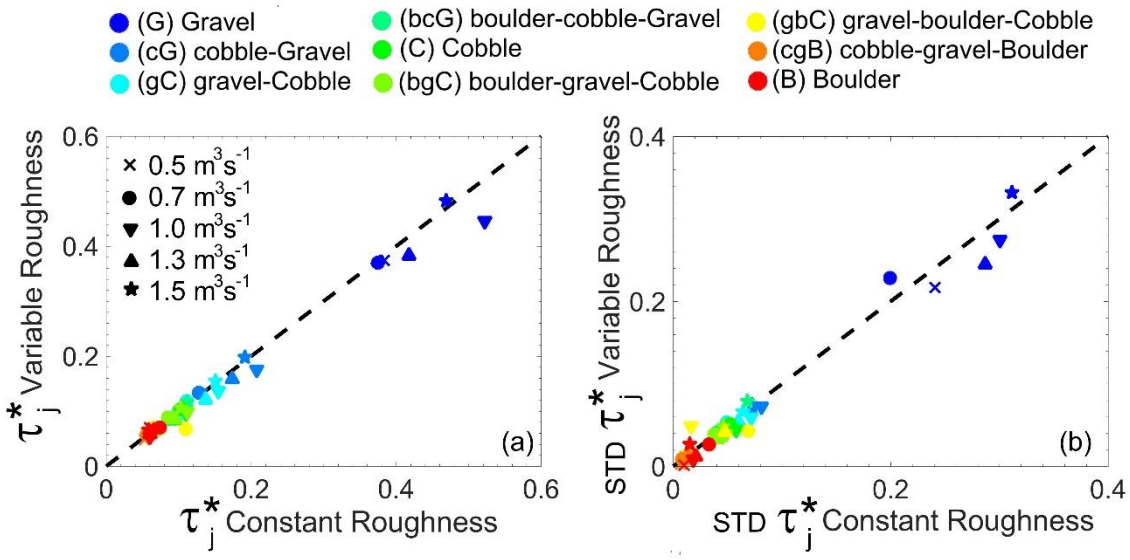

Figure C.1: Comparison between the predicted (a) dimensionless mean shear stress class and (b) standard deviation for each patch using a spatially constant or variable drag coefficient. A representative set of discharge for the 2010 data sets are shown. Markers have been colored by patch class while different shapes have been used for discharge.

Appendix D: Distribution of shear stresses

Parameter estimation for shear stress distributions was calculated using the maximum-likelihood estimation (MLE), where the objective is to find the model parameter values (θ) that maximize the likelihood function ($L(\theta) = \prod_{i=1}^{n} f(x_i \mid \theta)$, with x_i being the observed values) [*Fleiss et al.*, 2004]. One advantage of using the (MLE) is that is independent of the histogram bin size, which is required for example when the parameters are obtained via minimizing the χ^2 (see for example *Segura and Pitlick* [2015]). Notice that our calculations of χ^2 were not for parameter estimation but to test our null hypothesis (observed shear stresses comes from the reference probability distribution). To calculate the χ^2 score, in particular to estimate the histogram bin width we used the Freedman-Diaconis rule. If a given bin had less than five observations, based on the number of wetted nodes and shear stresses range in each patch class and discharge, we pooled it with neighboring bins until the count in each bin was at least five. Our results showed that no single probability distribution was systematically able to represent the observed spatially distributed shear stresses in each patch class and simulated discharge range with statistically confidence (Table D.1).

D.1 References

Fleiss, J. L., B. Levin, and M. C. Paik (2004), *Statistical Methods for Rates and Proportions*, 3rd ed., John Wiley & Sons, Inc., Hoboken, New Jersey, USA.

Segura, C., and J. Pitlick (2015), Coupling fluvial-hydraulic models to predict gravel transport in spatially variable flows, *J. Geophys. Res. Earth Surf.*, *120*, 834–855, doi:10.1002/2014JF003302.

Table D.1: Performance of the continuous probability distribution to predict the observed (from the model) shear stress distributions.

	Percentage of events where the observed shear stresses comes from the hypothesized continuous distribution with statistically confidence				
Data Sets	Normal	Lognormal	Gamma	GEV	Exponential
2010	12.61	17.72	18.62	18.62	1.20
2011	3.90	12.31	6.91	11.11	4.20
Each event correspond to a specific patch class and discharge. 2010 and 2011 correspond to the two data sets analyzed					

Appendix E: Hiding functions

Our sediment transport equations are based on the work of *Parker* [1990] and *Yager et al* [2012a, 2012b]. The hiding function we used, "Erlenbach - Mobile", is the one proposed by *Yager et al.* [2012a] (Table E.1), which is valid for the mobile sediment fraction and was developed using tracer particles in our study reach. To analyze the sensitivity of our predicted sediment volumes to the selected hiding function we calculated, using the Patch Mean method and a range of hiding functions, all the sediment transport events from the 2010 and 2011 data sets.

The dimensionless critical shear stress for the i^{th} grain size class at the j^{th} patch class is given by:

$$\tau^{*}_{ci\,j} = \alpha\left(\frac{D_{i\,j}}{D_{50}}\right)^{\beta}, \qquad \text{(E.1)}$$

where α and β were varied (Table E.1). The hiding functions were those by *Yager et al.* [2012a], the original *Parker* [1990] equation and one derived for the Rio Cordon [*Mao and Lenzi*, 2007], an alpine high-gradient, step–pool stream located in Italy.

Sediment volumes using the "Parker" hiding function *Parker* [1990] were almost always overpredicted by over an order magnitude and had the largest RMSE compared to the other hiding functions (Figure E.1). The "Rio Cordon" hiding function predicted sediment transport volumes more accurately than "Parker", but tended to underpredict values. The most accurate results were obtained using the two hiding functions of *Yager et al.* [2012a], "Erlenbach Total" and "Erlenbach Mobile". The selection of an adequate hiding function is therefore crucial to obtain accurate sediment transport predictions. In rivers that do not have calibrated hiding functions, a sensitivity analysis of hiding functions is recommended.

E.1 References

Mao, L., and M. A. Lenzi (2007), Sediment mobility and bedload transport conditions in an alpine stream, *Hydrol. Process.*, *21*(14), 1882–1891, doi:10.1002/hyp.6372.

Parker, G. (1990), Surface-based bedload transport relation for gravel rivers, *J. Hydraul. Res.*, *28*(4), 417–436, doi:10.1080/00221689009499058.

Yager, E. M., W. E. Dietrich, J. W. Kirchner, and B. W. McArdell (2012a), Prediction of sediment transport in step-pool channels, *Water Resour. Res.*, *48*(1), 1–20, doi:10.1029/2011WR010829.

Yager, E. M., J. M. Turowski, D. Rickenman, and B. W. McArdell (2012b), Sediment supply, grain protrusion, and bedload transport in mountain streams, *Geophys. Res. Lett.*, *39*, L10402, doi:10.1029/2012GL051654.

Table E.1: Hiding functions used in bed load calculations

Hiding Function	Hiding Function Coefficient	Hiding Function Exponent
Parker	0.0386	-0.9049
Erlenbach - Total bed	0.14	-0.62
Erlenbach - Mobile	0.07	-0.16
Rio Cordon	0.189	-0.639

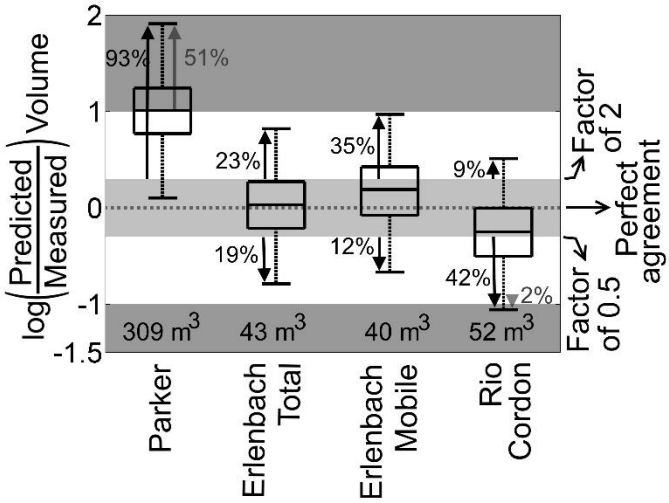

Figure E.1: The log of the ratio of the predicted to measured sediment volume when different hiding functions are used. "Parker" is the original hiding function of *Parker* [1990], "Erlenbach Total" and "Erlenbach Mobile" are those obtained by *Yager et al.* [2012a] and use the total bed grain size distribution and only the mobile grain fraction, respectively. "Rio Cordon" is the hiding function for the Rio Cordon [*Mao and Lenzi*, 2007]. See Figure 2.7 in Chapter 2 for other figure details.

Appendix F: Limited sediment supply

The upstream sediment supply was included by scaling the predicted total transport rate by the volumetric proportion of the bed covered by relatively mobile sediment $\left(Am / A_T\right) Z_m^*$, where $Z_m^* = Z_t / Z_{t0}$ is the ratio of the thickness of the mobile sediment deposit at the time of an individual flow event (Z_t) to that immediately after the last extreme event (Z_{t0}). The percent step protrusion ($p_{u\%t}$) varies with time [*Yager et al.*, 2012] and is related to the thickness of the mobile sediment deposit and the mean immobile grain diameter (D_I) through:

$$Z_t = D_I \left(1 - p_{u\%t}\right), \tag{F.1}$$

and

$$p_{u\%t} = 0.15 t^{0.21}, \tag{F.2}$$

where t is the time elapsed since the last extreme event (in units of months). Z_{t0} is calculated setting $t = 1$ in equation (F.2). Assuming D_I is constant during the period of analysis Z_m^* can be simplified as:

$$Z_m^* = \frac{Z_t}{Z_{t0}} = \frac{D_I \left(1 - 0.15 t^{0.21}\right)}{D_I \left(1 - 0.15 t^{0.21}\right)\Big|_{t=1}} = \frac{1}{0.85}\left(1 - 0.15 t^{0.21}\right), \tag{F.3}$$

F.1 References

Yager, E. M., J. M. Turowski, D. Rickenman, and B. W. McArdell (2012), Sediment supply, grain protrusion, and bedload transport in mountain streams, *Geophys. Res. Lett.*, *39*, L10402, doi:10.1029/2012GL051654.

Appendix G: Shear stress variations with median grain size for the entire wetted surface

In our $\overline{\tau}_j - \overline{\tau} - D_{50j}$ relations we only considered areas where the local dimensionless shear stress was higher than the dimensionless critical shear stress ($\tau_j^* \geq \tau_c^*$). This eliminates a portion of the low shear stress values, especially for coarse patches (i.e. Boulder patches), and improves the correlation between patch mean shear stress and median grain size. If the whole wetted area is considered (i.e. without filtering those values below τ_c^*) the patch mean shear stress ($\overline{\tau}_j$) still increased with higher D_{50j} for all patch classes except for Boulder patches (Figure G.1) Although Boulder patches did not follow the trend of the other patch classes, similar equations to the original $\overline{\tau}_j - \overline{\tau} - D_{50j}$ relations can be obtained and used for sediment transport calculations (Figure G.1 b and c).

$$c_p = 0.98\left(\frac{D_{50j}}{D_{50}}\right)^{0.82} \quad , \overline{\tau} = \overline{\tau}_{var\ D_{50}}, R^2 = 0.44 \tag{G.1}$$

$$c_p = 0.50\left(\frac{D_{50j}}{D_{50}}\right)^{0.93} \quad , \overline{\tau} = \overline{\tau}_T \quad , R^2 = 0.46 \tag{G.2}$$

$$e_p = -0.14\ln\left(\frac{D_{50j}}{D_{50}}\right) + 1.01 \quad , \overline{\tau} = \overline{\tau}_{var\ D_{50}}, R^2 = 0.43 \tag{G.3}$$

$$e_p = -0.14\ln\left(\frac{D_{50j}}{D_{50}}\right) + 0.99 \quad , \overline{\tau} = \overline{\tau}_T \quad , R^2 = 0.44 \tag{G.4}$$

We used the same test described in Chapter 2, section 2.4.3 to determine the accuracy of these relations when used in sediment transport equations. Equations (G.1) to (G.4) were almost as accurate as those obtained with the original $\overline{\tau}_j - \overline{\tau} - D_{50j}$ relations (Figure G.1), although a larger number of events were underpredicted.

G.1 References

Yager, E. M., J. M. Turowski, D. Rickenman, and B. W. McArdell (2012c), Sediment supply, grain protrusion, and bedload transport in mountain streams, *Geophys. Res. Lett.*, *39*, L10402, doi:10.1029/2012GL051654.

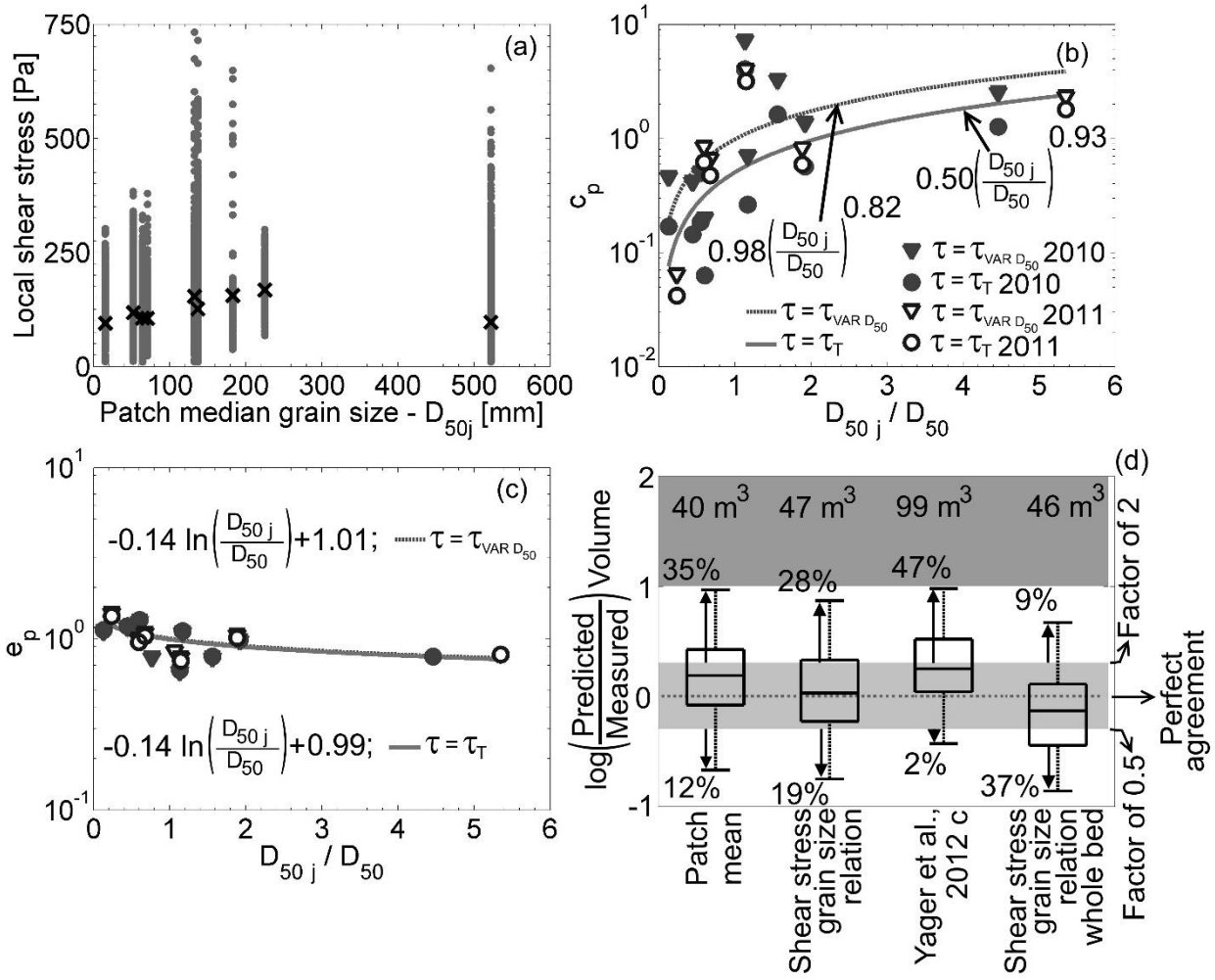

Figure G.1: Shear stress and sediment transport predictions using the whole wetted surface. (a) Local boundary shear stress versus local median surface grain size for a discharge of 1 m3/s for the 2010 data set and the whole wetted bed surface. Each circle represents a wetted node in the numerical model. Relations of (b) the coefficient and (c) exponent in equations (G.1) and (G.2). (d) Sediment transport volume predictions using equations (G.3) and (G.4) compared to those obtained by the "Patch mean", the original $\overline{\tau}_j - \overline{\tau} - D_{50\,j}$ relations and *Yager et al*. [2012 c]. See Figure 2.7 for an explanation of the box properties.

Appendix H: Prediction and measurements uncertainties

Even though our predictions represent an improvement over other published methods, only about 50% of the events were within a factor of 2 of the measured values. We made a number of simplifications that may have reduced the accuracy of our predictions. Our method does not route the sediment throughout the reach, which may affect the predictions because fine and coarse fractions of the bedload can be routed over different paths [*Clayton and Pitlick*, 2007]. We assumed that patches were stable throughout every hydrograph, and even more, during each data set. We did not change the bed topography, patch area or the grain size distribution even when some events were more than one year apart (in the 2010 data).

One particular source of uncertainty is the simplified term for sediment supply. In steep mountain channels, sediment supply is primary driven by episodic landslides and debris flows (e.g., *Bathurst et al.* [1986]; *Benda and Dunne* [1997]) and is sensitive to human activities in a watershed [*Yu et al.*, 2009], the presence and severity of wildfires [*Benda et al.*, 2003; *Goode et al.*, 2012], hillslope processes (i.e. degree of vegetation, [*Recking*, 2012]), and seasonal variations. We lack a mechanism to predict the exact timing and caliber of material that a landslide or debris flow delivers, and explicitly including them in bed load calculations is not feasible. We partially overcome this issue by using the protrusion of the immobile steps, as a proxy for sediment supply [*Yager et al.*, 2012], . Other important mechanisms, such as bed scour, sediment deposition, shear stress divergence, flow turbulence and hydrograph effects, were omitted in our study. Explicitly including them could improve future sediment transport predictions. Other potential sources of uncertainties come from our measured values of water surface elevation and the stage-discharge relation, especially for high discharges. Fluctuations in the observed water surface elevations indicate that there were local and temporal flow unsteadiness that the hydrodynamic model was not able to capture.

We used a sediment transport equation developed using reach-averaged properties (e.g. $\overline{\tau}$ and D_{50}) and applied it at the patch scale. We divided each patch into 25 sub-areas, which gave an average sub-area of 0.55 and 0.93 m^2, for the 2010 and 2011 data sets, respectively, with a minimum of approximately 0.05 m^2. Although no study, to the best of our knowledge, has defined the finest scale at which a certain sediment transport equation is applicable, most

2D and 3D models with sediment transport capabilities use a grid based algorithm. This approach has been successfully applied using finer or similar grid sizes to that used in this study. For example, sediment transport calculations has been used in numerical simulations of flume experiments using the STREMR HySeD model [*Abad et al.*, 2008] and field applications using the RMA2 [*King*, 1990; *Rathburn and Wohl*, 2003] and also the FaSTMECH models [*Maturana et al.*, 2014].

H.1 References

Abad, J. D., G. C. Buscaglia, and M. H. Garcia (2008), 2D stream hydrodynamic, sediment transport and bed morphology model for engineering applications, *Hydrol. Process.*, *22*(10), 1443–1459, doi:10.1002/hyp.6697.

Bathurst, J. C., G. J. L. Leeks, and M. D. Newson (1986), Field measurements for hydraulic and geomorphological studies of sediment transport - The special problems of mountain streams, in *Proceedings of the International Symposium on Measuring Techniques in Hydraulic Research*, pp. 137–151, Balkema, Netherlands.

Benda, L., and T. Dunne (1997), Stochastic forcing of sediment routing and storage in channel networks, *Water Resour. Res.*, *33*(12), 2865–2880, doi:10.1029/97WR02387.

Benda, L., D. Miller, P. Bigelow, and K. Andras (2003), Effects of post-wildfire erosion on channel environments, Boise River, Idaho, *For. Ecol. Manage.*, *178*(1-2), 105–119, doi:10.1016/S0378-1127(03)00056-2.

Clayton, J. A., and J. Pitlick (2007), Spatial and temporal variations in bed load transport intensity in a gravel bed river bend, *Water Resour. Res.*, *43*, W02426, doi:10.1029/2006WR005253.

Goode, J. R., C. H. Luce, and J. M. Buffington (2012), Enhanced sediment delivery in a changing climate in semi-arid mountain basins: Implications for water resource management and aquatic habitat in the northern Rocky Mountains, *Geomorphology*, *139-140*, 1–15, doi:10.1016/j.geomorph.2011.06.021.

King, I. P. (1990), *Program Documentation: RMA2-A Two-Dimensional Finite Element Model for Flow in Estuaries and Streams. Ver 4.3. Resource Management Associates, Lafayette, CA.*

Maturana, O., D. Tonina, J. A. McKean, J. M. Buffington, C. H. Luce, and D. Caamaño (2014), Modeling the effects of pulsed versus chronic sand inputs on salmonid spawning habitat in a low-gradient gravel-bed river, *Earth Surf. Process. Landforms*, *39*, 877–889, doi:10.1002/esp.3491.

Rathburn, S., and E. Wohl (2003), Predicting fine sediment dynamics along a pool-riffle mountain channel, *Geomorphology*, *55*(1-4), 111–124, doi:10.1016/S0169-555X(03)00135-1.

Recking, A. (2012), Influence of sediment supply on mountain streams bedload transport, *Geomorphology*, *175-176*, 139–150, doi:10.1016/j.geomorph.2012.07.005.

Yager, E. M., J. M. Turowski, D. Rickenman, and B. W. McArdell (2012), Sediment supply, grain protrusion, and bedload transport in mountain streams, *Geophys. Res. Lett.*, *39*, L10402, doi:10.1029/2012GL051654.

Yu, G., Z. Wang, K. Zhang, T. Chang, and H. Liu (2009), Effect of incoming sediment on the transport rate of bed load in mountain streams, *Int. J. Sediment Res.*, *24*(3), 260–273, doi:10.1016/S1001-6279(10)60002-9.

Appendix I: Field measurements used to predict sediment transport rates

For our reach-averaged velocity and sediment transport calculations the information summarized in Table I.1 was used. In the Table "m" denotes the relatively mobile sediment and parameters are proportion of the bed covered by mobile sediment (A_m/A_T), the depth of the mobile sediment (z_{mu}), the immobile-grain: protrusion (p_u), mean diameter (D), downstream spacing (λ_X), and downstream length (λ_W), D_{84} and D_{90} are the 84th and 90th percentile grain sizes, w is the channel width, w_{bottom} is the bottom width, L and H are the mean step length and height, respectively, KE and a are parameters in the *Egashira and Ashida* [1991] equation, α is the block concentration. "n/r" stands for not required for sediment transport predictions using the corresponding method (Chapter 2 for details). Ref1, Ref2 and Ref3 are *Nitsche et al.* [2011] *Yager et al.* [2012a], *and Yager et al.* [2012b], respectively.

I.1 References

Egashira, S., and K. Ashida (1991), Flow resistance and sediment transportation in streams with step-pool bed morphology, in *Fluvial Hydraulics of Mountain Regions*, edited by A. Armanini and G. Di Silvio, pp. 45–58, Springer-Verlag.

Nitsche, M., D. Rickenmann, J. M. Turowski, A. Badoux, and J. W. Kirchner (2011), Evaluation of bedload transport predictions using flow resistance equations to account for macro-roughness in steep mountain streams, *Water Resour. Res.*, *47*, W08513, doi:10.1029/2011WR010645.

Yager, E. M., W. E. Dietrich, J. W. Kirchner, and B. W. McArdell (2012a), Patch dynamics and stability in steep, rough streams, *J. Geophys. Res. Earth Surf.*, *117*(2), 1–16, doi:10.1029/2011JF002253.

Yager, E. M., W. E. Dietrich, J. W. Kirchner, and B. W. McArdell (2012b), Prediction of sediment transport in step-pool channels, *Water Resour. Res.*, *48*(1), 1–20, doi:10.1029/2011WR010829.

Table I.1: Field measurements used to predict sediment transport rates

Parameter	2010	2011	2004	2004 source
S (%)	9.9	9.8	9.8	Ref 2
w (m)	4.7	4.7	4.7	Ref 1; Ref 2
A_m/A_T	0.70	0.74	0.67	Ref 2
z_{mu} (mm)	310	302	310	Ref 1
p_u(mm)	144	110	130	Ref 1
D (mm)	454	412	442	Ref 2
D_{84} (mm)	n/r	n/r	494	Ref 2
D_{90} (mm)	n/r	n/r	619	Ref 3
λ_X (m)	4.0	4.0	4.0	Ref 1
λ_W (m)	1.3	1.3	1.3	Ref 1
C_m	0.44	0.44	0.44	Ref 1
w_{bottom} (m)	n/r	n/r	3.5	Ref 1
L (m)	n/r	n/r	7.86	Ref 1
H (m)	n/r	n/r	0.69	Ref 1
KE	n/r	n/r	0.48	Ref 1
a	n/r	n/r	2.5	Ref 1
α	n/r	n/r	0.14	Ref 1